

Body Posture Detection Using Strain Sensitive Clothing

A dissertation submitted to

ETH ZURICH

for the degree of
Doctor of Sciences

presented by

CORINNE MATTMANN

Dipl. El.-Ing. ETH/ MSc. ETH

born 18 July 1978

citizen of Eschenbach LU and Hochdorf

accepted on the recommendation of

Prof. Dr. Gerhard Tröster, examiner

Prof. Dr. Thomas Martin, co-examiner

To my family

Acknowledgments

First of all, I would like to thank my advisor, Prof. Dr. Gerhard Tröster, for giving me the opportunity to write this dissertation at the Wearable Computing Lab and for supporting me whenever necessary. I enjoyed in this lab the visionary thinking combined with pure science. His inputs substantially helped receiving the best paper award at ISWC2007.

I would also like to thank Prof. Tom Martin for being the second examiner of my dissertation and reviewing the thesis.

Special thanks belong to Frank Clemens from EMPA and his team for providing me the strain sensor. Without this sensor, the dissertation would not have been possible in this form.

Further, I would like to thank Tünde Kirstein for co-advising me during the first two years.

I am very grateful to the members of the Electronics Laboratory for the pleasant and inspiring atmosphere. Special thanks go to Holger Harms, Johannes Schumm, and Cornelia Setz.

I also want to thank my semester and master students (Christof Küng, Marco Guidali, Mirco Rossi, Valeria Hunkeler, Severin Hafner, André Linder, Sandra Schwendener, Dieter Schatz, Simon Steiner, Marianne Michel, Claudia Frischknecht, and Daniel Höhener) for their good work which helped me achieving the results of this thesis.

Special thank goes to Ruth Zähringer, our secretary, who solved many problems - even beyond her field of responsibility. I also owe thank to Urs Egger who designed and produced the PCB's for the prototype, Andreas Griesser for doing the body scans, and Roland Müller for providing the Vicon system.

Finally, I would like to thank my family, my boyfriend Andreas, and his parents for their support and for giving me a balance to the scientific work.

Contents

Abstract	xi
Zusammenfassung	xiii
1. Introduction	1
1.1. Research Objectives	2
1.2. Body Posture and Movement Measurement Systems	3
1.3. Approaches to Combine Electronics and Textiles	6
1.3.1. Conductive Fibers	6
1.3.2. Electronic Devices	7
1.3.3. Sensors and Actuators	7
1.4. Outline	8
2. Reference Measurement Method	11
2.1. Introduction	12
2.2. Method	12
2.2.1. Choice of Measurement System	12
2.2.2. Measurement Setup	13
2.2.3. Type of Markers	14
2.2.4. Garment and Marker Placement	16
2.2.5. Experiment	16
2.2.6. Post Processing	16
2.3. Results	18
2.4. Discussion and Conclusions	20
3. Textile Strain Sensor	23
3.1. Introduction	24
3.1.1. Related Work	24
3.2. Sensor Design	25
3.2.1. Sensor Material and Manufacturing	25
3.2.2. Sensor Attachment to Textile	26
3.3. Measurement Setup	29
3.4. Results and Discussion	31
3.4.1. Relaxation Behaviour	31
3.4.2. Hysteresis	32

3.4.3.	Sensitivity $\frac{\delta R}{\delta t}$ in Different Working Ranges . . .	33
3.4.4.	Dependency on Strain Rate	34
3.4.5.	Longterm Cycling	35
3.4.6.	Ageing	36
3.4.7.	Washability	37
3.5.	Conclusions	37
4.	Posture Classification Experiment	39
4.1.	Method	40
4.1.1.	Prototype	40
4.1.2.	Experimental procedure	41
4.1.3.	Classification methodology	43
4.2.	Results	44
4.3.	Conclusions	47
5.	Simulation of Strain in Tight-Fitting Clothing	49
5.1.	Introduction	50
5.2.	Animated Body Model	51
5.2.1.	Body Scan	51
5.2.2.	Animation	52
5.2.3.	Validation	53
5.3.	Cloth Simulation	54
5.3.1.	Particle Model	55
5.3.2.	Numerical Integration	58
5.3.3.	Collisions	58
5.3.4.	Sewing	61
5.3.5.	Fix Points	63
5.3.6.	Other Forces	64
5.4.	Simulation Process	64
5.4.1.	Input	64
5.4.2.	Simulation	66
5.4.3.	Calculation of Strain	68
5.5.	Results	69
5.6.	Conclusions	72
6.	Optimization of Sensor Placement	73
6.1.	Introduction	74
6.2.	Methods	74
6.2.1.	Input Data for the Optimization	75
6.2.2.	Mutual Information Feature Selection (MIFS)	77

6.2.3. Genetic Algorithm	79
6.3. Results and Discussion	81
6.3.1. Mutual Information Feature Selection	81
6.3.2. Genetic Algorithm	82
6.4. Conclusions	86
7. Sensitivity Analyses using Simulated Strain Patterns	89
7.1. Introduction	90
7.2. Sensitivity of Sensor Placement	91
7.2.1. Method	91
7.2.2. Results and Discussion	92
7.3. Effect of Sensor Failure on Classification Result	92
7.3.1. Method	92
7.3.2. Results and Discussion	93
7.4. Upwards Shift of Shirt at Waistline	96
7.4.1. Method	96
7.4.2. Results and Discussion	96
7.5. Does Posture Recognition Still Work for Different Body Proportions?	98
7.5.1. Method	98
7.5.2. Results and Discussion	99
7.6. Conclusions	100
8. Conclusions	103
8.1. Achievements	103
8.2. Outlook	105
A. Strain Patterns Measured with Reference Method	107
B. Simulated Strain Patterns (SSP)	113
C. SSP after Shift of Shirt at Waistline	119
D. SSP for Different Body Proportions	123
Glossary	127
Bibliography	131
Curriculum Vitae	141

Abstract

In this thesis, different aspects of a strain sensitive garment detecting upper body postures are presented.

A reference measurement method to capture strain patterns in the textile during different body postures was developed using an optical motion tracking system. With this method, the feasibility of a body posture recognition with a strain sensitive garment was shown. Additionally, the strain patterns were used to define requirements for a textile strain sensor.

In a collaboration with EMPA¹, a strain sensor was developed which was composed of a mixture of a thermoplastic elastomer and carbon black particles (50wt-%). The sensor has a diameter of $315\mu\text{m}$ enabling an unobtrusive integration into textile. The characterization showed high linearity, a small hysteresis, and only a minor dependance on the strain rate resulting in an error of 5.5% in strain. The working range of the sensor was 70% strain.

Using the characterized sensor thread, a catsuit prototype was built. A study was conducted with eight participants wearing the prototype and performing a total of 27 upper body postures. Nearly a complete recognition rate of 97% was achieved when the classification was adapted to the individual participants.

In order to answer theoretical aspects like the robustness of a system detecting the body posture by measuring the strain in a garment and to find an optimal sensor positioning, a model of the garment was developed. An already published simulation method, which was developed to simulate loose fitting clothing, was adapted to be used for tight-fitting garments. The simulation results matched to a large extent the strain patterns measured with the reference method.

Based on the simulation results, the sensor positioning was optimized using Mutual Information Feature Selection and a Genetic Algorithm. A small and a large sensor set (5 and 20 best sensor positions respectively) were defined for further analysis.

¹interdisciplinary research and services institution for material sciences and technology development within the ETH Domain

Using these two sensor sets, a sensitivity analysis was performed showing that

- An exact sensor positioning is not crucial. A shift of up to 11cm from the optimal sensor position decreased the recognition rate of the different body postures by less than 3%.
- Recognizing different body postures using a strain sensitive garment worked for different body proportions. The abdominal girth was varied between 86cm and 111cm .
- The number of sensors should not be minimized. A sensor set of 20 sensors showed advantages over using 5 sensors when a sensor fails and when the garment shifts at the waist level.
- A shift of the shirt at waist level caused the biggest drop in the recognition rate (up to 30% for a shift of 3cm). Therefore, the strain sensitive shirt should be fixed at waist level ensuring that it moves less than 1cm .

Zusammenfassung

In dieser Dissertation werden verschiedene Aspekte eines dehnungssensitiven Kleidungsstücks zur Messung der Oberkörperhaltung präsentiert.

Es wurde eine Referenzmessmethode entwickelt, mit der die Dehnungsverteilungen im Textil bei verschiedenen Körperhaltungen gemessen werden konnten. Diese Methode basierte auf der Messung mit einem optisches Trackingsystem. Damit konnte die Machbarkeit einer Haltungsmessung mit Dehnungssensoren gezeigt werden. Zusätzlich wurden Anforderungen an einen textilen Dehnungssensor definiert.

In Zusammenarbeit mit der EMPA² wurde ein Dehnungssensor entwickelt, welcher aus je 50wt-% thermoplastischem Elastomer und Ruspartikeln besteht. Der Sensor zeichnet sich durch eine hohe Linearität, eine kleine Hysterese und eine geringe Abhängigkeit von der Dehngeschwindigkeit aus. Dies führte zu einem Fehler von 5.5% bei einem Arbeitsbereich von 70%.

Es wurde ein Prototyp aus einem 'Catsuit' (einteiliges, enganliegendes Kleidungsstück) und der Sensorfaser gebaut. Daraufhin wurde eine Studie mit acht Teilnehmern durchgeführt, welche mit dem dehnungssensitiven Kleidungsstück 27 verschiedene Oberkörperhaltungen einnahmen. Es wurde eine fast perfekte Erkennungsrate von 97% erreicht, wenn die Klassifikation an jeden einzelnen Teilnehmer angepasst wurde.

Um theoretische Aspekte wie die Robustheit einer Haltungsmessung mit textil integrierten Dehnungssensoren zu betrachten, aber auch um eine optimale Sensorplatzierung zu finden, wurde ein Kleider-Modell implementiert. Eine für lose sitzende Kleidung publizierte Methode wurde angepasst, um sie für enganliegende Kleider verwenden zu können. Die Simulationsergebnisse stimmten weitgehend mit den Dehnungsverteilungen aus der Referenzmethode überein.

Basierend auf den Simulationsergebnissen wurde die Sensorpositionierung mittels "Mutual Information Feature Selection" und eines Genetischen Algorithmus optimiert. Für weitere Analysen wurde ein klei-

²interdisziplinäre Forschungs- und Dienstleistungsinstitution für Materialwissenschaften und Technologieentwicklung innerhalb des ETH-Bereichs

nes und ein grosses Sensorset (bestehend aus den 5 und den 20 besten Sensorpositionen) definiert.

Mit diesen beiden Sensorsets wurden Sensitivitäts-Analysen durchgeführt, die Folgendes zeigten:

- Eine exakte Sensorpositionierung ist nicht entscheidend für eine gute Haltungserkennung. Eine Abweichung um bis zu 11 Zentimeter von der optimalen Sensorposition reduzierte die Erkennungsrate verschiedener Körperhaltungen um weniger als 3%.
- Eine Haltungserkennung mit einem dehnungssensitiven Kleidungsstück funktionierte für Körperproportionen mit einem Bauchumfang zwischen 86cm und 111cm .
- Das Sensorset sollte nicht minimiert werden. Wenn ein Sensor ausfällt oder wenn das Kleidungsstück rutscht wurden mit 20 Sensoren bessere Resultate erzielt als mit 5 Sensoren.
- Ein Hochrutschen des Kleidungsstücks in der Taille verursachte den grössten Abfall der Erkennungsrate (bis zu 30% bei einem Verrutschen von 3cm). Deshalb sollte das Kleidungsstück an der Hüfte oder Taille fixiert sein, so dass es weniger als 1cm rutscht.

1

Introduction

In this Chapter, the research objectives of this dissertation are summarized.

Furthermore, an overview of different body posture and movement measurement systems is given. In recent time, portable systems emerged enabling new applications which are summarized in this Chapter.

Research is heading towards integrating measurement systems into the clothing which has some major advantages concerning comfort. A state-of-the-art of approaches to combine electronics and textiles is given. The Chapter finishes with an outline of the thesis.

1.1. Research Objectives

The goal of this thesis is to build and validate a measurement system to recognize body postures. This is realized by measuring strain in a tight fitting garment. With **tight fitting clothing** we assume a garment which has in all directions a certain pre-stretch when the wearer is in a normal, upright posture. When the wearer moves, the strain in the garment changes. By measuring this changing strain, the system can conclude back on the wearer's posture.

In this thesis, different aspects of a strain sensitive garment recognizing body postures are covered. The work includes the following contributions towards the goal of a textile body posture measurement system:

- *Reference measurement method:* Using a reference method to accurately measure strain patterns in the clothing, basic questions can be answered: How much is the garment stretched while worn? Do the strain patterns differ for different body postures?
- *Strain Sensor:* What are the sensor requirements for measuring strain in textiles? Can a suitable strain sensor be found to measure strain in the textile and what are the electrical properties of this sensor (characterization)?
- *Prototype:* Is it possible to build a prototype with the strain sensor? Can this prototype be used and how well can static postures be detected?
- *Sensor positioning optimization:* Where on the garment should the sensors be placed to achieve high recognition rates?
- *Sensitivity analyses/ robustness of system:* What happens if the sensors are placed imprecisely, one of the sensors fails, or the shirt moves? Does the method of recognizing the body posture with a strain sensitive garment still work for a person with different body proportions?

In the next two Sections, a state-of-the-art of aspects related to the present work is given. 1) In Section 1.2, different approaches of body posture and movement measurement systems are presented. There exist stationary measurement systems which are used in sports and rehabilitation. In recent times, however, portable systems emerged enabling

measurements independent of time and place. 2) As "portable" does not necessarily mean that the system is comfortable, there is a trend to integrate electronics into the clothing. This enables an unobtrusive measurement of user-related parameters while not interfering with the user. In Section 1.3, approaches how to combine electronics and textiles are presented.

1.2. Body Posture and Movement Measurement Systems

In the past, body posture¹ and movement² measurement (BPMM) was limited - either in the number of joints to be measured or in the location of the experiment:

- *Goniometers* measure the angle between two adjacent body segments [62]. Therefore, they allow joint measurements. However, capturing the whole body by measuring single joints is difficult to achieve. Also complex joints like the shoulder can hardly be measured by goniometers. Goniometers found their main application in clinical joint measurements.
- There are different types of *three-dimensional motion tracking systems*: optical (infrared), ultrasonic, and electromagnetic systems. They all have in common that they measure the three-dimensional position of markers placed on the body. From these marker positions, the body posture and movement can be reconstructed. The systems are accurate up to $1mm$, however, the setup is stationary meaning that the location of an experiment is restricted to a few square-meters. Motion tracking systems are mainly used in clinical applications (gait analysis), professional sports training, and in the movie and game industry (animation).

In recent time, new systems emerged which are portable and, therefore, not restricted to a single location. This opens the possibility of longtime measurements which enables new applications in different fields:

- **Rehabilitation:** Stroke patients with a paresis should get intensive exercise therapy [98]. If they do additional exercising, the

¹static

²dynamic

positive effect might even be improved. However, home rehabilitation is often self-directed with little professional feedback [87]. A portable BPMM system could measure the quality and quantity of exercise conduction and give a feedback to the patient. Furthermore, the therapist would get an independent feedback on the progress and performance of the patient.

- **Prevention:** Back pain is a widespread disease in developed countries causing costs of more than \$100 billion per year only in the United States [54]. For prevention, physical exercise is recommended [22]. A portable BPMM system could detect long periods of immobile sitting or standing. It could also report the total physical activity during the day and, therefore, help preventing back pain.
- **Sports:** During sports training, a portable BPMM system could give feedback about the duration, intensity, optimality and dynamics of exercise conduction. This could help the user improving and optimizing his or her workout (sports diary). Such a system would not be restricted to professional training but could also be an interesting system for hobby athletes.

Portable BPMM systems are based on different kind of sensors.

- *Accelerometers:* Hansson et al. [49] used accelerometers to measure joint angles. In [100] (Van Laerhoven et al.) and [68] (Martin et al.) the accelerometers were attached to pants to detect activities like walking and running. More recent, the influence of a loose fitting textile on the classification result was investigated in [50].

In the static case, accelerometers measure the gravitational acceleration. This enables the reconstruction of the orientation of 3-axes accelerometers with an accuracy of about 1 degree [50]. Therefore, static body postures can be measured accurately by attaching accelerometers to the body segments. However, in dynamic measurements, an inertial acceleration is measured additionally to the gravitation preventing an exact reconstruction of the orientation. Therefore, accelerometers were combined with gyroscopes and magnetometers. One example is the Moven system [5] where 18 "Attitude and Heading Reference Systems" (AHRS) modules were combined to capture whole body move-

ments. AHRS have an accuracy of better than 1 degree but are several cubic centimeters in size.

- *Piezoelectric film sensors:* In [35] a glove was realized using piezoelectric film sensors. The sensors were placed on the fingertips, on the mid-finger joints and on the exterior side of the index finger. The goal of this project was to replace a keyboard by the glove. Piezoelectric film sensors have the advantage of being thin and flexible, however, they react to several stimuli (pressure, bending) complicating the interpretation of a signal change.
- *Pressure sensors:* Dunne et al. [33] measured shoulder and neck movements with a textile piezo-resistive pressure sensor (polypyrrole-coated polyurethane foam). The sensor registered the pressure between skin and clothing. With this method they could recognize maximal shoulder movements, however, no test was performed to detect the foam reaction to shoulder movements of varying magnitudes.
- *Bending sensors:*
 - Toney et al. [97] used air-filled tubes in combination with conventional pressure sensors to measure finger joint angles. The tubes were mounted along the fingers. When the fingers were bent, the volume of the cylindrical tube changed and caused a signal change in the pressure sensor. With this setup, an accuracy of about 3 degrees was achieved.
 - A second approach is based on fiber-optic sensors. These sensors measure the amount of light passing the optical fiber which is proportional to the bend in the fiber. Fiber-optic sensors were used in a pressure suit [14] and to measure the seated spinal posture [32, 34].
- *Ultrasound:* SonoSens® (friendly sensors) is a commercially available system measuring the posture of the spine based on ultrasound distance measurements on the skin [3]. Pairs of sensors are directly attached to the skin measuring the distance between the sensors during movements.
- *Strain gauges:* Measuring upper limb movements with strain gauges was published in [39] by using knit strain sensors and in [45, 95] by using a conductive elastomer. In [44] a textile potentiometer was built to measure strain caused by joint movements.

1.3. Approaches to Combine Electronics and Textiles

Integrating measurement systems into the clothing has some major advantages over carrying such systems: clothing is personal, comfortable, close to the body, and worn almost anywhere and anytime. Additionally, clothing provides a large surface which can be used for sensing, actuating and integrating processing power.

Textile integrated technology still is in its very beginning. In the following, a brief state-of-the-art is given. The technologies are grouped into the categories conductive fibers, electronic devices, and sensors and actuators.

1.3.1. Conductive Fibers

For a textile interconnection of electronic devices or to connect sensors and actuators, conductive fibers are used. There are different products using a number of different materials. The products can be grouped into three main approaches:

1. Thin conductive wires (diameter of several micrometers) are combined to a multifilament to obtain a stable fiber (e.g. Bekaert [9] or Aracon by Micro-Coax [10]). These fibers typically do not quite have the textile feel, however, they have a good conductivity in comparison to other conductive fibers (dependent on the conductive material and its diameter, e.g. Bekinox®VN/HT: $5 - 15 \frac{\Omega}{m}$).
2. A polymer thread is coated with a conductive material (e.g. Statex [12]). Often silver is used as it is eudermic and does not corrode. These fibers have textile properties with a decreased conductivity (e.g. SHIELDDEX 235f34dtex 2 ply HC: $120 \frac{\Omega}{m}$).
3. Thin conductive wires are combined with a textile fibre - either by loosely combining them (e.g Ohmatex [11]) or by tightly enwind the textile fibre with the wire (e.g. Zimmermann/ novonic [8]).

These products can be used like conventional threads and integrated into the textile by traditional textile technologies like weaving, knitting, sewing, or embroidering.

All of the above listed products are non-elastic. There exist only few elastic conductive fibers (e.g. Zimmermann/novonic [8] and Ohmatex [11]) whereas both examples use approach 3. of the list above: They combine conductive wires with an elastic textile fiber. As the conductive

wire is non-elastic, it is attached in a way that the elasticity of the textile fiber remains.

1.3.2. Electronic Devices

There are only few approaches where electronic devices were integrated into the textile. They can be split into the three following main approaches:

- *Electronic devices with textile properties:* Electronics which is innately rigid is adapted to become textile properties like stretchable, drapeable, and soft. Some first approaches were presented in [48, 66] where textile transistors and other logical components are described. Using such textile logical components would enable to really integrate a circuit inside the textile.
- *Attach conventional electronics to the textile:* Electronic devices can be attached either as whole printed circuit board (PCB) as in [50, 60] where small conventional PCB's were attached or in [61, 81] where flexible PCB's were used. Another approach is to attach single components as in [64] where interposers were used to overcome the different pitches of the textile and the component.
- *Integrate electronics into textile accessories:* Instead of attaching the electronics to the textile, fashionable textile accessory can be used for "hiding" the electronics. In [86], the electronics was integrated into a button.

1.3.3. Sensors and Actuators

Several research projects aim for integrating sensors and actuators into textiles. A brief overview is given in the following table. For functionalities not listed in the table, conventional sensors and actuators have to be used and attached to the clothing where the comfort of the user is not affected.

<i>Pressure</i>	Two conductive layers were separated by a spacer foam to build a textile capacitance [74]. Conductive polypyrrole (PPy) coated polyurethane (PU) foam was used in [33].
-----------------	---

<i>Button</i>	SOFTswitch [13] has presented a keypad of conductive fabrics with a thin layer of elasto resistive composite that reduces its electric resistance when compressed [79].
<i>Strain</i>	Textile strain sensors were based on an elastomer filled with conductive particles (e.g. carbon black) [71, 95]. In [44] a textile potentiometer was presented.
<i>Temperature</i>	A textile temperature sensor was realized in [64] by measuring the resistance change in a copper wire ($R_{wire} = R_0(1 + \alpha_{metal} \cdot \Delta T)$).
<i>Electrodes</i>	Textile electrodes were realized by embroidering [57], weaving [31, 85], or knitting [80, 85] a conductive thread.
<i>Display</i>	Textile displays can be realized using an electroluminescent paste [76]. This paste is illuminated by applying a high-frequency voltage.
<i>Heating</i>	When applying a current to a textile conductive thread, the textile is heated according to $P = U \cdot I$. Companies selling heating textiles are e.g. novonic [8] and SOFTswitch [13].
<i>Cooling</i>	EMPA has developed a cooling vest based on aquatic evaporation [75].

1.4. Outline

Chapter 2 describes a reference measurement method to measure strain in the textile. This method was used to gain insight where and by how much clothing is stretched during different body postures. It was also used to define requirements for the textile strain sensor.

In Chapter 3, a textile strain sensor is presented which was developed in collaboration with EMPA. Furthermore, the sensor properties are discussed.

Using the strain sensor described in Chapter 3, a prototype setup was built. With this prototype, an experiment was performed showing that 27 upper body postures can be recognized almost perfectly when a user-specific training is used. This is shown in Chapter 4.

Chapter 5 presents a model that can be used to calculate the strain in an elastic, tight fitting clothing. This model was used to optimize the sensor positions using a Mutual Information Feature Selection method and a Genetic Algorithm. This optimization is described in Chapter 6.

In Chapter 7, different sensitivity analyses were performed like e.g. the robustness of the sensor placement and an upwards shift of the clothing at the waistline.

The dissertation finishes with conclusions in Chapter 8.

2

Reference Measurement Method*

In this Chapter a reference method to measure strain in textiles is presented. This enables an accurate determination of how and by how much clothing is stretched at different body postures. The method is based on measuring marker positions by using an optical tracking system. Recommendations on the markers and camera setup are given. The accuracy of the method and some general results on the measured strain patterns are presented.

*based on [72]

2.1. Introduction

As introduced in Chapter 1, the goal of this thesis was to build a prototype which can recognize upper body postures by measuring strain in the textile. However, so far it was not clear, where and how much strain appears during different body postures. Therefore, a reference method to measure strain in a textile was developed and is presented in this Chapter.

In the first part of this Chapter, the reference measurement method is described. As we focused on measuring the upper body posture, the method is presented exemplarily for measuring textile strain in the back region of a person. However, the method can also be used for other materials on other body regions and is not restricted to measuring textiles on the back (The same method was later used to measure the skin deformation in [82]). The output of the method is the measured strain pattern. In the second part of this Chapter, example strain patterns of three postures are shown.

2.2. Method

2.2.1. Choice of Measurement System

For measuring the strain pattern in a garment, a motion tracking system was utilized. These systems measure the three-dimensional position of markers. Usually, such systems are used for gait analysis [19, 42, 51] or for animating human models [18, 67] by measuring the skeleton movement with markers placed on the skin or the garment. In the presented method, the markers were attached to a garment. By looking at the varying distance between two markers, the strain in the garment was calculated.

There exist different motion tracking systems [108] (optical, magnetic, and ultrasonic). An optical system (VICON 370 [6]) was chosen for the following reasons:

- Optical tracking systems use several infrared (IR) cameras to measure the three-dimensional position of reflective markers. Reflective markers are passive elements (cable free). This has the advantage that more markers can be used than in active systems (magnetic, ultrasonic) which results in a better resolution of the final strain pattern. In theory, the number of passive markers is not restricted, however, in practice it is limited by the resolvable-

ness of the system and the reconstruction algorithm.

- The system can be used with markers as small as several millimeters. This is an advantage when placing many markers. Furthermore, very small and light markers do not influence the strain pattern in the textile in contrast to bigger markers or active elements.
- Amongst the different 3D motion tracking methods, the optical (IR) is the most accurate one. It has an accuracy of up to 1mm [36].

A disadvantage of the optical system is occlusion, which means that markers can be covered for example by an arm preventing the recording of this marker. The location data of the occluded marker is lost. However, occlusion can be minimized by an optimal arrangement of the cameras.

2.2.2. Measurement Setup

Optical motion tracking systems use a variable number of (at least two) infrared, stroboscopic cameras and passive, reflective markers. In a darkened room, the emitted IR-light is reflected by the markers, so that the cameras record only the markers, minimizing the necessary image processing. By knowing the exact position of the cameras, it is possible to reconstruct by triangulation the location of each marker that was detected by at least two cameras (see Fig. 2.1).

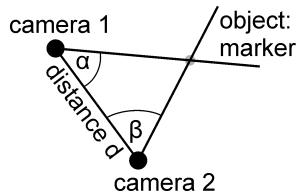


Figure 2.1. The marker location can be reconstructed by knowing the distance d between the cameras and the angles α and β (triangulation).

In the present work, the focus was on upper body postures. As strain was only expected on the back and the sides of the body, the cameras were arranged behind the subject to minimize occlusion. A VICON 370 system [6] with 5 cameras was used and it was set up in the configuration shown in Fig. 2.2. One camera was positioned in

the middle, at a height of 155cm and a distance of 150cm . This was a trade-off between the resolution (the resolution decreases with the distance) and still covering a large area (also while bending forward). The remaining four cameras were placed symmetrically on the sides, as far apart from each other as possible (80cm , 15cm respectively) minimizing the triangulation error.

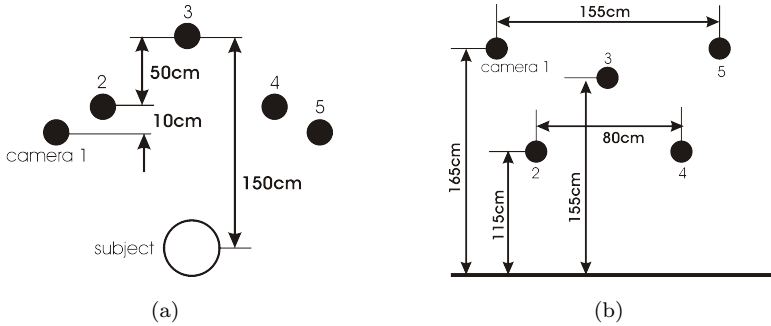


Figure 2.2. Arrangement of the cameras. Fig. 2.2(a): front view; Fig. 2.2(b): top view.

2.2.3. Type of Markers

Usually, reflective spheres are used as markers with the reconstructed marker location corresponding to the sphere center. However, using spheres might not be preferable when measuring strain in a plane as this results in a constant offset of the reconstructed location (see Fig. 2.3). This offset can produce an error which is dependent on the bending of the back. In contrast, the reconstruction point of flat markers lies in the plane of the back such that the marker position can directly be used for the calculation of strain.

In order to verify whether the same accuracy can be achieved with a flat marker as with a sphere (independent on the bending error), the accuracy of the markers shown in Fig. 2.4 was compared. The markers shown in Figs. 2.4(a) and 2.4(b) are commercially available [4] and are used for facial tracking. The marker in Fig. 2.4(c) was self-made by cutting circles out of a self-adhesive reflective material

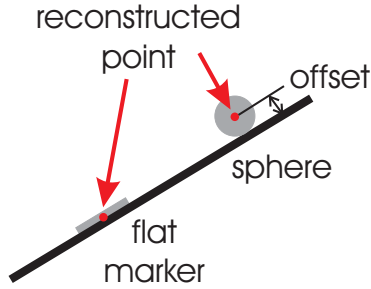


Figure 2.3. The offset is shown which results by using 3D markers.

(3MTM ScotchliteTM High Gain Reflective Sheeting 7610). The markers had a diameter between 3mm and 6.5mm.

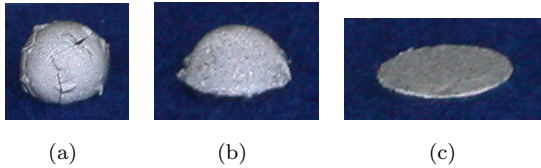


Figure 2.4. Different marker shapes which were compared: $\frac{3}{4}$ -sphere (Fig. 2.4(a)), hemisphere (Fig. 2.4(b)), circle (flat) (Fig. 2.4(c)).

The markers were placed in rows on a cardboard with a spacing s of 5cm. Several measurements were carried out, varying the orientation of the cardboard (no bending of the cardboard). The results showed that the measured distance between the markers varied at the most 0.6mm ($\max(s_i) - \min(s_i)$ with s_i being the spacing at sample i). This means that the accuracy was better than 1mm (error of less than 2% for a marker distance of 5cm). This is in accordance to the literature ([36]: VICON 370 mean abs. error of 0.94mm). No difference in the accuracy and the reconstruction rate was observed between the different markers. Therefore, a 6mm circular marker was chosen for the measurements (Fig. 2.4(c)).

2.2.4. Garment and Marker Placement

For the tight-fitting garment, a custom-made catsuit was used. It was adapted to the subject so that it was pre-stretched by about 10% in the normal upright posture. The textile used was elastic in both directions (course and wale, meandering path and sequence of stitching in knitting) and consisted of 95% viscose and 5% elasthan.

The markers were arranged in the back region of the garment in a grid with a spacing of 5cm (see Fig. 2.5). This resulted in 89 markers.

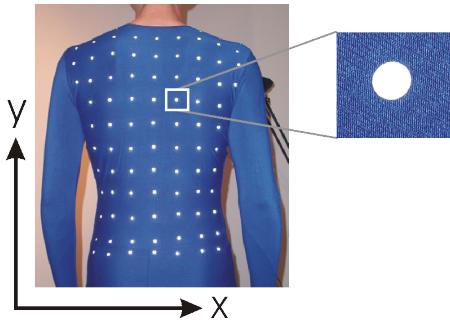


Figure 2.5. Photograph of the marker arrangement.

2.2.5. Experiment

An experiment to measure the strain pattern at different body postures was conducted with one subject (male, 26 years, body height 190cm, chest circumference 102cm, weight 80kg). The person was sitting on a chair without backrest during the whole experiment. A measurement cycle always started in the upright posture (see Fig. 2.6). This was at the same time the reference posture for the strain pattern calculation.

For each posture, a measurement cycle was performed. The subject started in the upright posture and moved to a certain posture. In this posture, he stayed for some seconds and moved back to the upright posture. This was repeated three times. The measured postures are listed in Table 2.1.

2.2.6. Post Processing

The output of the VICON motion tracking system was a stream (50Hz) of the marker positions [2]. From this data, the strain pattern be-



Figure 2.6. Reference posture (upright sitting).

Table 2.1. Sitting upper body postures measured with the reference method.

Sitting Postures	
<i>Rotation of trunk</i>	to the right to the left
<i>Bending trunk sideways</i>	to the right to the left
<i>Lifting shoulders</i>	both shoulders
<i>Slumped</i>	shoulders over hip
<i>Bending trunk forward</i>	bending (keeping arms along trunk) bending (arms down) strong bending (arms along trunk)
<i>Arm postures</i>	arms to the front arms to the sides arms overhead

tween two postures (with the upright posture being the reference (see Fig. 2.6)) was calculated according to the three following steps:

1. In a first step, 10 time frames of the reference and the posture to be compared were chosen. The frames were chosen at a point of time when the measured person did not move (verified by visualizing the marker positions). By averaging each marker position

over these frames ($\frac{1}{10} \sum_{i=1}^{10} p_i$), measurement inaccuracies were reduced resulting in an accuracy of the marker distance of about $0.5mm$.

2. In both postures, the distance of each marker to all neighbouring markers was measured. These distances were defined as $d_{reference}$ in the reference posture and $d_{posture}$ in the posture to be compared. The relative change between these two distances and, therefore, the strain was calculated by:

$$strain = \frac{d_{posture} - d_{reference}}{d_{reference}} \cdot 100[\%]. \quad (2.1)$$

3. This calculation was done in horizontal, vertical, and both diagonal directions separately.

2.3. Results

During the whole experiment, on average 94% of the markers were reconstructed. Therefore, only about 6% of the markers were occluded. At these positions, no strain could be calculated. However, by selecting time frames with minimal occlusion, this was not an issue: For most postures, time frames with zero to three occluded markers were selected (97% to 100% reconstruction rate) except for the bending forward postures where more markers were occluded.

In the experiment described in Section 2.2.5, measurements of different sitting postures were performed. The subject adopted the sitting posture for several seconds and straightened then up, back to the upright posture. In the following, three examples of these measurements are discussed, namely lifting the shoulders, bending the back and moving the arms forward. The results of the other postures are attached in Appendix A.

In all charts in Figs. 2.7 to 2.9, the color range covers strain values from -20% (dark blue) to $+20\%$ (dark red). Zero strain is shown in green. The asymmetric outer shape of the strain pattern in Figs. 2.8 and 2.9 is due to a missing marker so that no strain could be calculated at this position. As mentioned in Section 2.2.6, the strain was calculated separately in the horizontal and vertical direction. In order to get a better resolution, the $5cm$ -grid was linearly interpolated resulting in a grid of $1cm$.

When lifting the shoulders (see Fig. 2.7), no significant strain was measured in horizontal direction in the lower back (Fig. 2.7(b)) whereas

in the upper back, there was a negative strain of up to -20% . This seems reasonable as lifting the shoulders anatomically moves them together while the lower back stays at about the same width. In vertical direction (Fig. 2.7(c)), the measured strain was up to 11% on the sides, which is caused by a prolongation of the side of the body when lifting the shoulders.

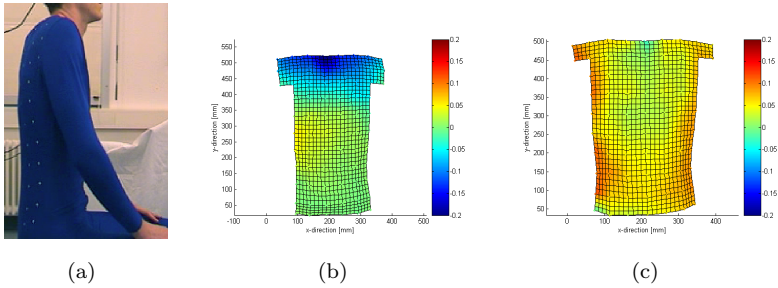


Figure 2.7. Measured strain pattern (in [%]) in the back side of the garment while lifting the shoulders. For a smoother pattern, the strain values were linearly interpolated. Fig. 2.7(a): measured posture; Fig. 2.7(b): strain in horizontal direction; Fig. 2.7(c): strain in vertical direction.

For the bending posture (Fig. 2.8), a strain of up to 17% in the lower back in vertical direction (Fig. 2.8(c)) was observed. In horizontal direction (Fig. 2.8(b)) we encountered strain in the upper back for

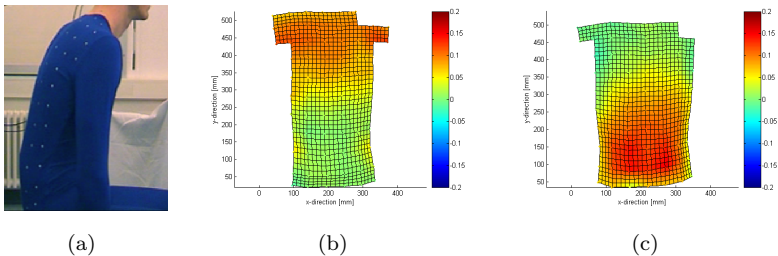


Figure 2.8. Measured strain pattern (in [%]) in the back side of the garment while bending forward. For a smoother pattern, the strain values were linearly interpolated. Fig. 2.8(a): measured posture; Fig. 2.8(b): strain in horizontal direction; Fig. 2.8(c): strain in vertical direction.

which not only the change in the back position was responsible but also a shoulder movement. The shoulders and also the arms moved forward when the back was bent. When comparing Fig. 2.6 to Fig. 2.8(a), this arm and shoulder movement while bending the upper part of the body can be registered.

To verify that the strain in the upper back in Fig. 2.8(b) was caused by an arm and shoulder movement, the posture of holding the arms to the front was captured. As expected, it can be seen in Fig. 2.9 that the arms provoke a strain in the upper back region. Strain of 15% to 20% was measured in the upper back in horizontal direction (Fig. 2.9(b)). In vertical direction (Fig. 2.9(c)), a strain of about 7% was measured in the lower back.

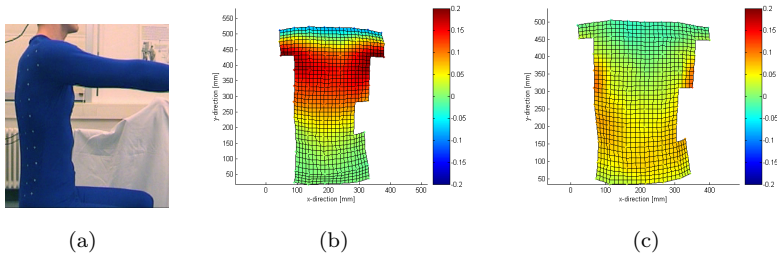


Figure 2.9. Measured strain pattern (in [%]) in the back side of the garment while moving the arms forward. For a smoother pattern, the strain values were linearly interpolated. Fig. 2.9(a): measured posture; Fig. 2.9(b): strain in horizontal direction; Fig. 2.9(c): strain in vertical direction.

2.4. Discussion and Conclusions

A method to measure strain patterns in garments during different body postures was presented. The method was based on measurements using an optical motion tracking system. Reflective markers were attached to a garment in a rectangular grid of 5cm . When moving the body, the markers shift relative to each other. From this shift, the strain was computed using Equation 2.1.

For the markers, 6mm circles of reflective adhesive tape were chosen. Compared to sphere markers, flat markers have the advantage that the reconstructed point lies in the plane of the garment such that a

direct calculation of the strain was possible. The precision of the marker distance when using the $6mm$ circle markers was better than $1mm$. With a marker distance of $5cm$, the achieved accuracy of the strain patterns was better than 2% ($\frac{1mm}{50mm} = 0.02$).

During the experiment, 94% of the markers were reconstructed (5 cameras were used). This could be improved by using more cameras. The cameras should be arranged such that marker occlusion is minimized during the whole experiment.

Several measurements were performed with a single subject. Thereby, we concentrated on the back region while the person took different sitting postures. Based on these measurements, the following points were identified:

- In the back region of the garment, strains of up to 20% were measured.
- For the measured postures, distinct strain patterns were identified indicating the feasibility of a body posture measurement using textile integrated strain sensors. As a generalization, the following correlations between movements and strain in the garment can be given (see Fig. 2.10):

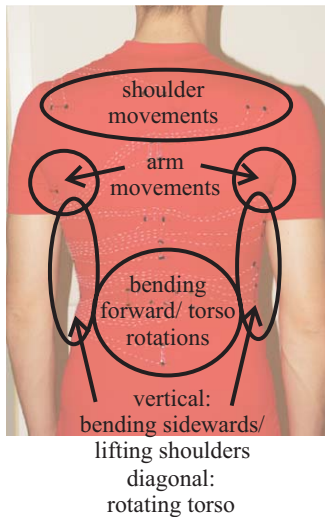


Figure 2.10. Regions of strain for characteristic movements.

- The region in the upper back is stretched in horizontal direction when the shoulders move forward.
- Arm movements cause mainly strain in the armpit region.
- Bending forward causes strain in vertical direction, mainly in the lower back region.
- Strain in diagonal direction on the back and the side of the torso is measured when rotating the torso.
- Bending sideways and lifting the shoulders causes strain on the side of the torso in vertical direction.

3

Textile Strain Sensor*

This Chapter focuses on a novel carbon filled elastomer sensor which was developed in collaboration with EMPA. After presenting the sensor material and its attachment to the textile, the properties of the sensor thread are addressed. Beside the relaxation behaviour, hysteresis, and ageing effects, the properties after several washing cycles are also discussed.

*based on [71]

3.1. Introduction

As shown in the last Chapter 2, measuring strain in a textile requires a strain sensor with a measurement range of at least 20%¹. Therefore, commercially available strain gauges based on a metallic foil pattern (typical measurement range of 1% strain) cannot be used and new technologies need to be developed.

Beside a suitable electric characteristic like e.g. linearity and stability, some additional properties are required for a sensor measuring strain in a textile:

- The measurement range of the sensor must be at least 20% strain plus a certain pre-stretch of the textile.
- The sensor must have textile stress properties. This means that the force needed to stretch the sensor must be in the same range as the counter-force of the fabric. To have a convenient wearing comfort, force in the textile should not exceed 2N measured in a 5cm band [56].
- It is important that the sensor property is not influenced by bending.
- The sensor should be washable.

In this Chapter, a carbon black filled elastomer sensor which was developed in collaboration with EMPA, Switzerland is presented. The sensor material and its attachment to the textile are described. This is followed by an electrical characterization of the sensor.

3.1.1. Related Work

Measuring strain in textile is addressed by different research groups. Farrington et al. [39] built a knitted strain sensor which was integrated into a jacket and was used to measure upper body movements. Gibbs et al. designed a textile potentiometer to measure joint movements [44]. In [63] a thin layer of polypyrrole (using chemical vapor deposition) was applied on the fabric substrate at low temperature (-26°C). With this configuration, a measurement range of up to 50% strain and a gauge factor ($\frac{\Delta R \cdot l_0}{R_0 \cdot \Delta l}$, l_0 and R_0 are the initial length and resistivity respectively, Δl and ΔR the change in length and resistivity) of 80

¹Throughout this thesis, strain is defined as $strain = \frac{l-l_0}{l_0} \cdot 100[\%]$, where l is the current length and l_0 the initial length of the sensor.

was achieved. Das et al. investigated ethylene-vinyl acetate (EVA) and ethylene-propylenediene rubber (EPDM) composites for sensor applications [30]. Such carbon composite materials show high dependance on the strain rate: When doubling the strain rate, the resistivity was also doubled at the maximal measured strain of 30%. An elastomer/carbon black-composite (CE) was used by Tognetti et al. to measure arm and finger movements. This sensor showed an overshooting of 30% in the resistivity and a relaxation time of several minutes [65, 95, 96].

When using thermoplastic elastomer (TPE) based composites, no curing is necessary (unlike e.g. CE). Therefore, such polymers are interesting when developing strain sensors [26, 27, 70, 93]. In [27], Cochrane et al. presented a sensor of a thermoplastic elastomer filled with carbon black (27.6vol-%). They focused on noncyclic strain sensing and looked at influences of temperature and humidity on the resistance. The sensor showed a dependance of the resistance on the humidity (up to 40% in resistance) but not on the temperature (less than 10% up to a relative humidity of 70%). In this dissertation a similar composition (50wt-%/32vol-% carbon black) was used. However, the focus was on the characterization of the sensor's dynamic behaviour, as sensors integrated into textiles are exposed to repeated strain cycles.

3.2. Sensor Design

3.2.1. Sensor Material and Manufacturing

For the development of the strain sensitive conductive fiber, EMPA used a mixture of a TPE (thermoplastic elastomer) and carbon black particles. No curing is necessary when using TPE based composites and thermoplastic processing technology can be used for shaping. The TPE material was SEBS-Block copolymer THERMOLAST K® (FD-Series), Compound No. TF7-ATL produced by KRAIBURG TPE GmbH, Germany. The carbon black powder was ENSACO 250 produced by TIMCAL, Belgium. The density of the TPE was $0.89 \frac{g}{cm^3}$ and $1.8 \pm 0.2 \frac{g}{cm^3}$ of the carbon black powder. The primary particle size and the specific surface area of the carbon black powder were $54nm$ and $65 \pm 5 \frac{m^2}{g}$ respectively.

For the fibre manufacturing, TPE pellets were filled in an electrically heated torque rheometer (Rheomix 600, Fisher Scientific, Germany) with roller blade configuration. After melting the thermoplastic part of the TPE, carbon black powder was added and subsequently

homogenized and dispersed into the polymer during 1 hour at 180°C. The rotation speed was constant (10rpm) during the whole procedure.

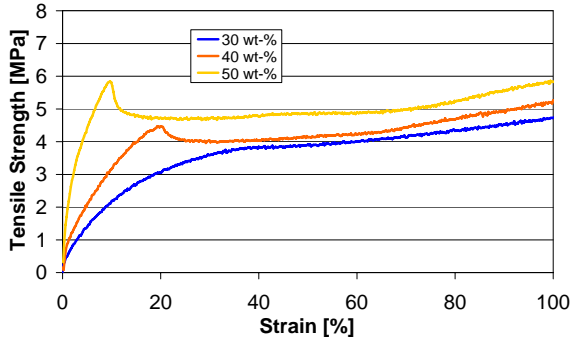
After compounding, the fibre was produced by using a capillary rheometer (Rosand RH 7, Malvern Instruments, Germany) and an extrusion die with an orifice of 300 μm in diameter. The composite material was preheated and -compacted in the cylinder of the rheometer for 2min and a pressure of 0.5MPa at 180°C before extruding with speed of 3.5mm/min. Because of die swelling, the fibre diameter increased to 315 μm .

In a previous investigation [92], different contents of carbon black were added to the TPE polymer to study the electromechanical properties of the fibres. Fig. 3.1 shows the influence of the carbon content on the mechanical (tensile strength) and the electrical (resistance) properties of the extruded fibre.

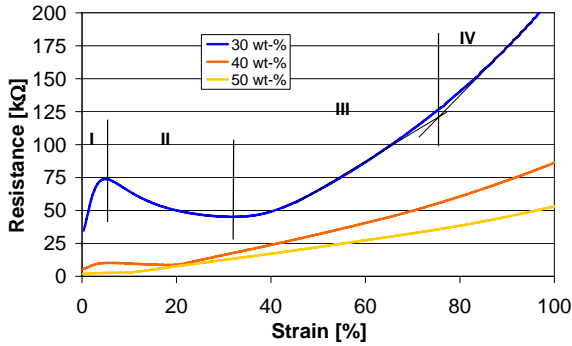
As expected, varying the content of carbon black in the compound influences the mechanical and electrical properties. Above a certain amount of carbon black (40wt-%), a yield point occurs in the mechanical stress strain curve of the sensor fibres (at 20% strain). The electrical behaviour of the fibre changes too. For low filling levels of carbon black (30wt-%) the resistivity curve can be separated into four sections as described by Flandin et al. - initiation (I), reversible (II), re-coverable damage (III) and depercolation (IV) [40]. As the same resistivity occurs at different strains in a range of 100% strain, the 30wt-% compound was not suited for our application. Fibres with a carbon black content around 40wt-% show a plateau in the electrical resistivity (10%) which changes to a continuous increase for higher filling levels (50wt-%). A further increasing of the filling level results in a brittle fibre which is unacceptable for sensor applications. Therefore, a 50wt-% composite (1.21 $\frac{\text{g}}{\text{cm}^3}$, 32vol-%) was used to produce the textile strain sensors in this study (see Fig. 3.2(a)). This filling level results in a resistance of approximately 700 Ω/cm at a sensor diameter of 315 μm .

3.2.2. Sensor Attachment to Textile

The sensor was designed to measure strain in textiles. Therefore, the sensor thread described in Section 3.2.1 (see Fig. 3.2(a)) needed to be integrated or attached to a textile before characterization. We realized this attachment with a silicone film (Dow Corning 732) (see Fig. 3.2(b)). Silicone was used for the following reasons:



(a)



(b)

Figure 3.1. Influence of the carbon black filler content on the mechanical (Fig. 3.1(a)) and the electrical (Fig. 3.1(b)) properties of the extruded fibre with a gauge length of 5cm . In Fig. 3.1(b), the four regions described by Flandin et al. [40] are shown for a filling level of 30wt-%.

- Silicone is very elastic (maximal strain of 540%, Dow Corning 732). Further advantageous properties of silicone can be found in [1].
- Silicone builds a good bonding to textiles: When removing, the silicone (tensile strength 333.6psi ($= 2.3\text{MPa}$), Dow Corning 732) tore before it detached from the textile. This means that the con-

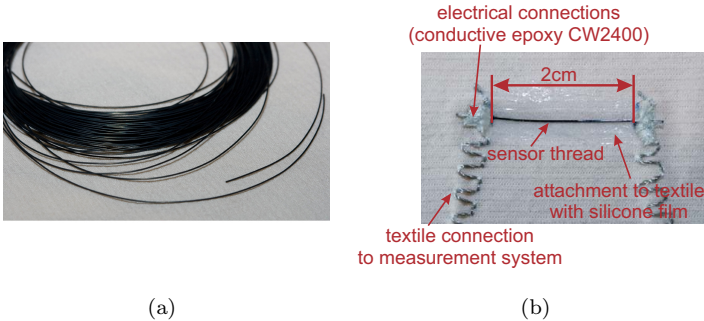


Figure 3.2. Fig. 3.2(a): Sensor thread after extrusion. Fig. 3.2(b): Sensor thread attached to the textile with a silicone film.

nection between the textile and the silicone could withstand more than 2.3MPa .

- When stretching the sensor material described in Section 3.2.1 alone, it experiences a permanent plastic deformation: The sensor lengthened by about 28% when a strain of 80% was applied and did not return to its original length. Therefore, the sensor material alone has a reduced working range of the applied stretch minus the permanent deformation ($\frac{1.8}{1.28} = 40.6\%$). However, when the sensor is attached to the textile using silicone, the sensor is forced back almost to its original length and, therefore, has a larger working range of more than 70% ($= \frac{1.8}{1.05}$, see Section 3.4.1).

For connecting the sensor to a measurement system, a *SHIELDEX*[®] yarn (235f34dtex 2-ply HC) was used. This nylon yarn is silver coated and has a resistivity of $120\Omega/m$. In order to keep the elasticity of the textile, the thread was sewn using an elastic stitch. For the connection between the sensor and the silver coated yarn, a conductive epoxy (CW2400, CHEMTRONICS CIRCUITWORKS) was used.

In Fig. 3.3 the assembling of the sensor is shown. It comprised the following steps:

1. In a first step, the sensor was temporarily attached to the textile using adhesive tape. Thereafter, the textile was attached to a cardboard with fixing pins under light tension in order to prevent shifting when using the conductive glue and to prevent the building of ripples when applying silicone.

2. The sensor was then connected to the conductive thread using conductive epoxy (see Fig. 3.3(a)). This step needed a drying period of 24 hours.
3. In a next step the sensor was attached to the textile with silicone using a palette-knife (see Fig. 3.3(b)). The silicone needed some hours to cure.
4. After having removed the adhesive tape and the fixing pins, the textile strain sensor was finished (see Fig. 3.3(c)).

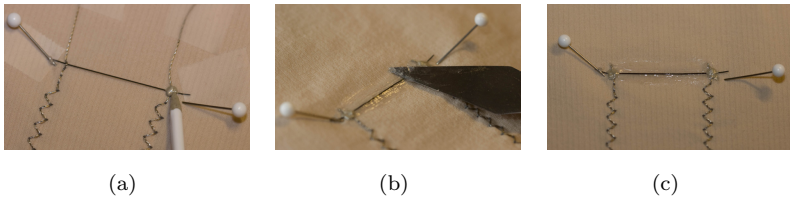


Figure 3.3. Assembling of the textile strain sensor. Fig. 3.3(a): Connecting the sensor to the conductive thread using conductive epoxy. Fig. 3.3(b): Attaching the sensor to the textile using silicone. Fig. 3.3(c): Sensor attached to the textile.

3.3. Measurement Setup

Several cyclic strain measurements (extension - retraction) were performed in order to characterize the sensor. For these measurements, the sensor thread was attached to the textile as described in Section 3.2.2. The sensor length was always 2cm . This is the same length as used in the prototype in Chapter 4.

The strain was applied to the sensor using a strain tester (Zwick/Roell DO-FB0.5TS). The resistance was measured in parallel with a multimeter HP34401. If not specified differently, the measurements were done at a speed of $200\text{mm}/\text{min}$ which corresponds to a strain rate of $16\%/sec$ (sensor length 2cm). The waiting times at maximal and minimal strain were 3sec .

The following measurements were taken. For each of these measurements, a different sensor was used.

increasing range The measurement range was slowly increased (steps of 10%) starting with a range of 10% up to a range of 100% strain. With this experiment, insight was gained on the influence of the measurement range on the sensor characteristics.

decreasing range Starting with applying a strain of 80%, the range was decreased in steps of 20%. This measurement should confirm that the characteristic curve (= strain-resistivity characteristics) only depends on the maximal strain applied and remains constant for arbitrary (smaller) strains.

varying speed The strain rate was varied between $50\text{mm}/\text{min}$ and $600\text{mm}/\text{min}$ (50, 100, 200, 400, and $600\text{mm}/\text{min}$). This measurement gave information about an influence of the strain rate on the sensor characteristics.

waiting times of 2 minutes The waiting times at maximal and minimal strain was increased to 2min in order to see the relaxation behaviour of the sensor.

long-term cycling (16 hours) The sensor was permanently cycled for 16 hours. This showed whether there is a change in the characteristics of the sensor while in permanent use.

long-term measurement (2 months) During two months, the characteristics of the sensor was measured once a week in order to find ageing effects of the sensor.

washing test The sensor was washed 8 times at 30°C in a washing machine using a conventional cleaning agent (no fabric softener). After each washing cycle, the characteristics of the sensor was measured. This trial shows whether the sensor endures this procedure and the properties change due to washing.

All measurements were done with the sensor attached to two different textiles (486 Meryl (88% PA, 12% lycra, knitted) and Keller AG 88018 (49% PA, 51% EL, woven)) which have different elasticities. The Meryl textile is about three times more elastic than the weave from Keller AG. However, the sensor characteristics were the same with both textiles so that the kind of textile is not considered in the following Sections.

3.4. Results and Discussion

In the following section, the textile integrated sensor thread is characterized. The following sensor properties were examined: relaxation behaviour, hysteresis, sensitivity, dependency on strain rate, longterm cycling, ageing, and washability. We did not look at influences by temperature and humidity as this is covered in [27] where a similar sensor was used. They found a dependance of the resistance on the humidity (up to 40% variance in resistivity) but not on the temperature. As our sensor is protected with a silicone film (so far only on one side, however, a thin layer of silicone could be put down on the fabric before attaching the sensor to protect it from both sides), we expect the influence of the humidity to be eliminated.

3.4.1. Relaxation Behaviour

In Fig. 3.4(a), the resistance over time is shown for a cycling strain. The upper plot depicts the applied strain. The sensor was cycled between 0% and 80% strain at a speed of $200\text{mm}/\text{min}$ and waiting times at minimal and maximal strain of 2 minutes. In the lower plot the measured resistance is shown which varied between $2\text{k}\Omega$ and $19\text{k}\Omega$ (for a sensor length of 2cm).

It is apparent that this sensor has a small relaxation: When the strain is kept constant at 80%, it relaxes by $1.5\text{k}\Omega$ (see Fig. 3.4(a))

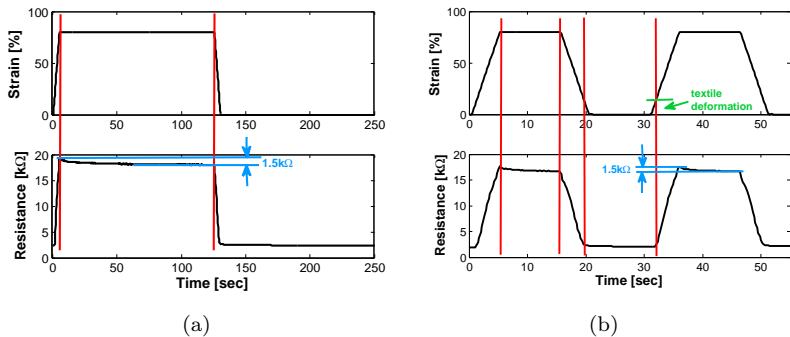


Figure 3.4. Response of sensor to a given strain (sensor length 2cm). Fig. 3.4(a): waiting time 2 minutes. Fig. 3.4(b): waiting time 10 seconds

while the total range is $17k\Omega$. This results in an inaccuracy of 8.8% caused by the relaxation.

For strains lower than 10% it can be seen in Fig. 3.4(b) that the resistance does not follow the applied strain. It stays at the resistance level which corresponds to a strain of about 10%. This is caused by a temporary deformation of the textile due to the large strain applied (marked as "textile deformation" in Fig. 3.4(b)) which reduces to about 5% after some hours. This is not an issue when measuring strain in a garment as the textile is pre-stretched when worn and the sensor, therefore, is used in the working range only.

3.4.2. Hysteresis

A resistance vs. strain plot is shown in Fig. 3.5 for an applied strain of 80%, indicating a linear rise in resistance when applying strain and only a small hysteresis: The maximal hysteresis error is $\pm 3.5\%$ (7%) in strain at $16k\Omega$. The mean hysteresis error over the working range is $\pm 2.25\%$ (4.5%) in strain.

A system with hysteresis is defined as a system whose output does not only depend on the current input but also on the history of the input. Typical causes for hysteresis are friction and structural changes in the material [41]. However, so far it is not clear whether these effects account for the hysteresis in the present sensor.

The temporary deformation of the textile, which was described in Section 3.4.1, can also be seen in Fig. 3.5. In this plot it appears as a plateau at low strains.

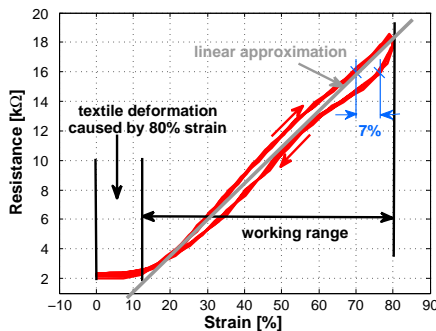


Figure 3.5. Response of sensor to a given strain illustrated as a resistance vs. strain plot (sensor length 2cm).

3.4.3. Sensitivity $\frac{\delta R}{\delta l}$ in Different Working Ranges

In this Section it is analyzed whether the sensitivity of the sensor remains stable when the sensor is used in different strain ranges. Two tests were conducted where a variable strain range was applied, the first one without pre-stretching the sensor before the test, the second with the pre-stretch.

In Fig. 3.6, an increasing strain was applied to the sensor without pre-stretching it. It can be seen that the sensitivity changes with each increase in strain. Within each of these regions, the sensitivity remains stable, however, at different values. Therefore, dependent on the maximal strain applied, the strain sensor has a different sensitivity.

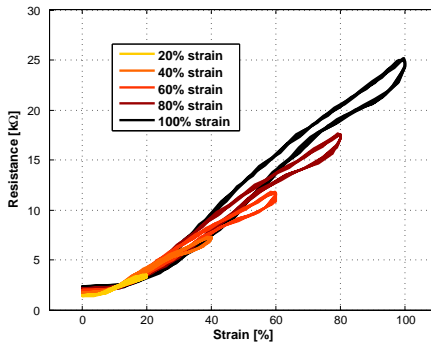


Figure 3.6. Applying an increasing strain to the sensor without pre-stretching it (sensor length 2cm). The sensitivity of the sensor changes.

In Fig. 3.7, a pre-stretch of 80% (extension - retraction cycle to 80% strain) was first applied to the sensor (black curve). After that, different smaller strains were applied (60%, 40%, and 20%). The Figure shows that the sensitivity (slope) of the sensor remains stable: The sensor has a sensitivity $\frac{\delta R}{\delta l}$ of $1.14 \frac{k\Omega}{mm}$ ($= \frac{16k\Omega}{14mm} = 229 \frac{\Omega}{\% \text{ strain}}$). Therefore, the sensor needs to be pre-stretched to its full working range before its first usage so that the sensitivity becomes stable. This also means that during usage, no larger strain than the pre-stretch value should be applied.

To show that a pre-stretched sensor remains stable over a longer period of time, smaller strains (20%, 40%, and 60%) were applied to a sensor 24 hours after a pre-stretch to 80%. The result was the same

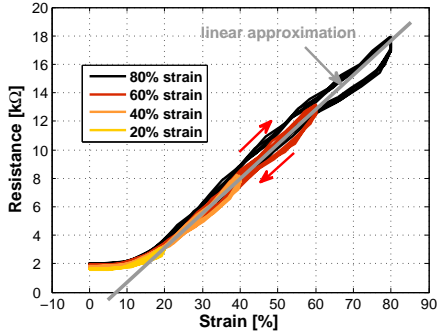


Figure 3.7. Applying a pre-stretch of 80% to the sensor (black curve) followed by different smaller strains (sensor length 2cm). The sensor sensitivity remains constant. We call this the pre-stretched case, which means that the sensor is stretched to its full range before any other (smaller) strain is applied.

sensitivity in all measurements (as in Fig. 3.7) confirming that a pre-stretching ensures stable sensitivity.

During the PhD, around 100 sensors were measured showing all similar characteristics (the resistance did not vary more than 10%). During these measurements, no failures occurred when a strain of up to 80% was applied. When applying a strain of 100% around 20% of the sensors failed and only a minority of the sensors still worked at 150% strain. Therefore, we specify the range of the sensor to be between 0% and 80% strain (working range of 70% when the textile deformation is considered, see Section 3.4.1). This results in a sensitivity of $1.14 \frac{k\Omega}{mm}$ and a gauge factor ($\frac{\Delta R \cdot l_0}{R_0 \cdot \Delta l}$) of ~ 20 at a sensor length of 2cm.

Failures usually occurred while stretching the sensor for the first time. Once stretched to a certain amount without breaking, the sensor worked reliably afterwards. Typically two types of failures appeared: The sensor either failed due to a rupture of the sensor thread at one of the ends of the sensor (at the transition to the epoxy) or as cracks in the conductive epoxy such that the connection between the sensor and the conductive thread failed.

3.4.4. Dependency on Strain Rate

The dependency on the strain rate is shown in Fig. 3.8. The strain velocity was increased from 50mm/min to 600mm/min (50, 100, 200,

400, and 600 mm/min). This increase in speed shows a marginal rise in resistance (+2 $k\Omega$ at 80% strain). The maximal error increases from $\pm 3.5\%$ to $\pm 7.5\%$ when doing a linear approximation over all five measured speeds and using a range of 80% strain. The mean error increases from $\pm 2.25\%$ to $\pm 5.5\%$.

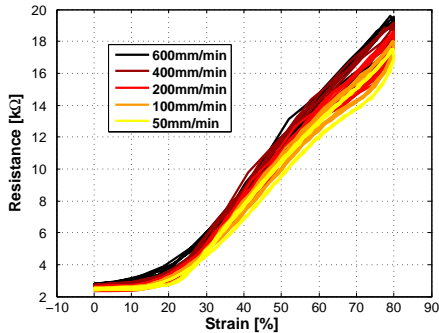


Figure 3.8. Sensor characteristics at different measurement speeds (50, 100, 200, 400, and 600 mm/min , sensor length 2 cm).

3.4.5. Longterm Cycling

The sensor was cycled for 16 hours at a cycling rate of $\sim 250 \frac{cycles}{hour}$, resulting in a total of ~ 4000 cycles in order to verify the stability of the sensor properties. The maximum and minimum resistance values of the first 8 hours are shown in Fig. 3.9. It can be seen that the minimal resistance shows a marginal increase of about 0.5 $k\Omega$. This increase is probably caused by a slowly increasing textile deformation (see Section 3.4.1). Also the first step at the beginning is caused by textile deformation, however, when the sensor is pre-stretched as described in Section 3.4.3, this step is reduced from 1 $k\Omega$ to less than 0.5 $k\Omega$. The maximal resistance decreases in the first half an hour by 1 $k\Omega$ (6%). This phase is followed by a slow increase of the maximal resistance approaching the initial level. Therefore, the sensitivity of the sensor ($\frac{\delta R}{\delta l}$) can be assumed to be widely constant with time.

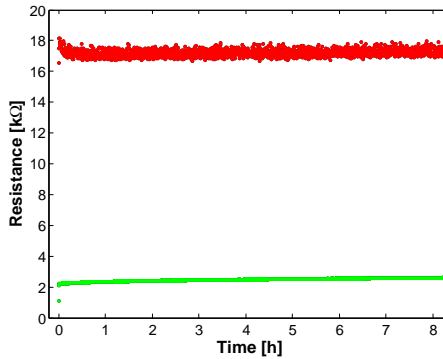


Figure 3.9. The sensor was cycled for 16 hours whereas the maximum and minimum resistance values of the first 8 hours are shown.

3.4.6. Ageing

In order to show the longterm-stability of the sensor signal, the measurements were repeated once a week during two months. During this time, only a minor increase in the sensor signal of less than $1k\Omega$ at an applied strain of 80% was found (see Fig. 3.10).

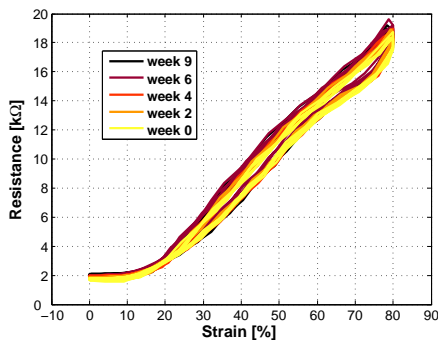


Figure 3.10. Repeated measurements during 2 months (one measurement per week, sensor length $2cm$, measurement speed $200mm/min$), showing a minor increase in the sensor signal of less than $1k\Omega$ at an applied strain of 80%.

3.4.7. Washability

The strain sensor was washed 8 times (over a period of 2 months) at 30°C in a washing machine using a conventional cleaning agent. During this procedure, the sensor signal increased by less than $1k\Omega$ at an applied strain of 80% (see Fig. 3.11). This is the same increase as caused by the ageing effect in the same period of time (see Fig. 3.10). Therefore, the washing had no influence on the sensor properties. One reason for this durability is the attachment of the sensor using silicone. This protects the sensor against many factors.

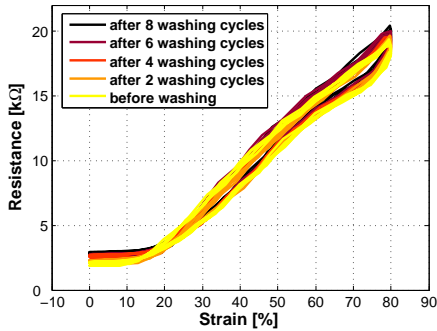


Figure 3.11. The sensor properties remained stable also after 8 washing cycles.

3.5. Conclusions

In this Chapter, a strain sensor was presented with a working range of 70% strain. Conventional strain gauges (based on a metallic foil pattern) reach a higher linearity but at a very reduced working range of less than 1%.

Due to this large measurement range and the fiber-shaped form (diameter of $0.315mm$), this sensor has the potential to be fully integrated into textiles. Thereby, it has to be assured that a restoring force is present, forcing the sensor back to its original length. This is necessary, as the sensor material alone experiences a permanent plastic deformation when stretched (see Section 3.2.2) which results in a smaller working range and different sensor properties. In this thesis,

the restoring force was achieved by using silicone to attach the sensor to the textile.

Different characteristics of the sensor were presented and are summarized in the following. These properties qualify the sensor for strain measurement in a garment.

- widely linear resistance vs. strain characteristic over a working range of 70% strain,
- a small hysteresis and a minor dependence on the strain rate resulting in a total mean error of $\pm 5.5\%$ in strain,
- stable sensor properties while in continuous usage,
- no ageing effect,
- a high sensitivity of $1.16k\Omega/mm$ (sensor length $2cm$) and a gauge factor of ~ 20 ,
- thread-like shape,
- washable.

Before usage, the sensor needs to be pre-stretched to 80% in order to get a stable sensitivity.

4

Posture Classification Experiment*

A prototype of a strain sensitive clothing was built using the strain sensor presented in the previous Chapter. Experimental data obtained with this prototype was used to classify a selection of 27 upper body postures. The following Sections present the prototype setup, the experimental protocol, the classification method, and its results. With this prototype, the feasibility of detecting 27 upper body postures with a strain sensitive garment was verified on eight subjects.

*based on [69]

4.1. Method

4.1.1. Prototype

Using the strain sensor described in Chapter 3, a prototype of a clothing recognizing upper body postures was built (see Fig. 4.1). 21 sensors were attached to the back region of the garment (see Fig. 4.2). It will be shown in Chapter 7 that placing more sensor than minimally necessary increases the robustness of the result. The sensors were fixed to the textile using silicone as described in Section 3.2.2. For the garment, a commercially available catsuit (one-piece, tight-fit garment) with a front zipper (medium-sized) was used.

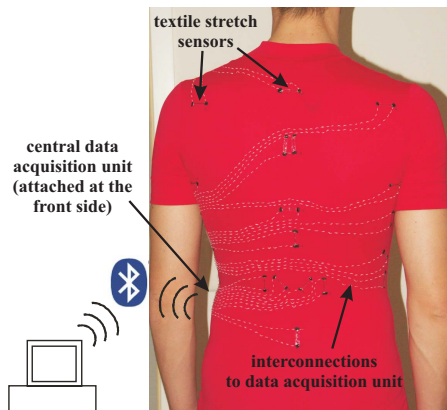


Figure 4.1. Architecture overview of a prototype recognizing upper body postures using strain sensors.

The sensors were connected to a small data acquisition unit, which digitized (four 8-channel MAX147, 12bit) and transmitted the measured signal to a PC via Bluetooth (MSP430F149, BlueNiceComIII). These connections to the data acquisition unit were realized with a *SHIELDDEX*[®] yarn (235f34dtex 2-ply HC) (see Section 3.2.2). A graphical user interface was implemented which visualized the measured strain values and stored the data into a file. An overview of the setup is given in Fig. 4.1 [73].

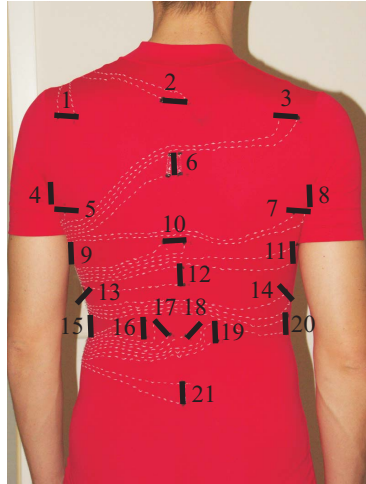


Figure 4.2. Placement of 21 strain sensors.

4.1.2. Experimental procedure

A set of frequently used body postures covering the degrees of freedom in trunk and arm movement were defined. This initial set was adapted to cover both sitting and standing postures resulting in a final set of 15 sitting and 12 standing posture classes (see Fig. 4.3). Tab. 4.1 summa-



Figure 4.3. Visualization of the sitting and standing upper body postures included in the study.

Table 4.1. Sitting and standing upper body postures included in the study. The postures are visualized in Fig. 4.3.

Base Posture	Class	
<i>Standing upright</i>	-	arms relaxed
Sitting Postures	Class	
<i>Rotation of trunk</i>	1	to the right
	2	to the left
<i>Bending trunk sideways</i>	3	to the right
	4	to the left
<i>Lifting shoulders</i>	5	right shoulder
	6	left shoulder
	7	both shoulders
<i>Slumped</i>	8	shoulders over hip
<i>Bending trunk forward</i>	9	with bent back
	10	with straight back
	11	bending maximally, hands beside the feet
<i>Forced upright</i>	12	
<i>Arm postures</i>	13	arms to the front
	14	arms to the sides
	15	arms overhead
Standing Postures	Class	
<i>Rotation of trunk</i>	16	to the right
	17	to the left
<i>Bending trunk sideways</i>	18	to the right
	19	to the left
<i>Lifting both shoulders</i>	20	
<i>Slumped</i>	21	
<i>Bending trunk maximally forward</i>	22	hands approaching toes
<i>Forced upright</i>	23	
<i>Extending arms to the front</i>	24	
<i>Squatted</i>	25	maintaining straight back
<i>Flexing torso sideways</i>	26	to the left
	27	to the right

rizes the posture set that was considered in the study. An additional base posture was defined as standing upright with relaxed arms along the body axis. This posture was used for a very basic adaptation of the prototype to the user.

Eight male participants aged between 26 and 31 years were included in the study. The mean body height was 179cm , standard deviation (SD) 4.1cm . The mean chest circumference was 95cm (SD 4cm) and the waist circumference was 84cm (SD 4.1cm).

The participants were instructed to assume the different postures for approximately two seconds in a predefined sequence while wearing the garment prototype. A picture was shown to the participants to indicate each posture, however, the postures were not explained or trained beforehand. Each posture was repeated three times and the whole set of postures was recorded twice, such that each posture was recorded six times in total (repetitions 1 to 3 and 4 to 6 are referenced as set 1 and 2 respectively). The complete data set included 1296 postures from the 27 posture classes and eight participants.

The strain sensor values were acquired using a central data acquisition unit attached at the waist level (see Section 4.1.1), recording at a sampling rate of 33.5 Hz. The postures were labelled during the recordings.

4.1.3. Classification methodology

The strain data of all 21 garment-sensors was used as feature set for the posture classifications. In a pre-processing step, the strain values were adapted to each wearer: The mean value of each sensor during base posture was subtracted from each participant's data set. This method compensated for the variable body compositions and hence a variable pre-strain in the garment among the different participants.

The influence of the degree of user adaptation on the classification result was evaluated. A *user-specific* training of the classifier was compared to a training and testing that included sensor data from *all users* and to a subject-wise leave-one-out split representing a *new user* scenario.

All classifications were performed on every sample of the data with

a Naïve Bayes classifier:

$$\begin{aligned} \text{selected class} &= \operatorname{argmax}_{c_j} \{p(c_j|S)\} \\ &= \operatorname{argmax}_{c_j} \left\{ p(c_j) \prod_{k=1}^n p(s_k|c_j) \right\}, \end{aligned} \quad (4.1)$$

where c_j is a class j , s_k the value of sensor k , n the number of sensors, and S the values of all sensors. A sample was labelled with the class c_j that achieved the highest posterior probability $p(c_j|S)$. A normal distribution of the sensor values was assumed so that $p(s_k|c_j)$ was calculated according to:

$$p(s_k|c_j) = \frac{1}{\sigma_{kj} \sqrt{2\pi}} e^{-\frac{(s_k - \mu_{kj})^2}{2\sigma_{kj}^2}}, \quad (4.2)$$

where μ_{kj} and σ_{kj} were the mean and standard deviation of sensor k in class j .

A 6-fold cross-validation procedure was used to split training and testing data for the user-specific and all-users evaluations. The splitting procedure was designed to use each repetition of the posture only once for testing. For the new-user evaluation the data was sliced according to the number of study participants into eight iterations. For each iteration the data from seven of eight participants was used for training and the left out data set for testing.

To compare classification results with unequal number of test observations in each class, a normalized accuracy measure was used. The classification result was derived as mean of the class-relative accuracies (normalized accuracy):

$$nAcc_{Total} = \frac{1}{N_C} \sum_{i=1}^{N_C} \frac{Recognized_i}{Relevant_i}, \quad (4.3)$$

where N_C is the total number of classes, $Recognized_i$ and $Relevant_i$ are the number of correctly identified and the total number of observations in class i respectively.

4.2. Results

In the user-specific classification an accuracy of 0.97 was achieved with minor confusions of the classes 9 (bending forward with bent back), 10 (bending forward with straight back) and 25 (squatted) only.

We analyzed the influence of training-testing partitioning by reducing the number of cross-validations from 5 to 2 and consequently, reducing the number of training observations from 80% to 50%. The accuracy dropped to 0.8. From this result we concluded that differences exist between the two consecutive posture recording sets (repetitions 1 to 3 compared to repetitions 4 to 6) but only minor variability within each set. Possible reasons for this result are 1) accurate repetition of the postures within each set but slightly different postures between the sets, 2) not enough variance in each set since three repetitions were performed only, 3) sensor inaccuracies and 4) movements of the clothing in comparison to the skin.

Figs. 4.4 and 4.5 show the all-user and the new-user classification results respectively (actual class in rows, predicted class in columns). The plot is obtained from the confusion histogram matrix by normalizing each row by the row sum (number of relevant observations for the corresponding class). While the all-user analysis achieved a performance of 0.84, the performance dropped for the new-user evaluation to 0.65. A summary of these classification results is shown in Fig. 4.6, including the minimal and maximal results achieved.

The matrix plots in Figs. 4.4 and 4.5 show that certain similar

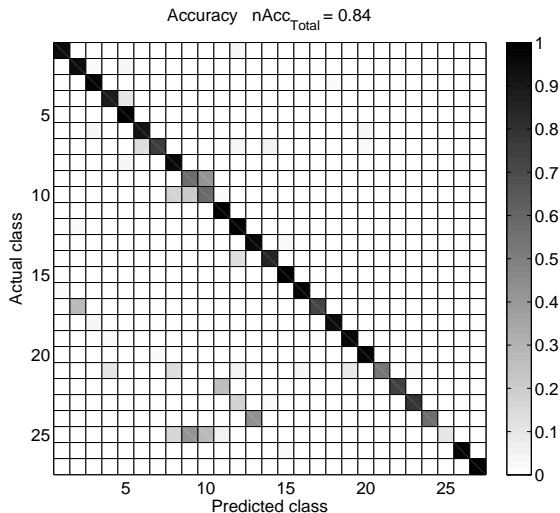


Figure 4.4. Confusion matrix of the all-user classification of 27 postures.

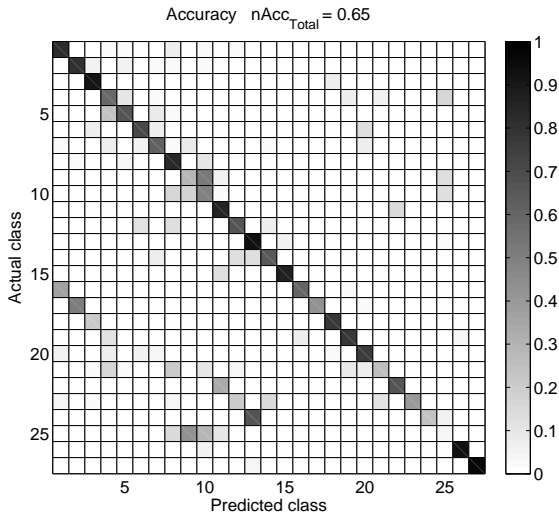


Figure 4.5. Confusion matrix of the new-user classification of 27 postures.

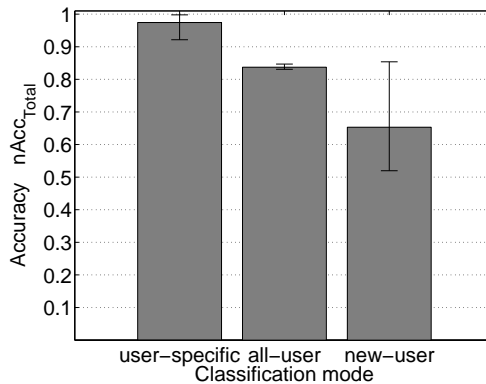


Figure 4.6. Summary of the classification performances.

postures could not be discriminated. Two types of error were evident: 1) Confusions appeared between the corresponding sitting and standing postures, e.g. postures 13 and 24 (extending the arms to the front while sitting and standing). 2) Similar postures could not be differentiated like e.g. postures 9, 10 and 25 (bending the trunk forward with

a bent and a straight back and squatted). Therefore, the same analysis was repeated for the sitting postures only (postures 1 to 15). The results increased from 65% to 74% for the new-user classification. Hence, this indicates that a posture classification is feasible for many (not too similar) classes even for new-users, however, sitting and standing can hardly be distinguished with the current setup.

4.3. Conclusions

With the presented prototype, a study was performed where 29 sitting and standing postures were classified. From this study, the following can be concluded:

- The method of detecting body postures by measuring the strain in the clothing works for a user-specific training. An accuracy of 97% was achieved when doing a user-specific classification.
- When doing a user-independent training, the classification rate dropped to 65%. Mainly, similar postures could not be differentiated. This indicates that a user-dependent training is necessary.
- The test subjects did not report any discomfort caused by the strain sensors. Therefore, the attachment of the sensors using silicone is suitable for textile applications.

5

Simulation of Strain in Tight-Fitting Clothing

In the last Chapter 4, a strain sensitive garment prototype with intuitively placed sensors was presented. However, there might be better sensor positions. Therefore, in the following two Chapters a method to optimize the sensor positioning is introduced.

With an animatable body model, different body postures were created. A cloth model was then applied to these postures, enabling the calculation of the strain in the clothing. In the subsequent Chapter 6 a method is presented to derive the optimal sensor position from the calculated strain patterns.

5.1. Introduction

In order to calculate the strain pattern in the clothing, three steps were necessary which are described in this Chapter:

- **Body Scan:** Four 3D scans of the torso of one person were recorded. This step is described in more detail in Section 5.2.1
- **Animation:** One of the scans (basic posture) was animated using *3ds Max* (Autodesk, San Rafael, USA). The other three scans were used for validation. These steps are described in Sections 5.2.2 and 5.2.3. There were several reasons for building an animatable model instead of scanning the user in several postures.
 - There exist methods to build animated body models using some body parameters [25, 89] which could even replace the single scan. This is more convenient for the user than taking several scans.
 - An animated body model enables a clear definition of even small changes in the body posture difficult to achieve when scanning the person.
- **Cloth simulation:** A cloth simulation was performed enabling the calculation of strain patterns in the clothing for the different postures. A particle model which is described in Section 5.3 was used to simulate the clothing. The calculated strain patterns were utilized to optimize the sensor positions (see Chapter 6).

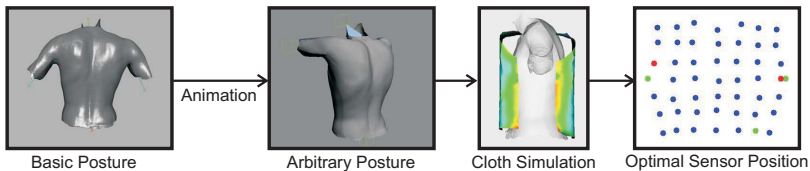


Figure 5.1. Data flow for optimizing the sensor position: scan of a person, animation, cloth simulation, optimization of sensor position.

5.2. Animated Body Model

5.2.1. Body Scan

To achieve an accurate body model, the torso of one person was scanned. Four different postures were measured whereas one posture (basic posture, see Fig. 5.2) was animated and the three remaining postures (see Fig. 5.3) were used for validation of the animation. An animated body model has the advantage that the strain pattern of arbitrary postures can be simulated without rescanning the person.

For scanning, the OSCAR scan system developed at ETH Zurich [47] was used. This is an active capture system consisting of four digital cameras. Each camera reconstructs part of the surface by using a light pattern. By using several cameras, the whole surface can be assembled. Also other methods could be used to generate a body model like e.g. [25, 89, 90].

Each of the upper body scans consists of around 150'000 triangles which results in elements of the size of $5 - 10\text{mm}^2$.

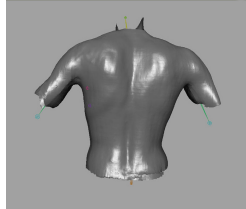


Figure 5.2. Scan of the upper body; basic posture.

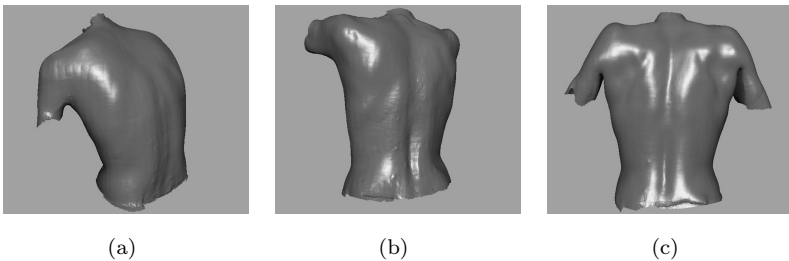


Figure 5.3. Scan of the upper body; Fig. 5.3(a): bent posture, Fig. 5.3(b): arms forward, Fig. 5.3(c): lifted shoulders.

5.2.2. Animation

To animate the body model, *3ds Max 8* (Autodesk) was used. The basic posture scan (see Fig. 5.2) was animated so that the three other posture scans (see Fig. 5.3) were reproduced as accurate as possible. The following parameters were optimized:

- **skeleton:** Like in a real body, animatable body models contain a skeleton [78, 106]. By moving the "bones", the corresponding surface also moves. The skeleton has to be defined once whereas the number, size, and shape of the bones can be varied. In this thesis, 16 vertebrae were used so that the flexibility of the spine could be ensured (see Fig. 5.4(a)). To prevent the abdominal region from collapsing, so called fins were used (see Fig. 5.4(b)). In order to better control the shoulder region, bladebones were modelled with a user-defined shape.
- **skinning:** In order to also move the skin when the skeleton is animated, the skin has to be attached to the skeleton. This procedure is referred as "skinning". In *3ds Max*, two regions have to be defined on the skin for each bone. The region above the bone is only influenced by that particular bone. In the adjacent region the surface can be influenced by several bones. The amount of the effect is weighted by the distance to the bone. The skinning can be done automatically by *3ds Max*. Only few regions (mainly in the armpit region) were adapted manually.

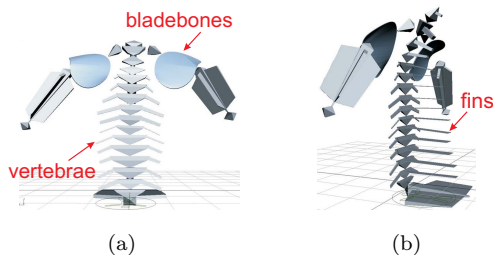


Figure 5.4. Skeleton of the animated torso using *3ds Max*.

5.2.3. Validation

A skeleton and skinning were applied to the basic posture scan to get an animated body model. This animated model was then altered to get the postures of the three other scans (see Fig. 5.3). The similarity of the animated postures and the scans was determined by calculating the distance between the two surfaces (see Fig. 5.5). This distance calculation was realized by intersecting the normal vectors of the scanned surface with the surface of the animated model (see Fig. 5.6). *vtk* [7] was used to determine the similarity of the two surfaces.

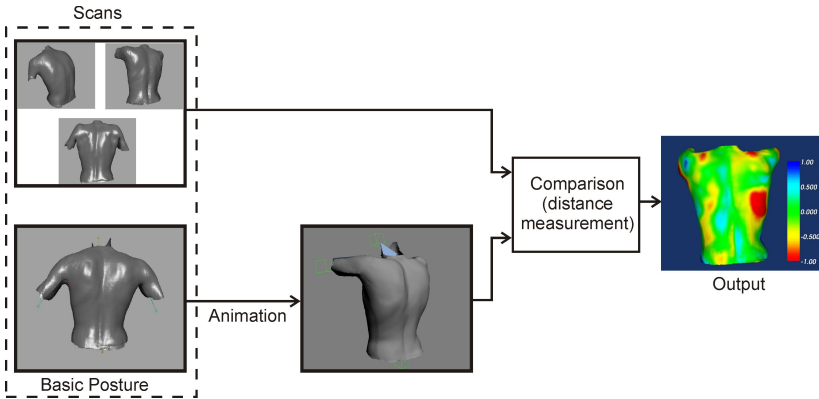


Figure 5.5. Validation of the animated scan: Comparison between animated and scanned postures.

The resulting mean error was 3.5mm whereas the maximal error was 2cm . The mean error was calculated as

$$\bar{e} = \frac{1}{n} \sum_{i=1}^n d_i, \quad (5.1)$$

where n was the number of points (corner points of the elements) of the scanned model and d_i the distance to the animated surface in each point (see Fig. 5.6). In order to verify the influence of this error on the simulated strain pattern, a cloth simulation (see next Section 5.3) was performed with both models - the scanned surface and the animated model. The difference between these two simulated strain patterns was on average 2% in strain.

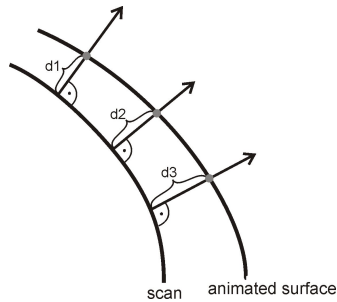


Figure 5.6. Distance measurement for comparing the animated model to the scanned surface of the same posture. This was done by intersecting the normal vectors of the scan with the surface of the animated model.

5.3. Cloth Simulation

The cloth simulation problem was addressed by the textile and the computer graphics community. However, they focused on different aspects of the same problem: While the textile community was interested in the mechanical behaviour of textile, the computer graphics community focused on geometric structures resembling cloth. In literature, the many different approaches of cloth modelling are summarized according to the following categories [20, 77]:

- *Peirce Model* [55, 91]: The textile community approached cloth modelling from a mechanical engineering point of view and tried to understand the mechanical properties of textiles: The Peirce Model describes the geometric relationships among yarn crossings (low-level structure). Also, they measured and modelled the mechanical behaviour of cloth and studied tensile, bending, and shearing properties.
- *Continuum mechanics/ Finite Element Model (FEM)* [15, 24, 37, 38, 43, 107]: Low-level structural models turned out to be too complex to model cloth drape [20]. Therefore, FEM-based methods were used by the textile community for simulating cloth drape. In FEM, mechanical equations are applied to single mesh elements of the discretized surface (triangles or quadrangles).
- *Geometric Approaches* [77, 105]: The computer graphics community is interested in a model looking like cloth not necessarily

being an exact mechanical approximation. Therefore, they implemented geometric approaches where the folds in a cloth were approximated by geometric curves and surfaces.

- *Physically Based Approaches* [21, 28, 59, 84, 94, 99, 101, 104]: Physically based approaches can be divided into "Mass and Spring Models", "Elasticity-Based Models", and "Particle Models". In these techniques, cloth models are represented as triangular or rectangular grids, with points of finite mass at the intersections. The forces or energies are calculated for these points in relation to its neighbour points (local interactions). Although these approaches were developed by the computer graphics community and, hence, were not optimized for accuracy, they approach the accuracy of Finite Element Models: In 2005 Volino et al. [104] presented a particle model as accurate as a nonlinear first-order Finite Element Model [102].

In this thesis, the particle model of Volino et al. [104] was used to simulate strain in the garment. As this model was optimized for simulating wrinkles in loose fitting garments, the algorithm was adapted to simulate strain in a tight fitting garment.

5.3.1. Particle Model

A particle model was used for simulating the strain in a tight fitting clothing. In particle models, the surface is discretized and considered as a bunch of points. Each of these so called particles has an assigned position, velocity, acceleration, and mass. They are locally connected so that triangles or quadrangles emerge. As only these local connections are considered in the model, it is possible that the simulation converges not to a global but to a local minimum.

The cloth model of P. Volino [104] was chosen for calculating the strain pattern in a garment. This is a force based particle model which works on triangles. Using triangles instead of quadrangles has the advantage that the shape of the surface to be modelled can be chosen arbitrarily, whereas with quadrangles, step-like borders cannot be avoided. Another advantage of this model is its accuracy: It is equivalent to a nonlinear first-order finite element model [102].

The simulation is performed in two main steps: 1) In each triangle, the strain is calculated enabling the identification of the force acting on the neighbouring triangles (this Section). 2) By integrating these forces

($F = m \cdot d\ddot{x}$), the new particle positions is determined (Section 5.3.2). This corresponds to one iteration step and is repeated until the changes in the particle positions are small.

Model of P. Volino [104]

The strain in each triangle at the current time step is calculated by comparing the triangle to the original, undistorted triangle. The original triangle is described by 3 2D points (u_a, v_a) , (u_b, v_b) , (u_c, v_c) (see Fig. 5.7). The corresponding coordinate system is defined as $(1, 0, 0)$ and $(0, 1, 0)$ and relates to the directions of the threads in the garment to be simulated (e.g. weft-warp in a woven textile). In order to find the deformed thread directions \mathbf{u} and \mathbf{v} , the transformation matrix \mathbf{A} is calculated. \mathbf{A} transforms the undistorted triangle into the deformed triangle (P_a, P_b, P_c) ,

$$(P_a \ P_b \ P_c) = \mathbf{A} \cdot \left(\begin{pmatrix} u_a \\ v_a \end{pmatrix} \begin{pmatrix} u_b \\ v_b \end{pmatrix} \begin{pmatrix} u_c \\ v_c \end{pmatrix} \right). \quad (5.2)$$

From \mathbf{A} \mathbf{u} and \mathbf{v} can be calculated using $\mathbf{A} = (\mathbf{u} \ \mathbf{v})$. This results in the thread directions \mathbf{u} and \mathbf{v} shown in Equation (5.3) and (5.4) for the deformed triangles.

$$\mathbf{u} = \frac{(v_b - v_c)P_a + (v_c - v_a)P_b + (v_a - v_b)P_c}{u_a(v_b - v_c) + u_b(v_c - v_a) + u_c(v_a - v_b)} \quad (5.3)$$

$$\mathbf{v} = \frac{(u_c - u_b)P_a + (u_a - u_c)P_b + (u_b - u_a)P_c}{u_a(v_b - v_c) + u_b(v_c - v_a) + u_c(v_a - v_b)} \quad (5.4)$$

From this, the current in-plane strain ϵ can be calculated according to Equation (5.5).

$$\epsilon_{uu} = |\mathbf{u}| - 1 \quad \epsilon_{vv} = |\mathbf{v}| - 1 \quad \epsilon_{uv} = \frac{|\mathbf{u} + \mathbf{v}|}{\sqrt{2}} - \frac{|\mathbf{u} - \mathbf{v}|}{\sqrt{2}} \quad (5.5)$$

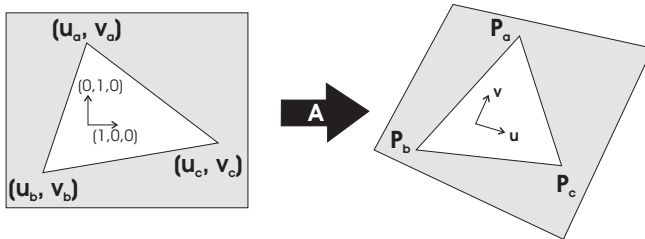


Figure 5.7. Left: Original, undistorted triangle; Right: deformed triangle.

The general viscoelastic stress(σ)-strain behaviour is a function of the strain in different directions and its first derivatives:

$$\begin{aligned}\sigma_{uu} &= (\epsilon_{uu}, \epsilon_{vv}, \epsilon_{uv}, \epsilon'_{uu}, \epsilon'_{vv}, \epsilon'_{uv}) \\ \sigma_{vv} &= (\epsilon_{uu}, \epsilon_{vv}, \epsilon_{uv}, \epsilon'_{uu}, \epsilon'_{vv}, \epsilon'_{uv}) \\ \sigma_{uv} &= (\epsilon_{uu}, \epsilon_{vv}, \epsilon_{uv}, \epsilon'_{uu}, \epsilon'_{vv}, \epsilon'_{uv})\end{aligned}\quad (5.6)$$

As viscosity was neglected in the present model, the following formulae result to calculate the stress σ from the strain ϵ (isotropic, linear material):

$$\begin{aligned}\sigma_{uu} &= \frac{E}{1 - \mu^2} \cdot (\epsilon_{uu} + \mu \cdot \epsilon_{vv}) \\ \sigma_{vv} &= \frac{E}{1 - \mu^2} \cdot (\epsilon_{vv} + \mu \cdot \epsilon_{uu}) \\ \sigma_{uv} &= \frac{E}{2 \cdot (1 + \mu)} \cdot \epsilon_{uv}\end{aligned}\quad (5.7)$$

whereas μ is the so called poisson's ratio (contraction in one direction when the sample is stretched in the other direction) and E the Young's modulus.

$$\mu = -\frac{\frac{\Delta x}{x_0}}{\frac{\Delta y}{y_0}} = -\frac{\epsilon_{xx}}{\epsilon_{yy}}\quad (5.8)$$

From the stress σ , the force (F_a, F_b, F_c) in each corner (particle) of the element can be calculated according to Equation (5.9).

$$\begin{aligned}F_a &= \frac{1}{2} [((v_c - v_b)\sigma_{uu} + (u_b - u_c)\sigma_{uv}) \frac{\mathbf{u}}{|\mathbf{u}|} \\ &\quad + ((v_c - v_b)\sigma_{uv} + (u_b - u_c)\sigma_{vv}) \frac{\mathbf{v}}{|\mathbf{v}|}] \\ F_b &= \frac{1}{2} [((v_a - v_c)\sigma_{uu} + (u_c - u_a)\sigma_{uv}) \frac{\mathbf{u}}{|\mathbf{u}|} \\ &\quad + ((v_a - v_c)\sigma_{uv} + (u_c - u_a)\sigma_{vv}) \frac{\mathbf{v}}{|\mathbf{v}|}] \\ F_c &= \frac{1}{2} [((v_b - v_a)\sigma_{uu} + (u_a - u_b)\sigma_{uv}) \frac{\mathbf{u}}{|\mathbf{u}|} \\ &\quad + ((v_b - v_a)\sigma_{uv} + (u_a - u_b)\sigma_{vv}) \frac{\mathbf{v}}{|\mathbf{v}|}]\end{aligned}\quad (5.9)$$

This model was validated with a "virtual" tensile test in [104]. For a strain up to 50%, the accuracy was better than 1% when measuring along arbitrary directions.

5.3.2. Numerical Integration

The output of the particle model described in the last Section are the forces F_i in each particle. By using Newton's equation of motion $F_i = m_i \cdot \ddot{x}_i$ and one, respectively two integration steps, the particle velocity \dot{x}_i and position x_i of the next time step are calculated. For this integration, the semi-implicit Euler method of the first order was used (Equation (5.10)). As in this thesis a static simulation was performed where computation time is not critical (not real-time), the choice of the integration method was not crucial. For better readability, the subscript i was removed:

$$\begin{aligned}\dot{x}_{t+dt} &= \dot{x}_t + \frac{1}{m} \cdot F(x_t, \dot{x}_t) \cdot dt \\ x_{t+dt} &= x_t + \dot{x}_{t+dt} \cdot dt,\end{aligned}\tag{5.10}$$

where m is the particle mass. In comparison to the explicit Euler method, the "new" velocity \dot{x}_{t+dt} is used to calculate the "new" position x_{t+dt} . Explicit Euler: $x_{t+dt} = x_t + \dot{x}_t \cdot dt$. If computation time is not an issue, the accuracy can be improved by reducing the time step dt .

5.3.3. Collisions

So far, the particle model (Section 5.3.1) and the subsequent numerical integration (Section 5.3.2) were described. However, the body model is not included so far: The garment would neither stop at the body model nor would it be influenced by the garment itself. Therefore, so called "collision detection" is required to restrict the garment to stay "outside" the body model. Typically, two types of collisions are added to the model:

- **Self collisions** are collisions of the clothing with itself, e.g. wrinkles (see Fig. 5.8). Self collisions are not an issue when modelling a tight-fitting clothing and were, therefore, neglected.
- **Collisions between the garment and the body model** (see Fig. 5.9) need to be considered in order to achieve an interaction between the body and the clothing. If neglected, the garment would "fly" through the body model.

In order to eliminate collisions, two methods are described in literature [29]:

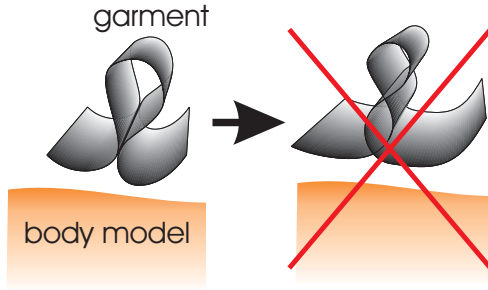


Figure 5.8. Self collision: "Collision detection" methods avoid clothing from intersecting with itself in simulations.

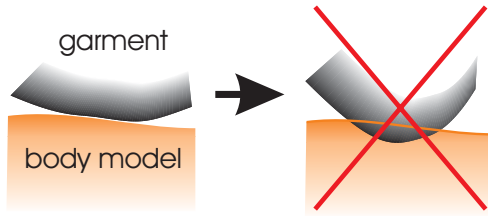


Figure 5.9. Penetration of the garment into the body model is prevented by using "collision detection".

- **Mechanical and dynamic reactions:** After a collision, the *forces* of the particles are adapted, e.g. using a repulsive force between the particle and the surface of the body [16].
- **Geometric reactions:** *Position and velocity* of the particle are directly changed in order to simulate the effect of a collision [53].

In the case of a mechanical reaction, a force function has to be defined which increases with a decreasing distance between the particle and the surface of the object. This ensures that the particle is pushed back when approaching the skin, preventing a penetration. However, large forces emerge when the clothing is close to the skin which decreases the numerical stability of the simulation. Therefore, a geometric approach was implemented:

Similar to [53], in each time step and for each particle, it is verified whether the particle crossed the body surface during the last time step.

If the line between the actual position x_t and the position of the particle in the last time step x_{t-dt} intersects with the human body surface, there was a collision in the last time step. In the case of a collision, the particle is temporarily set back to the position p where it penetrated the body (see Fig. 5.10(a)) and the velocity is recalculated so that an elastic impact results. The components \vec{n} and \vec{t} of this new velocity $\vec{v}_{t,new}$ can be damped separately. A damping of the tangential velocity \vec{t} simulates friction between the textile and the human body. The normal component \vec{n} was completely damped (set to zero) in our implementation in order to prevent instabilities (a bounce back can cause oscillation and cause instability). The new position $x_{t,new}$ can then be calculated by adding the new velocity $\vec{v}_{t,new}$ to the penetration point p .

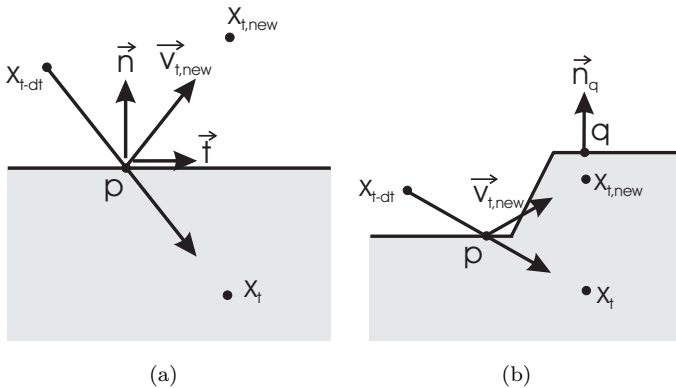


Figure 5.10. Fig. 5.10(a): When a collision is detected, the particle is temporarily set back to position p and a new velocity \vec{v}_{new} is calculated assuming a perfect elastic impact, so that the new position of the particle is $x_{t,new}$. Fig. 5.10(b): If the new position $x_{t,new}$ is still inside the body, $x_{t,new}$ is shifted to position q .

In a second step, it is verified whether the penetration into the body could be prevented and the new position $x_{t,new}$ is outside the body. This is done by looking for the closest point to $x_{t,new}$ on the surface (q , see Fig. 5.10(b)) and checking the direction of its normal vector \vec{n}_q (An angle between \vec{n}_q and $\overrightarrow{x_{t,new}q}$ of less than 90° means that the particle is inside the body. Otherwise it is outside.). If the particle is still inside

the body, it is set to position q . This approach can be summarized as follows:

1. \forall particle, if $\overline{x_{t-dt}x_t} \cap \text{body surface} \neq \emptyset$
 - $\vec{v}_{t,old} + \vec{n} = \vec{t}$, $\vec{v}_{t,new} = a \cdot \vec{t} + b \cdot \vec{n}$, where a and b are damping factors of the tangential and normal component respectively
 - $\vec{x}_{t,new} = \vec{p} + \vec{v}_{t,new} \cdot \frac{\overline{x_t p}}{|\vec{v}_t|}$
2. if $\vec{v}_{t,new} \cdot \vec{n}_q < 0$
 - $x_{t,new} = q$

5.3.4. Sewing

Inspired by the real assembly of clothing, simulated garments are built by "stitching" several sewing patterns together: The patterns are arranged around the body model and external forces are defined at the border of the patterns so that always two particles approach each other (see Fig. 5.11). One can imagine these forces to be caused by virtual elastic threads. As soon as the seams are closed, the particles are defined to stay together for the remainder of the simulation.

There are several methods for garment sewing (e.g. [103]), however, these methods were designed for nonelastic clothes. In the approach

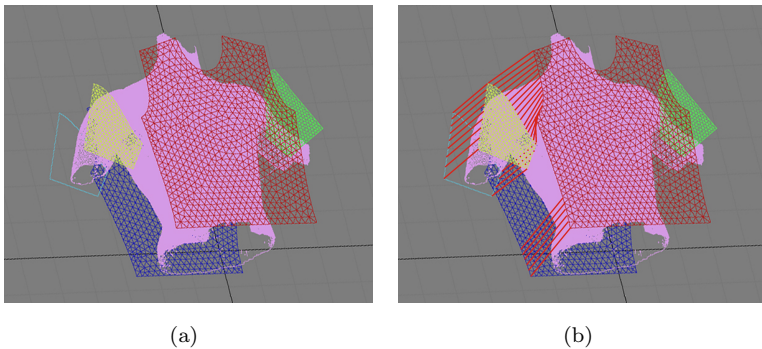


Figure 5.11. Sewing of the patterns. A virtual force is defined between corresponding particles.

of Volino et al. [103], forces are applied to the border particles. This works fine when the textile is nonelastic. However, if applied to elastic garments, a stable simulation could only be achieved by cumbersome fine-tuning of the parameters. The following problems appeared:

- **Simulation became instable:** The forces steadily increased until they were larger than the forces in the clothing. This caused the corresponding particles at the seam approaching each other. However, when the seam was closed, the force was still larger than in the garment and was only slowly damped. This resulted in a overshooting of the particles or in instability.
- **Seam never closed:** The forces never became large enough to overcome the elastic forces of the clothing, so that the seam did not close.

Hence, an algorithm was implemented which manipulates directly the velocities of the particles. The algorithm works in two phases:

1. **Calculate velocity correction:** A velocity correction $\vec{d\dot{x}}$ is added to the velocities of two particles a and b which are sewn together. This correction is calculated as

$$\vec{d\dot{x}} = \frac{\vec{dx}}{dt \cdot N}, \quad (5.11)$$

where \vec{dx} is the vector between particles a and b ($x_b - x_a$) and dt is the duration of one iteration step. Parameter N is the number of time steps which is used to close the seam. This number is continuously decreased during the simulation.

The velocity correction is then added to the current velocity of particle a and subtracted from the velocity of particle b .

2. **Keep common position:** As soon as the distance between particles a and b is below a certain limit, these particles change to a second phase. The goal of this phase is to keep the common position. This is done by manipulating the velocity and the position of the particles:

velocity: The mean velocity of two corresponding particles a and b is calculated by weighting the velocities with their masses m_a and m_b :

$$\vec{x}_{a,b,mean} = \frac{m_a \cdot \vec{\dot{x}}_a + m_b \cdot \vec{\dot{x}}_b}{m_a + m_b} \quad (5.12)$$

This velocity is applied to both particles a and b .

position: Particle a is set to the position of particle b and vice versa. Thereby, the patterns first overlap, however, this is balanced during the next iterations as larger internal forces result. That way, the particles converge to a common position.

5.3.5. Fix Points

With the procedure described so far, the patterns are not attached to the body model at all. Therefore, the textile will converge so that it is not stretched in vertical direction. It can even happen that the patterns move upwards until the body model is undressed (e.g. when the arms show upwards) as this minimizes the force in the patterns. This can be prevented by attaching the textile at the waistline and the arms as shown in Fig. 5.12. Additionally, one particle at the shoulder and armpit respectively was fixed. This prevents the result to strongly depend on the initial placing of the patterns which can happen as particle models look for a local and not a global solution.

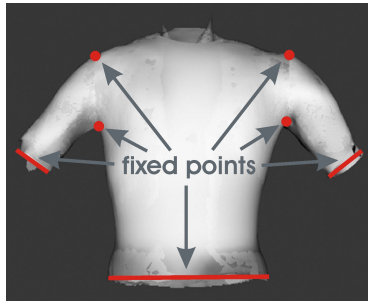


Figure 5.12. Points where the patterns were attached to the body model. The fixation at the sleeves and the waistline was added to prevent slipping, at the shoulder and the armpit to be independent of initial conditions.

The fixation was realized by manipulating the velocities similar to the approach described in Section 5.3.4 with the difference that point b is a fix point on the body model and, therefore, has no velocity assigned. This implies that the second step "keep common position" was changed to setting the velocity of particle a to zero and the position to x_b . Point b of the body model was not changed.

5.3.6. Other Forces

5.3.6.1. Gravitation

In general, gravitation has only a minor influence on the strain in a textile. This influence increases with a higher elasticity (smaller Young's modulus E) or a bigger self-weight of the textile. The force acting on a particle i can be calculated as

$$F_i^G = m_i \cdot G, \quad (5.13)$$

where G is the gravitational constant $G = (0, 0, -9.81) \frac{m}{s^2}$ and m_i the mass of particle i . The force F_i^G was added to the force in each particle.

No influence was observed in the results when adding F_i^G so that the gravitation was not considered in the model.

5.3.6.2. Mechanical Damping

Mechanical damping works against the movement of the particle and depends on the velocity \dot{x}_i of the particle:

$$F_i^D = -D \cdot \dot{\mathbf{x}}_i \quad (5.14)$$

When using mechanical damping, the system can reduce kinetic energy, which e.g. helps reducing periodic oscillations. This increases the stability of the model, however, does not alter the result. F_i^D was added to the force in each particle.

5.3.6.3. Bending Forces

Bending forces have been neglected in the described model as they do not influence the result when the clothing is tight fitting. These forces are only important when looking at wrinkles and the dynamic behaviour of loose fitting clothes.

5.4. Simulation Process

5.4.1. Input

Body model The preparation of the body model was described in Section 5.2. Using this animated body model, different body postures were created and utilized as an input to the cloth simulation. As the cloth simulation described in the last Section 5.3 does not

require a closed mesh (dependent on the collision method), the "holes" at the arms and the hip were left open.

Pattern To simulate strain in a shirt (upper body), six pattern parts were used: a front part, a back part and a front and back piece respectively for both sleeves. These patterns were prepared once in a pre-processing step using *3ds Max*: 1) In a first step, the border line of the pattern was defined (e.g. by importing a photograph of a real pattern and tracing its border). 2) A mesh of the area defined by the border line was created. The mesh consisted of triangles as this was required by the particle model described in Section 5.3.1. It was important to make sure that border lines which were sewn together had the same number of border particles, such that a unique seaming was possible. This was realized by defining equidistant points on the border lines before building the mesh (see Fig. 5.13). In Table 5.1, the number of particles and triangles of each pattern are given. The single mesh elements (triangles) had a side length of about 1.5cm.

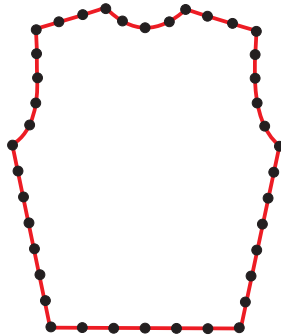
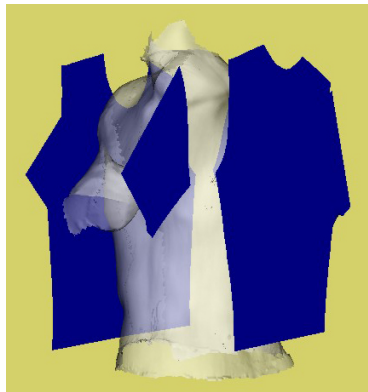


Figure 5.13. Border line of a pattern with defined equidistant points. This information was used for building a mesh of the pattern.

In a next step, the patterns were arranged around the body model (see Fig. 5.14), so that the body model was inside the clothing when closing the seams. Attention had to be paid to keeping the patterns in the x-y-coordinate plane as the particle model described in Section 5.3.1 assumes the initial pattern to be limited to two dimensions. Therefore, the patterns should not be rotated.

Table 5.1. Number of particles and triangles of the used meshes.

pattern	number of particles	number of triangles
front	780	1442
back	777	1446
right sleeve front	320	589
right sleeve back	288	526
left sleeve front	320	589
left sleeve back	292	534

**Figure 5.14.** Initial arrangement of the patterns.

Define seams and fix points As a last input, the seams and the fix points were indicated. The seams were defined by specifying pairs of particles to be sewn together. For the fix points, the border points to be fixed were indicated together with the point on the body model where it was attached to.

5.4.2. Simulation

In Fig. 5.15 the data flow during the simulation is shown. The trapezoidal boxes are the inputs described in Section 5.4.1, square boxes are functions in the simulation program.

The simulation starts with applying external forces (e.g. gravitation) and adds to these external forces the internal forces which are calculated according to the particle model described in Section 5.3.1

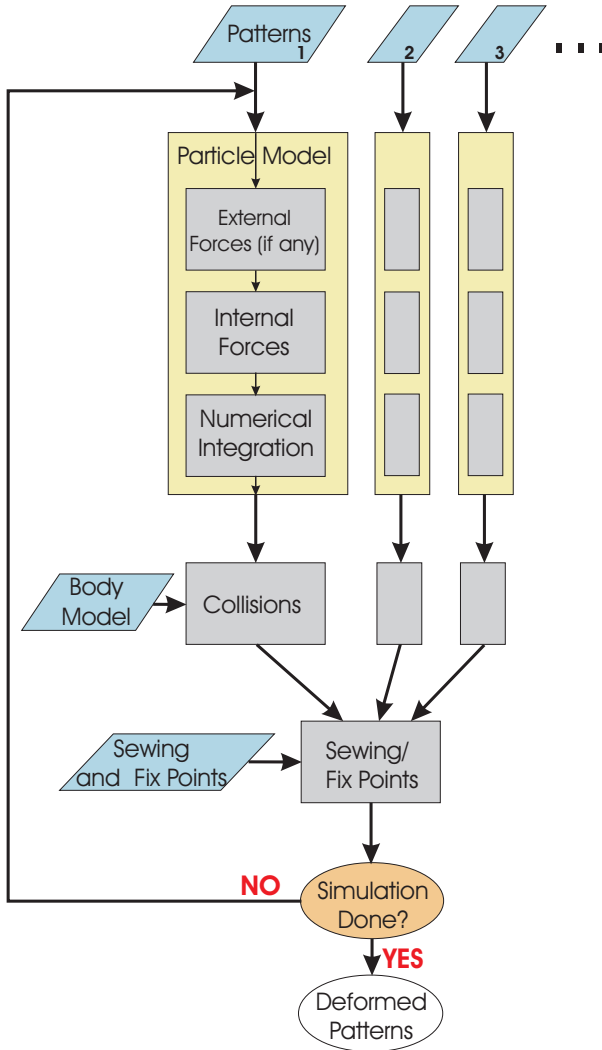


Figure 5.15. Data flow during the simulation.

by using the current strain. This is followed by a numerical integration (Euler, see Section 5.3.2) of the forces which results in new velocities and positions of the particles. The new positions are then tested for

collision with the human body model (see Section 5.3.3). In a last step the sewing and fix points are applied to the particles (see Section 5.3.4).

This sequence is repeated until the seams are closed plus a user defined number of follow up steps in order to let the textile approach the body and balance the forces in the garment. In the simulation results presented in this thesis, 500 follow up steps were used which turned out to be more than sufficient. Other constants used in the simulation are summarized in Table 5.2. The parameters do not have an influence on the result but need to be tuned in order to get a stable simulation. Also they are related to each other, e.g. if the Young's modulus is increased by a factor k , the time step has to be decreased by \sqrt{k} for the simulation to remain stable (as $x \sim F \cdot dt^2 \sim E \cdot dt^2$ using Equations (5.10) and (5.9)).

Table 5.2. Constant parameters used for the simulation.

Parameter	Value
Gravitation	neglected
particle mass	$111\mu g$
Young's modulus	$200 \frac{mN}{mm^2}$
time step	$7.7\mu sec$
poisson coefficient	0.0
damping	$25 \cdot \text{time step} (192.5 \frac{kg}{sec})$

5.4.3. Calculation of Strain

The output of the simulation are the deformed patterns (front, back, four sleeve parts) (see Fig. 5.15). The body model is not altered.

In a last step, the strain in the back pattern is calculated¹. This is done the same as in the particle model (Equations (5.2) to (5.5)), taking the upright "normal" posture (Fig. 5.2) as the undistorted mesh and the animated as the deformed one.

In Fig. 5.16 some examples are shown (bending forward, holding arms forward, lifting shoulders). The strain is calculated in horizontal and vertical direction.

¹The strain is calculated in the back pattern only as the focus of this thesis is to measure upper body postures. Of course the strain in the other pattern can be calculated accordingly.

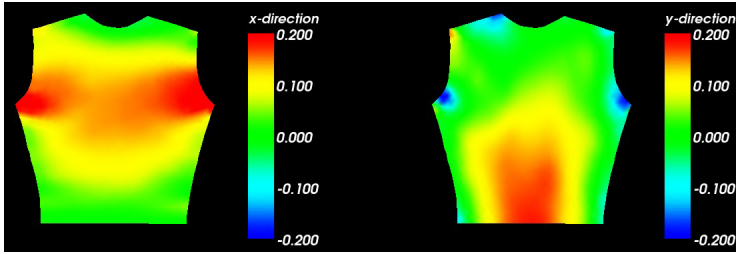
5.5. Results

The simulation results shown in Fig. 5.16 were compared to the reference measurements described in Section 2 (see Fig. 5.17). To allow a better comparison, the border of the simulated region was added in Fig. 5.17.

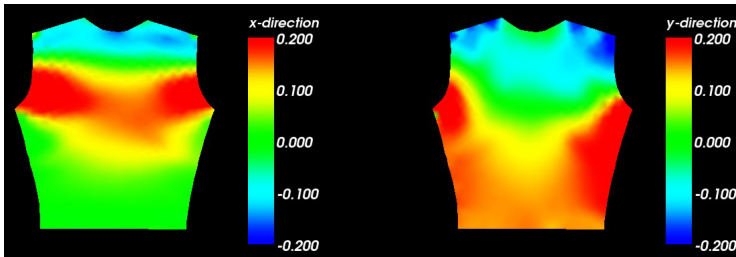
When comparing e.g. the bending forward posture (Figs. 5.16(a) with 5.17(a)), the strain patterns look similar: They both have a strain in horizontal direction in the upper back region and a vertical strain in the lower back. The strain values in the lower back are similar, however, in the upper back they differ by about 5% (20% in the simulated versus 15% in the reference measurement). As it was not verified whether the postures of the simulated and the real person were exactly the same, it is assumed that this difference in the strain value is caused by slightly different postures. The difference of 5% strain in the upper back in horizontal direction can be explained by a stronger forward movement of the shoulders in the model.

In the example where the arms are hold forward (Figs. 5.16(b) and 5.17(b)), the absolute strain values in horizontal direction are the same (20%) in the simulation and the measurement. However, there is a difference of about 10% in strain in vertical direction at the sides of the body.

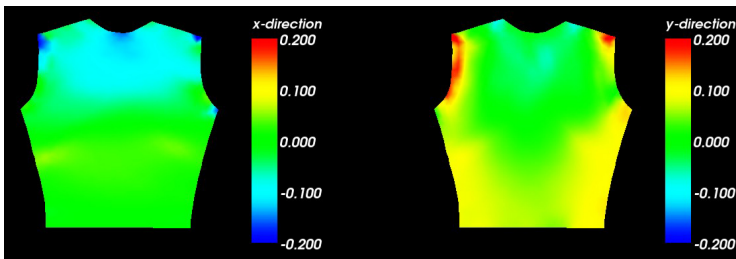
When lifting the shoulders (Figs. 5.16(c) and 5.17(c)), the strain in vertical direction is about 10% in the simulation as well as in the measurement. In horizontal direction, there is strain of zero and smaller in both patterns. The negative strain is larger in the measurement, however, as the strain sensor cannot measure negative strain, this difference is not relevant.



(a)



(b)



(c)

Figure 5.16. Calculated strain distributions for bending forward (Fig. 5.16(a)), holding arms forward (Fig. 5.16(b)), and lifting shoulders (Fig. 5.16(c)). Strain in horizontal direction is shown on the left, strain in vertical direction on the right.

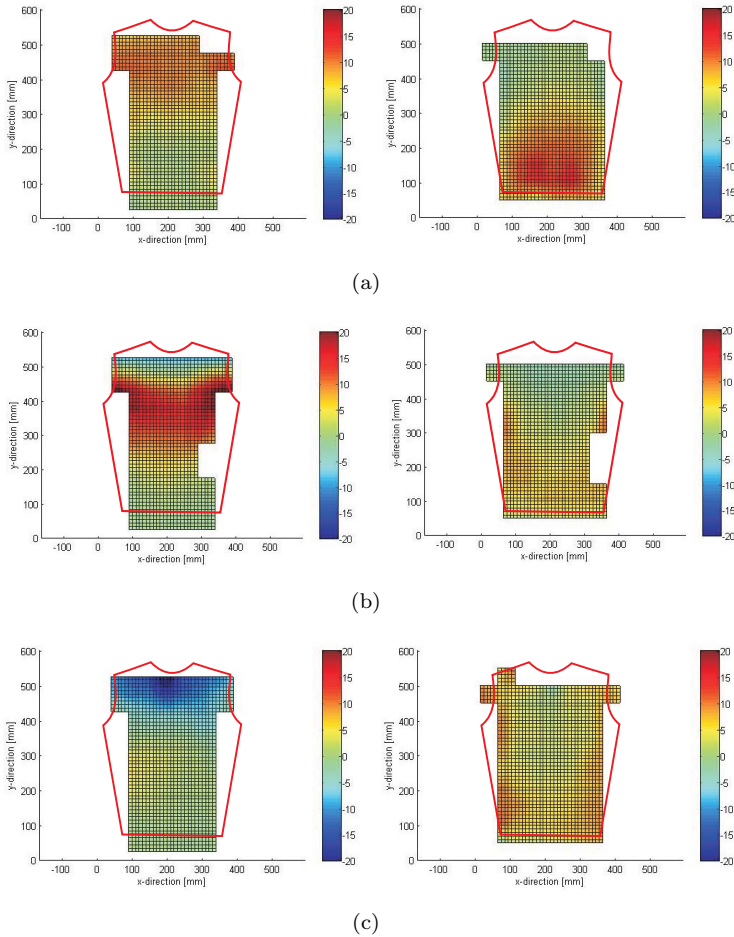


Figure 5.17. Measured strain distributions with the optical method described in Section 2 for bending forward (Fig. 5.17(a)), holding the arms forward (Fig. 5.17(b)), and lifting the shoulders (Fig. 5.17(c)). Strain in horizontal direction is shown on the left, strain in vertical direction on the right. Overlaid is the border of the simulated pattern so that the strain can be better compared to Fig. 5.16.

5.6. Conclusions

In this Chapter a simulation method was shown to calculate the strain distribution in a tight-fitting clothing. Six pattern parts were used to cover the upper body - a front part, a back part, and four sleeve parts (a front and a back piece for each arm).

A particle model published by P. Volino [104], which was originally designed for simulating loose-fitting clothing, was used. With some adjustments in the seaming process, the model was adapted to be used for tight-fitting clothing.

By comparing the simulation results to the reference strain measurement described in Section 2, it was shown that the strain patterns were similar, however, that the absolute strain values differed up to 10%. We assumed that the postures were not exactly the same as this was not ensured.

6

Optimization of Sensor Placement

Finding sensor positions leading to a maximal recognition rate is important when designing a strain sensitive garment for detecting different body postures. In this Chapter, a method is shown to find the most relevant sensor positions on the back. The analysis is based on the simulation results presented in the previous Chapter 5.

6.1. Introduction

When recognizing body postures by using the strain values of textile integrated strain sensors, the positioning of the sensors is important to achieve a high recognition rate. Two methods are presented to find the most relevant sensor positions. The methods are based on the simulation results shown in the previous Chapter and are shown exemplarily for one example.

6.2. Methods

The problem of finding an optimal set of sensors can be regarded as a feature selection problem with the features being the simulated strain values (~ 1500 , 777 strain values in horizontal and 777 in vertical direction, see Table 5.1). From this feature set, the best ones (best sensor positions) should be determined.

There exist many different feature selection methods which can be categorized into two different approaches: Filter and wrapper methods [58]. The basic difference is the goal of the optimization. Filter methods optimize the features - they choose the features with the best quality measure - whereas wrapper methods optimize the system as a whole (classification result). They try to find those features which lead to the best classification result.

- **Filter Methods:** Filter methods rate each feature independent of the subsequent classification. The features with the highest rating are selected. Filter methods can be split into three methods [83]:
 1. *Max-Dependency:* Find a feature set S with m features x_i , which jointly have the largest dependency on the target class c .
 2. *Max-Relevance:* Each feature is rated individually without considering the other features. This approach has the drawback that several highly correlated "good" features can be selected although they give no additional information. Examples are Mutual Information, ANOVA, Kruskal-Wallis.
 3. *Min-Redundancy:* Additionally to an individual rating, the correlation between the features is considered. Therefore, the

concurrent selection of highly correlated features can be prevented. An example is the Mutual Information Feature Selection (MIFS) Algorithm.

- **Wrapper Methods:** Wrapper methods select a subset of features depending on the classification result. Therefore, they use a search algorithm to find a feature set leading to an optimal classification result. This method optimizes over the whole search room, however, depending on the search algorithm, not necessarily the global optimum (maximal recognition rate) is found. Examples for search algorithms are the Genetic Algorithm (GA) and Simulated Annealing.

In this thesis, a filter and a wrapper method were used for optimizing the sensor positions. For the filter method, the MIFS algorithm was used which includes the correlation between features (Min-Redundancy). Including the correlation is necessary for this problem as neighbouring sensors are highly correlated. For the wrapper method, a Genetic Algorithm was used.

6.2.1. Input Data for the Optimization

For optimizing the sensor positions, simulated data as described in Chapter 5 was used. The strain pattern of ten different body postures was calculated. The used body postures and the strain patterns are visualized in Appendix B.

For a given posture, the simulation resulted in a unique strain pattern (also in several runs). Therefore, one data set was available per posture (class) and noise was added to simulate variation in the data. An equally distributed noise of $\pm 5.5\%$ was added. This value was chosen as the total mean error of the sensor was $\pm 5.5\%$ as shown in Chapter 3. The biggest portion to this amount of error was caused by the hysteresis and the dependance on the strain rate as can be seen in Fig. 3.8. If an equal distribution of the strain rate is assumed, every path in Fig. 3.8 is passed equally often and also the recorded resistance values for a given strain appears approximately equally frequent. Therefore, an equal distribution of the noise was selected. After adding the noise, negative strain values were set back to 0% as the physical strain sensor cannot measure negative strain. In order to prevent problems in the subsequent calculations (when setting values to zero, a mean and standard deviation of zero is possible causing problems in the Naïve Bayes

classification (Equation 4.1)) normally distributed noise was added to the zero values.

That way, an additional set of 99 strain patterns was generated for each posture, resulting in 100 samples per posture. Therefore, a total of 1000 samples was used for the optimization, equally distributed among the ten classes. This data set was used for both optimization methods (MIFS and GA).

6.2.1.1. Data Reduction

For the Genetic Algorithm it turned out that using all 1500 features resulted in a computationally expensive algorithm. The reason was probably a weak optimum so that the algorithm converged slowly. Additionally, a time-consuming leave-one-out cross-validation¹ was used. Therefore, the data was reduced. In Section 7.2, it will be shown that a shift in the sensor positioning of up to 11cm reduced the classification result by less than 3%. This small drop indicates that taking an equally distributed subset of the sensors is valid.

For reducing the data, neighbouring sensor positions on the back were combined. This was realized by selecting an equally distributed subset of the potential positions (see Fig. 6.1). To each original sensor position p_i , the closest position of the subset was assigned building virtual regions around each point of the subset. The mean strain value of each region was then assigned to the position of the subset. Thus, beside data reduction, this step also filtered the data. The data reduction can be summarized as follows:

1. Select an equally distributed subset s_i of the sensor positions p_i .
2. Assign each potential sensor position p_i to the closest subset sensor position s_i .
 - For each p_i find the closest s_i
 - Assign p_i to the closest s_i : $S_i = \{S_i, p_i\}$
3. For each s_i , the mean strain value of all assigned sensor positions p_k is calculated: $strain_{s_i} = \frac{1}{size(S_i)} \sum_{k=1}^{size(S_i)} strain_{p_k}$

¹leave-one-out cross-validation: The data is split into $(n - 1)$ training and one test sample where n is the number of samples. Every sample is used once for testing so that n classification steps are necessary. In a last step, the mean of the n classification results is taken.

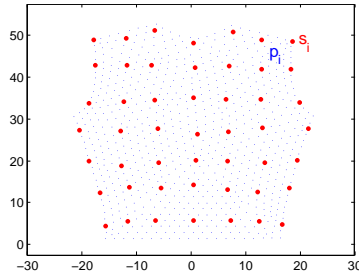


Figure 6.1. The reduced set of potential sensor positions (s_i , shown in red) is shown in relation to the total set of simulated positions p_i .

In Fig. 6.2, the sensor numbers of the subset are shown for further reference.

Note: The data reduction was applied before adding noise (directly to the 10 simulated postures), in order not to refilter out the noise.

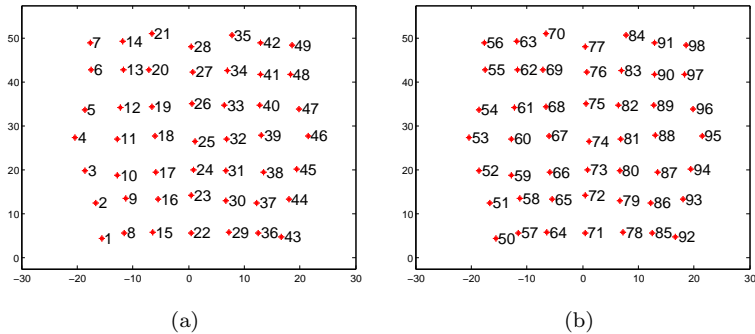


Figure 6.2. The defined sensor numbers of the reduced set of potential sensor positions are shown. The numbers shown in Fig. 6.2(a) represent the sensors in horizontal direction, in Fig. 6.2(b) the ones in vertical direction.

6.2.2. Mutual Information Feature Selection (MIFS)

MIFS is a feature selection algorithm which examines the information value of the feature and also considers the correlation between

the features [17]. This should prevent the selection of similar (highly correlated) features.

The information value of each feature is calculated using mutual information. The mutual information between a class and a feature is calculated as

$$I(c, f) = P(c, f) \log\left(\frac{P(c, f)}{P(c)P(f)}\right), \quad (6.1)$$

where $P(c)$ is the probability of a certain class c , $P(f)$ is the probability of feature f , and $P(c, f)$ is the joint probability of f and c . Using $I(c, f)$, the mutual information of a feature f can be calculated by summing (discrete case) over all classes c (the set of all classes c is defined as C):

$$I(C, f) = \sum_c I(c, f) \quad (6.2)$$

From this value, the weighted Mutual Information (MI) between the feature and all already selected features is subtracted which is calculated as

$$I(F_s, f) = \sum_{f_s} I(f_s, f), \quad (6.3)$$

where f_s is one selected feature and F_s are all selected features.

The features with the highest weighted difference between Equation (6.2) and (6.3) are selected according to the following procedure [17]. This is called MIFS algorithm.

1. F is a set of all features, F_s a set of the selected features (empty at the beginning).
2. Calculate $I(C, f)$ for each feature $f \in F$.
3. *Find the first feature:*
 - Find f which maximizes $I(C, f)$.
 - Remove f from F : $F = \{F \setminus f\}$
 - Add f to F_s : $F_s = \{F_s, f\}$
4. *Find further features:*
 - Calculate $I(f, F_s)$ for all f .
 - Find $f \in F$ which maximizes $I(C, f) - \beta \cdot I(F_s, f)$
 - Remove f from F : $F = \{F \setminus f\}$

- Add f to F_s : $F_s = \{F_s, f\}$

5. Repeat step 4 until the number of required features is selected.

β is a weighting factor of the correlation between the features. The bigger β , the more is the MI penalized by the correlation between the features. In literature, β is usually chosen between 0 and 1. For the results described in section 6.3.1, a β of 0.4 was used.

6.2.3. Genetic Algorithm

The Genetic Algorithm was first mentioned in 1975 by Holland [52]. Since then it has evolved to a popular search algorithm which is classified as a global search heuristic. As indicated by its name, the algorithm was inspired by the principle of natural evolution:

- The information to be optimized is coded in a gene-like string of ones and zeros,
- and "child" populations emerge by inheritance, mutation, selection, and crossover.

The fittest children survive and can build new populations. With this principle, the population gradually improves until an optimum is reached. The decision of who survives is based on a fitness function which can be an arbitrarily chosen function. In the present problem of sensor position optimization, the fitness function was chosen to be the recognition rate of the body postures (Naïve Bayes classifier (Equation 4.1) with a leave-one-out cross-validation where each sample was once used for testing) corrected by the weighted number of selected sensors [88]. This correction was added for the GA to select a minimal set of sensors. The weighting factor was chosen as 0.01 so that a good classification result was preferred over a minimal set of sensors:

"fitness = leave-one-out classification result - 0.01 * number of selected sensors".

The Genetic Algorithm has some major advantages over other search algorithms:

- By looking at populations, the algorithm works in parallel on a set of potential solutions. Therefore, the chance of finding a global maximum is increased.

- Beside a fitness function, no other additional information is required.
- GAs use probabilistic transition rules [46], contributing to the algorithm's robustness.

A weakness of the GA is that it can converge to a local maximum. Once converged, the population can only find better solutions by mutation (random search) which scans the search space slow compared to inheritance and crossover of populations [23].

Genetic Algorithms have quite a big number of parameters one can influence. However, the mechanism of a GA is so robust, that in our analysis the result was stable for a wide range of parameters. Therefore, the choice of parameter was not a crucial factor. In this thesis, the following parameters were used (only the most important parameters are shown):

number of individuals: In each generation step, the population size was 60 individuals.

number of generations: 70 generation steps were performed.

method for crossing: In each generation step, the crossing between individuals was performed with a "mask"-method. This means that a random mask (containing ones and zeros) was generated of the length of an individuuum. Wherever the mask contained a one, the genes of one parent individuuum were taken, where it contained a zero, from the other parent.

reinsertion method: In order to prevent losing good individuals, usually the best parent individuals survive (instead of only the children). There are different methods whereas in this thesis the " $(\mu + \lambda)$ - strategy" was used. This is a method where all individuals of the parent and the child population are put together and the best half is chosen for further inheritance.

mutation rate: The mutation rate was chosen such that on average one gene per individual and generation was mutated.

Further information about Genetic Algorithms can be found in [46].

6.3. Results and Discussion

6.3.1. Mutual Information Feature Selection

In Fig. 6.3, the selected sensor positions are shown when selecting the best 4, 6, 8, and 10 features according to MIFS. From this it can be seen that the sensors in the armpit region in horizontal and vertical direction are the most relevant ones (see Fig. 6.3(a)). When selecting more sensors, sensors in vertical direction on the side of the body are selected additionally to the ones in the armpit region (Fig. 6.3(b)). For the results in Fig. 6.3, a β of 0.4 was used.

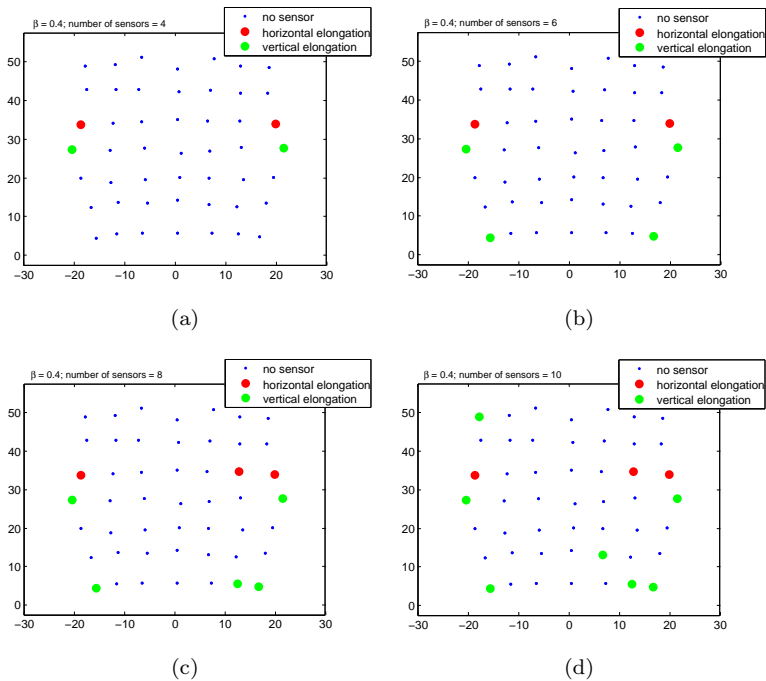


Figure 6.3. Result of the MIFS algorithm ($\beta = 0.4$) when selecting 4, 6, 8, and 10 sensor positions ((a), (b), (c), and (d) respectively). Therefore, the sensor positions in the armpit region are the most relevant ones (see Fig. 6.3(a)).

Using the selected best sensor positions, a classification was performed based on the data described in Section 6.2.1. In Fig. 6.4, the recognition rates for different β and number of sensors are shown using a Naïve Bayes classifier (Equation 4.1) with a leave-one-out cross-validation. This Figure shows that with the first four selections, a fast improvement of the recognition rate is achieved. After that, the improvement slows down until with 10 sensor positions a recognition rate of almost 100% is achieved for all β between zero and one. For more than 10 sensor selections, the recognition rate remains at 100% except for a "beta" of one where a small decrease can be noticed. The reason for this decrease is an overvaluation of the correlation between the features meaning that minimizing the correlation between features is weighted more than a "good" feature with a high Mutual Information. Selecting features with a low information value can lower the recognition rate.

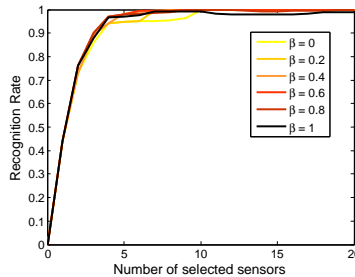


Figure 6.4. Recognition rates for different β and number of sensors.

6.3.2. Genetic Algorithm

The Genetic Algorithm was applied 60 times (60 runs) to the reduced data set described in section 6.2.1. The improvement in the recognition rate is shown in Fig. 6.5 for 10 exemplary runs. From this plot it can be seen that a fast improvement is achieved: After about 20 generations, all runs achieve an optimal result of 100% recognition rate.

The result of the Genetic Algorithm was not ONE optimal result, but different combinations of "good" sensors. In Fig. 6.6, the number of occurrences of each sensor position over all 60 runs are shown whereas the numbers on the x-axis corresponds to the sensor numbers shown in Fig. 6.2. It is apparent that five sensor positions (5, 46, 53, 85, and 95) are selected in almost all runs. Additionally to these five sensors,

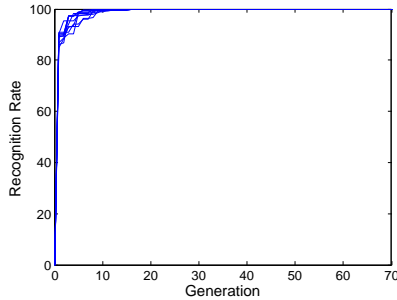


Figure 6.5. Improvement of Genetic Algorithm (ten example runs). The algorithm improved quickly in the first 10 generations.

a varying set of other sensors is chosen in order to achieve the 100% recognition rate. In Fig. 6.7, all selected positions are represented by a red (horizontal measurement direction) and green (vertical measurement direction) point. The cumulative number of selections of each position is encoded in the size of the points.

From these plots, the relevant sensor positions can be determined:

- In **horizontal direction**, the most important sensor positions are in the middle level of the back, particularly on both sides of the body close to where the sleeves are attached.
- In **vertical direction**, two distinct positions are on both sides in the armpit region. Additionally, it is also important to measure in the lower back region (lowest row of sensors).

In Fig. 6.8, the different selected combinations of sensor positions are shown for 60 runs of the GA. From this it can be seen that some sensor positions complete one another, meaning that often at least one of them is selected. This indicates, that there is no perfect position but good sensor regions as it was implicitly assumed in Section 6.2.1.1 when the data was reduced. Examples of such completing sensor positions are shown in Table 6.1.

In Fig. 6.9, the recognition rate for a varying amount of most frequently chosen sensor positions is shown. It can be seen that with five and more sensors, an almost perfect classification result can be achieved.

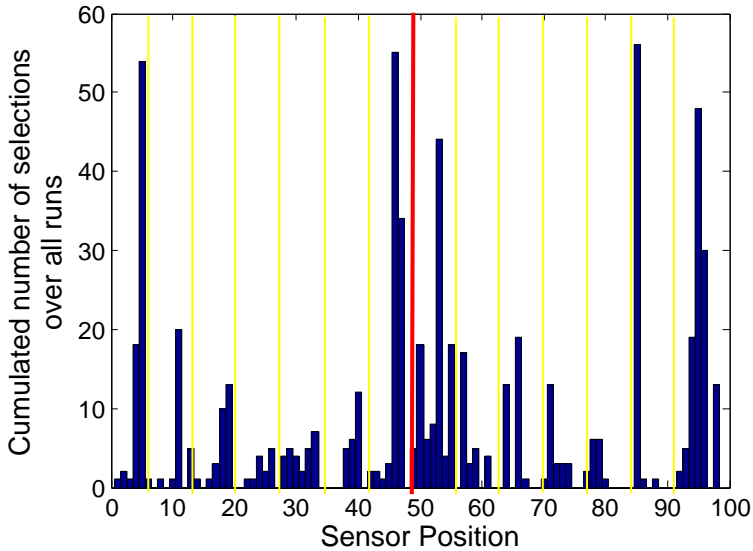


Figure 6.6. This plot shows the number of selections of each sensor position (corresponding to the numbers introduced in Fig. 6.2) during 60 runs of the GA.

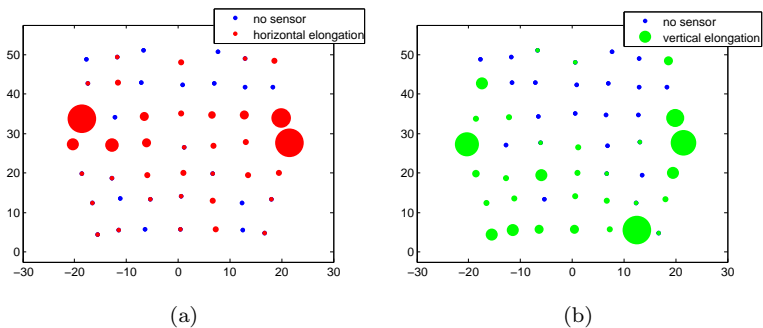


Figure 6.7. All selected sensor positions by the Genetic Algorithm during 60 runs. The size of the points corresponds to the number of selections. In Fig. 6.7(a), the selected sensors in horizontal and in Fig. 6.7(b) in vertical direction are shown.

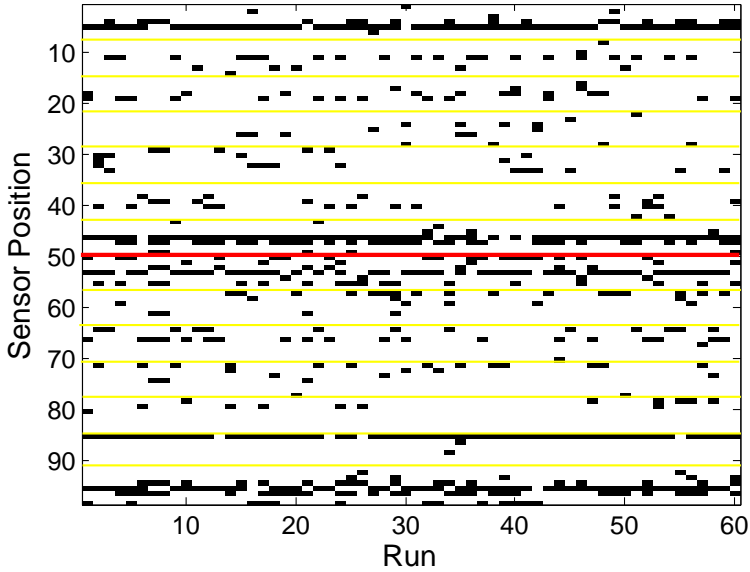


Figure 6.8. Combinations of selected sensor positions by the Genetic Algorithm. The numbers on the y-axis represent the sensor positions as shown in Fig. 6.2. The red line splits the sensors arranged in horizontal direction (1-49) from those in vertical direction (50-98). Along the x-axis, different runs of the GA are shown.

Table 6.1. Sensor positions where often at least one of them was selected and their occurrence (in %) in 60 runs of the GA.

Sensor numbers	Appearance during 60 runs (in %)
4, 5	98.3
46, 47	95
53 - 55	93.3
95, 96	95
50, 85	96.7

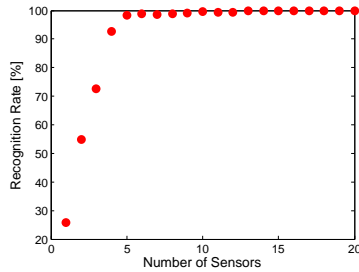


Figure 6.9. Recognition rate when selecting the best x sensors.

6.4. Conclusions

When comparing the results of the MIFS and the GA algorithm, they were quite similar. Both of them found the most relevant sensor positions to be in the armpit region, in both - horizontal and vertical - direction. Therefore, both of them can be used for optimizing the sensor positions on a strain sensitive clothing. However, there are also some differences and restrictions for each method:

MIFS MIFS reached the highest possible recognition rate, however, the quality of the result depends on the choice of β : If β is chosen "too large", uncorrelated sensor positions are selected (including "bad" positions) which can lead to a decrease in the recognition rate after a first increase. If β is chosen "too small", correlated sensors are selected such that the sensor set is not minimal. These effects were not very distinct in the presented results (see Fig. 6.4) as the sensor set was reduced to 98 positions before selection (see Section 6.2.1.1). With the original 1500 positions, these effects can be better seen (see Fig. 6.10).

In return, the MIFS was computationally fast (The MIFS used about ten seconds on a Pentium®4 CPU 2.8GHz, the GA 20 hours on a Sun Fire X4600 2.8GHz. Both implementations were not optimized for speed.)

GA The GA always found a result with 100% recognition rate. Adding the corrections to the fitness function as described in Section 6.2.3 reduced the selected number of sensors by a factor of about two to three (the number of selected sensors decreased from around 20 to 30 down to 10) while keeping the 100% recognition rate.

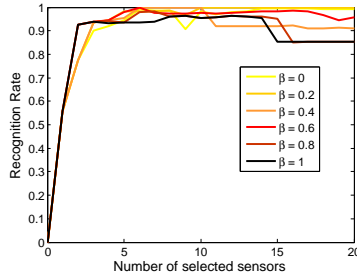


Figure 6.10. Recognition rate using MIFS when applying it to the original feature set of 1500 sensor positions.

From this result, the number of sensors could further be reduced, however, resulting also in a slightly lower recognition rate (trade-off). With 5 sensors, a recognition rate of 98.4% was achieved (see Fig. 6.9). When further reducing the number of sensors, a large drop was found (92.6% for 4 sensors). Hence, at least five sensors should be used in order to achieve a high recognition rate.

7

Sensitivity Analyses using Simulated Strain Patterns

In the previous Chapter, an optimal set of sensors was determined for one subject leading to recognition rates of almost 100%. However, what happens if the sensors are placed differently, one of the sensors fails, or the shirt moves? Does the method of recognizing the body posture with a strain sensitive garment still work for a person with different body proportions? These questions are answered in this Chapter.

7.1. Introduction

In this Chapter, several sensitivity analyses are presented to show the robustness of recognizing the body posture with a strain sensitive garment. In Section 7.2, the sensitivity of the sensor placement is analyzed. This is followed by an analysis on the influence of sensor failures on the classification result (Section 7.3). One of the major issues when using a strain sensitive clothing is a good fixation of the clothing at the arms and the hip. In Section 7.4, an upwards shift of the garment at the waist level is analyzed. In the last Section 7.5, it is shown whether the method of recognizing the body posture with a strain sensitive garment works for a person with different body proportions.

For the analyses, a small (5 sensors, Fig. 7.1(a)) and a large (20 sensors, Fig. 7.1(b)) set of sensors was used. The positions are the 5, respectively 20 best sensor positions according to the Genetic Algorithm (see Section 6.3.2).

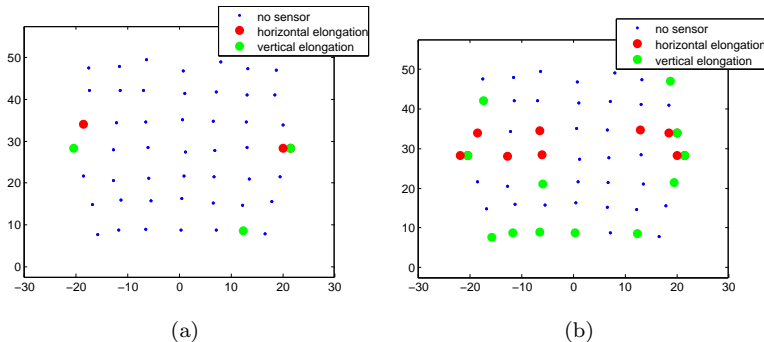


Figure 7.1. Best sensor positions according to the Genetic Algorithm (see Section 6.3.2). In this Chapter, the 5 (Fig. 7.1(a)) and the 20 (Fig. 7.1(b)) best sensor positions were used.

The same data as described in the Section 6.2.1 was used: The data set included 1000 samples from ten different posture classes (100 samples per class). In all examinations of this Chapter a Naïve Bayes classifier (Equation 4.1) was utilized to categorize the data.

For better comparison of the different influence factors, the relative

change of each analysis was calculated:

$$\text{relative change} = \frac{cr(original) - cr(adapted)}{cr(original)}, \quad (7.1)$$

where $cr(original)$ is the classification result of the original analysis, and $cr(adapted)$ the classification result when one of the parameters is changed.

7.2. Sensitivity of Sensor Placement

7.2.1. Method

With the Genetic Algorithm, the optimal sensor positions were calculated (see Section 6.3.2). However, it is not clear how accurate the sensors need to be placed on the garment in order to achieve the "best" possible recognition rate. Therefore, the influence of the sensor placement on the classification result was analyzed. For this analysis, the five best sensors were used (see Fig. 7.1(a)). Each of the sensors was shifted separately between 1cm and 11cm , while the other sensors were held constant. They were shifted in eight directions (see Fig. 7.2, $x_1 - x_8$). Where possible, the strain value at these positions was calculated by interpolation (less directions were used for border points) and the classification results were determined. A leave-one-out cross-validation was used, using the shifted sensor values for training and testing. In a last step, the mean value of these classification results was taken:

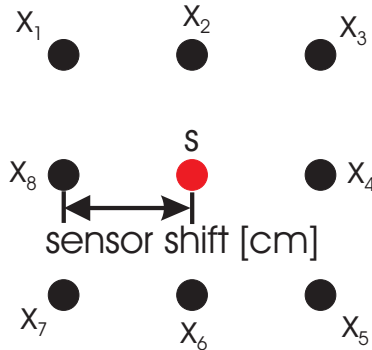


Figure 7.2. Positions where the sensor was shifted to ($x_1 - x_8$). The shift was varied between 1cm and 11cm .

$$\text{mean recognition rate} = \frac{1}{n} \sum_{i=1}^n cr(x_i), \quad (7.2)$$

where n is the number of neighbours, cr the classification result when using the shifted sensor position x_i .

7.2.2. Results and Discussion

In Fig. 7.3, the classification result is shown in relation to the shift in the sensor placement. It can be seen, that even a quite large shift of 11cm causes a drop in the recognition rate of less than 3% (relative change of 0.03) when using a Naïve Bayes classifier to distinguish between ten postures. These results show that the influence of the exact positioning has a much lower influence on the classification result compared to other effects (e.g. shift of the shirt as presented in Section 7.4). This indicates that the positioning of the individual sensors is not the most limiting factor.

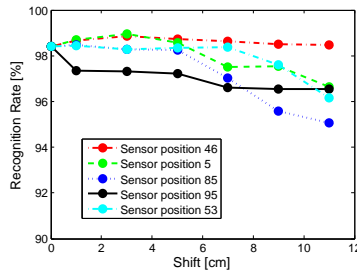


Figure 7.3. Recognition rate when shifting the sensor position. The sensors shown in Fig. 7.1(a) were shifted (sensor numbers 5, 46, 53, 85, and 95 in Fig. 6.2).

7.3. Effect of Sensor Failure on Classification Result

7.3.1. Method

Although the sensors worked reliable during usage (Chapters 3 and 4), it can happen that they fail. One of the main reasons is an over-stretching of the sensor: If the sensor is stretched to more than 80%,

the probability of breaking increases. A second reason is the connection between the sensor and the textile thread (see Fig. 3.2(b)): It can happen that cracks appear in the conductive glue causing a failure of the connection. Out of this reason, the effect of sensor failures on the classification result was analyzed. This was done on the 5 and 20 best sensors (see Fig. 7.1). All combinations of sensor failures were considered resulting in 31 combinations

$$\text{number of combinations} = \sum_{k=1}^n \binom{n}{k} \quad (7.3)$$

for the 5 best sensors ($n = 5$), respectively 1'048'575 for the 20 best sensors (Equation 7.3, $n = 20$). The mean, standard deviation, and minimal and maximal values of the classification results were calculated.

Two different classification strategies were performed:

1. The reduced set of sensors was used for training and testing (leave-one-out cross-validation). This simulates the case when the shirt is retrained after a failure showing whether the shirt can still be used with the broken sensor(s) without any replacement.
2. The training was performed on the sensor set without any failures, the testing on the reduced set while the strain value of broken sensors was set to zero. Setting sensor values to zero was done under the assumption that broken sensors can be recognized. Training on the full set and testing on the reduced sensor set corresponds to the more realistic case (than 1.) of a sensor failure during usage and no retraining of the shirt.

7.3.2. Results and Discussion

In Figs. 7.4 and 7.5, the mean recognition rate, its standard deviation, and the minimal and maximal recognition rates are plotted against the number of failures. In Figs. 7.4(a) and 7.5(a), the five best sensor positions are used for the analysis while the 20 best sensor positions are employed in Figs. 7.4(b) and 7.5(b).

The last data point in these Figures always has a value of 10%. The reason is that a classification with zero sensors (all failed) leads to a random recognition resulting in 10% correct classifications (10 classes).

The analysis in Fig. 7.4 shows the results when the reduced set of sensors is used for training and testing. It can be seen, that the

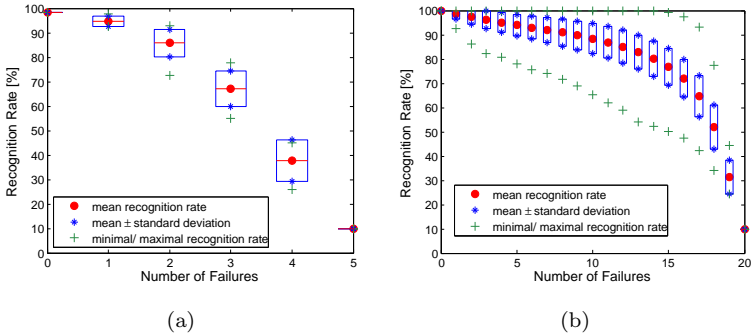


Figure 7.4. The mean recognition rate, its standard deviation, and the minimal and maximal recognition rates are plotted against the number of failures. The reduced set of sensors was used for training and testing. In Fig. 7.4(a), the five best sensor positions were used for the sensor failure analysis, in Fig. 7.4(b) the 20 best sensor positions.

recognition rate drops fast when five sensors are used (Fig. 7.4(a)): The first failure causes a drop of 3.6% in recognition (from 98.4% to 94.8%), the second failure a drop of another 9% (94.8% to 85.8%). This means that when using five sensors, each sensor is important. On the other side, when a set of 20 sensors is used (Fig. 7.4(b)), the classification rate drops much slower. It still can drop quite fast (see the minimum values in Fig. 7.4(b)), however, the mean value decreases slowly: Ten sensor failures still result in a mean recognition rate of 88.4%.

Therefore, a larger sensor set than minimally necessary to achieve a good recognition rate should be placed on the garment so that a shirt with broken sensors can still be used after a retraining.

In Fig. 7.5, the results of a failure during usage are shown. The classifier was trained on the data containing all 5, respectively 20 sensor values and tested on the data where the strain values of the broken sensors were set to zero. In comparison to Fig. 7.4, the recognition rate drops much faster. However, again the drop is much slower per sensor failure when using more sensors. The relative changes are summarized in Table 7.1. Even if the same percentage of sensors fail (4 when using 20 sensors compared to 1 when using 5), the recognition rate is better when using 20 sensors. This can be explained by the larger redundancy

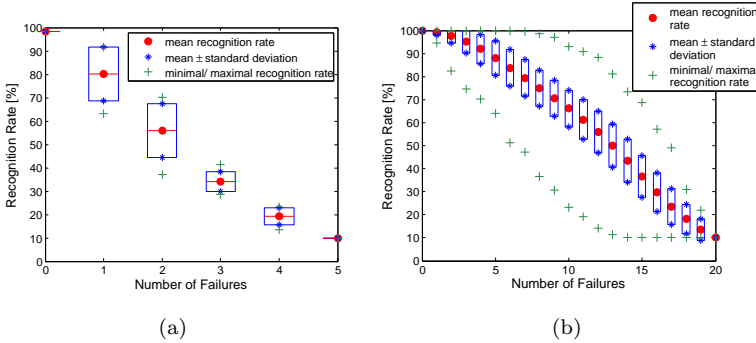


Figure 7.5. The mean recognition rate, its standard deviation, and the minimal and maximal recognition rates are plotted against the number of failures. The classifier was trained on all 5, respectively 20 sensors and tested on the data where broken sensors were set to zero. In Fig. 7.5(a), the five best sensor positions were used for the sensor failure analysis, in Fig. 7.5(b) the 20 best sensor positions.

Table 7.1. Relative changes in the recognition rate when one sensor fails.

rel. change	without retraining	with retraining
5 sensors	0.037	0.185
20 sensors	0.0123	0.0065

in the sensor data so that less information is lost compared to using only 5 sensors.

Therefore, to prevent large drops in the recognition rate due to sensor failures while in usage (no retraining), the set of sensors should not be minimized.

When looking at the maximal and minimal values in Fig. 7.5(b) there is a large range. This means that some sensors can fail without reducing the recognition rate. On the other hand, the recognition rate can drop down to e.g. 50% if the best six sensors fail. With a retraining, the recognition rate can be improved to 80% (see Fig. 7.4(b)) and the garment can still be used with an acceptable recognition rate.

7.4. Upwards Shift of Shirt at Waistline

7.4.1. Method

Shifting of the shirt is a crucial factor restricting the accuracy of a posture recognition with strain sensitive clothing. Therefore, the influence of an upwards shift at the waist level is discussed in this Section. New simulations were performed as described in Chapter 5 with the fix points at waistline (see Section 5.3.5) defined higher at the body (shift of 1cm, 2cm, and 3cm). A shift of 2cm is visualized in Fig. 7.6. Based on the new simulation results (strain values), the recognition rate was calculated for the small and the large sensor set (see Fig. 7.1).

The sensor positions were kept constant on the shirt, meaning that they also shifted upwards with the clothing.

A Naïve Bayes classification was performed, using the original strain values for training and the ones after the upwards shift for testing.

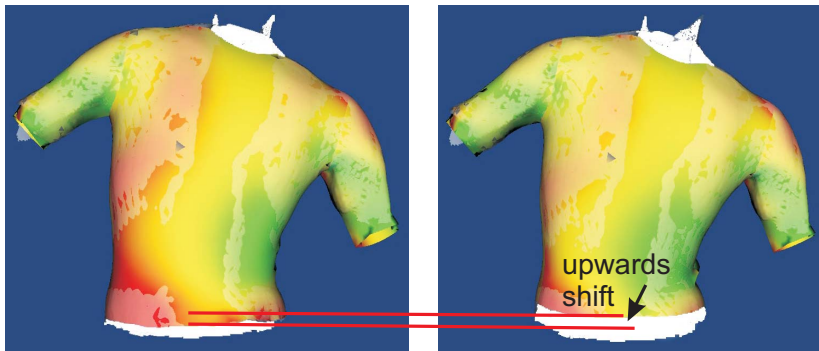


Figure 7.6. Visualization of a shift of 2cm of the shirt at the waistline.

7.4.2. Results and Discussion

In Fig. 7.7, the influence of the shift is shown for shifts up to 3cm. It can be seen that when only five sensors are used, the recognition rate drops by more than 30% when the shirt moves by 3cm. Even for a smaller shift of 1cm, the recognition rate drops by 10%. However, if more sensors are placed the recognition rate is generally higher, confirming the statement of Section 7.3 that a larger than a minimized sensor set should be chosen. When using 20 sensors, the drop can be

reduced to 1.7% (98.3%) for a shift of 1cm . The relative changes are summarized in Table 7.2 Therefore, additionally to using a not minimized set of sensors, it is recommended to fix the shirt at the waist level such that it moves less than 1cm .

Table 7.2. Relative changes in the recognition rate when the shirt shifts at waist level.

rel. change	shift of 1cm	shift of 3cm
5 sensors	0.088	0.336
20 sensors	0.017	0.215

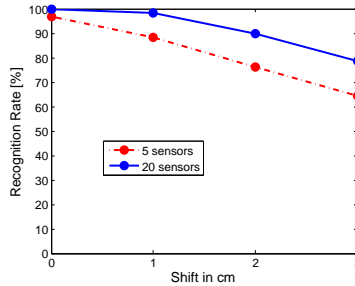


Figure 7.7. Classification results for a shift at the waistline of up to 3cm for the small and the large sensor set (see Fig. 7.1).

To obtain a deeper insight into the reason of the drop in the recognition rate, the recognition rates for each posture are shown in Figs. 7.8 and 7.9. It can be seen that some of the postures are still recognized almost perfectly (e.g. posture 1, 2, 4, 8, and 9, see Appendix B) whereas e.g. postures 3 or 6 cannot be recognized at all. This seems reasonable as the postures which could not be recognized tend to be those with the major strain in vertical direction in the lower back. When shifting the shirt upwards, these strain values are changed and the recognition fails. On the other hand, the postures still recognized well are basically those incorporating the arms (arms forward, arms upwards). Postures of the arms result predominantly in strain in horizontal direction in the upper back, which is not influenced by an upward shift of the shirt, so that these postures can be recognized.

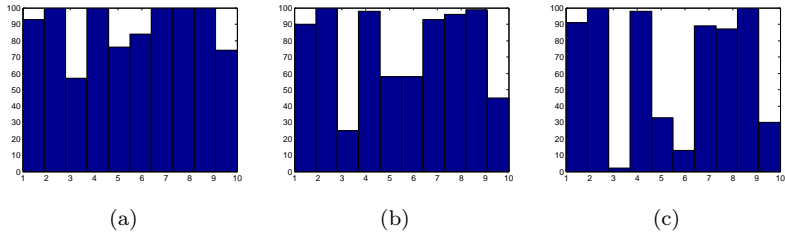


Figure 7.8. Recognition rate of each posture using the 5 best sensors (Fig. 7.1(a)). Fig. 7.8(a): Shift of 1cm, Fig. 7.8(b): Shift of 2cm, Fig. 7.8(c): Shift of 3cm.

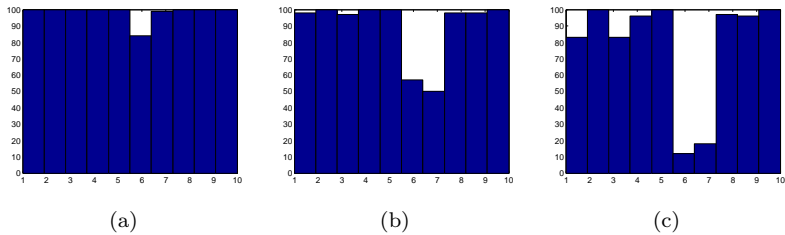


Figure 7.9. Recognition rate of each posture using the 20 best sensors (Fig. 7.1(b)). Fig. 7.9(a): Shift of 1cm, Fig. 7.9(b): Shift of 2cm, Fig. 7.9(c): Shift of 3cm.

7.5. Does Posture Recognition Still Work for Different Body Proportions?

7.5.1. Method

To show that recognizing different body postures with a strain sensitive garment is not restricted to a standardized body, the abdominal girth of the body model was altered from 86cm to 111cm (see Fig. 7.10(a)). With this body model, the same 10 postures as with the original model were generated and used for calculating the strain patterns (the resulting strain distributions are shown in Appendix D).

A classification was performed using the same sensor positions as for the standardized body (see Fig. 7.1). The strain values calculated

with the adapted body model were used for training and testing (leave-one-out cross-validation).

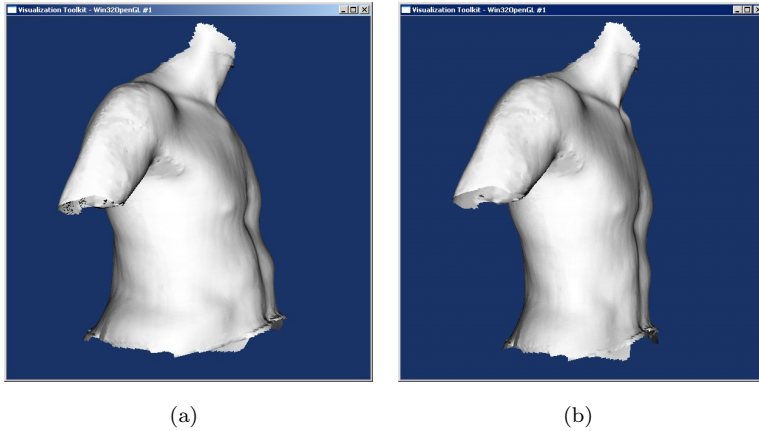


Figure 7.10. Fig. 7.10(a): body model with a bigger abdominal girth (used in this Section); Fig. 7.10(b): original body model for comparison.

7.5.2. Results and Discussion

The classification results are plotted in Fig. 7.11 up to the best 20 sensors. This can be directly compared to Fig. 6.9 which contains the values calculated for the original body proportions.

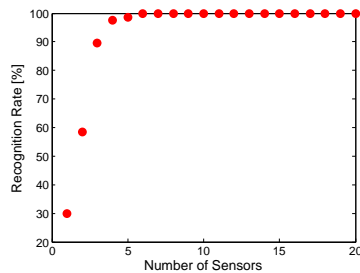


Figure 7.11. Recognition rate when selecting the best x sensors.

When comparing these two Figures, they look similar. The recognition rates of the original body proportions are even slightly lower, particularly when using 3 sensors (89.7% vs. 72.6%). Therefore, the method of recognizing different body postures using a strain sensitive garment worked for a tested range of the abdominal girth of 86cm to 111cm.

	20 best sensors	5 best sensors
adapted body posture	100.0%	98.5%
original body posture	99.9%	98.4%
relative change (Eq. 7.1)	0.001	0.001

Additionally, from the similar recognition rates it can be concluded that the same sensor positions can be used as calculated for the original body model, meaning that the optimization of the sensor positions has to be done only once for a specified set of body postures.

However, the strain sensitive garment should be trained on each person separately: When using the strain values of the original model for training and the ones calculated with the adapted body model for testing, the recognition rate drops to 80.8% when using the best 20 sensors, respectively to 73.8% for the best five sensors.

7.6. Conclusions

In this Section, several sensitivities of the model were analyzed. From these analyses, the following conclusions can be drawn:

- The exact positioning of the sensors is not a critical factor when detecting body postures with strain sensors. A shift of up to 11cm of a single sensor reduces the recognition rate by less than 3% (relative change of 0.03).
- The sensor set should not be minimized such that sensor failures do not have a major effect on the classification result: When using 20 sensors, the relative change of one sensor failure was reduced to 0.0065 compared to 0.185 when using 5 sensors (with retraining).
- The shirt should be fixed at the waist level in a way that it moves less than 1cm. Otherwise, postures incorporating bending of the back (in any direction) cannot be recognized: A shift of 3cm of

the shirt at waist level caused a relative change in the recognition rate of 0.215 (20 sensors).

- Using a strain sensitive garment to recognize the body posture worked for different body proportions: The abdominal girth was varied between 86cm and 111cm (relative change of 0.001). The same sensor positions can be used which has the advantage that the optimization has to be done only once for a specified set of body postures.

8

Conclusions

8.1. Achievements

Recognizing different body postures with textile integrated sensors enables an unobtrusive posture detection not interfering with the user. This allows longtime-measurements and opens new applications in sports, rehabilitation, or prevention. By continuously measuring the posture of the wearer, an immobile sitting posture could be detected and a feedback given. This could help preventing back pain. Also rehabilitation exercises could be monitored enabling a feedback on the performance.

The goal of this thesis was to build and validate a textile approach of recognizing the body posture. Measuring the strain in the garment for detecting the body posture appeared to be a promising approach. Textile strain sensors were slowly emerging whereas other sensor technologies were far away from being "textile" like e.g. accelerometers or bending sensors.

During the PhD studies, the following contributions have been made to approach the goal of a textile body posture measurement system:

- A reference measurement method was developed to measure

strain patterns in the clothing. The precision when using 6mm circle markers was better than 1mm . With a marker distance of 5cm , the achieved accuracy of the strain patterns was better than 2% ($\frac{1\text{mm}}{50\text{mm}} = 0.02$). This reference measurement method enabled the determination of how and by how much clothing is stretched at different body postures. Furthermore, requirements for the textile strain sensor were defined.

Using this method, the following conclusions were drawn:

- Different strain patterns were measured implying that a body posture detection by measuring strain is feasible.
 - The strain sensor should cover a measurement range of at least 20% plus a certain pre-strain. However, as even larger strain can appear, the sensor range should be larger or it should be protected against overstretching. Furthermore, the elastic force of the sensor should be in the range of the textile it is used for and it should be washable.
- A textile strain sensor was developed together with EMPA. The sensor consists of a thermoplastic elastomer and is filled with $50\text{wt-}\%$ carbon black. It was attached to the garment with a silicone film which resulted in a working range of 70% strain. The sensor properties of this garment attached strain sensor were studied: The relaxation behaviour, hysteresis, strain rate dependency, longtime cycling behaviour, and ageing effects were characterized with a strain tester and a multimeter. The total mean error was $\pm 5.5\%$ in strain. The sensor was washed 8 times which neither influenced its electrical properties nor its visual appearance.
 - A prototype was built by attaching 21 strain sensors to the garment. This prototype was used for an experiment where 27 upper body postures were recognized. It turned out that a user-specific training is necessary. This resulted in a recognition rate of 97% .
 - A model to describe the strain in the garment for different body postures and body proportions was developed. It was based on an already published model [104] but had to be adapted in order to work with tight-fitting garments.
 - Using simulation results of this model, the sensor positioning was optimized using Mutual Information Feature Selection and a Genetic Algorithm. A minimal sensor set of 5 sensors and a set of

20 sensors were selected to be used for further analyses. It was shown that better results can be achieved with the larger sensor set. The most restricting factor turned out to be a shifting of the clothing at waist level (relative change in the recognition rate of up to 0.336). Therefore, it should be ensured that the garment does not shift when detecting body postures with strain sensors.

In conclusion, this thesis shows the feasibility but also limits of recognizing body postures with a strain sensitive garment.

8.2. Outlook

In this PhD thesis, a prototype of a strain sensitive garment to detect body postures was presented. This prototype has the basic functionality, however, there are still many improvements required in order to achieve a reliably functioning product. Some aspects where further research is necessary, are discussed in the following paragraphs.

- So far, the sensor was attached to the textile with a silicone film. This is not satisfactory for mass production. Therefore, a full integration into the textile is necessary. When integrating the presented sensor into the textile, it has to be assured that a restoring force is present, forcing the sensor back to its original length. Also the connecting "cables" to the hardware need to be integrated and the electrical contacting to the sensor should be examined to become mass producible.
- Using a simple linear approximation, the strain sensor had an error of $\pm 5.5\%$. By using a more advanced model, a further reduction of this error is possible.
- A further research topic is to proceed from static postures to dynamic movement measurements. This would require that a distinction between all possible body postures is possible (not "only" 27 as tested in Chapter 4). However, so far it is not clear whether each possible posture has a unique strain pattern. This would first have to be confirmed.
- It was shown that a shifting of the garment at the waist level caused the largest drop in the recognition rate. Therefore, designs or methods need to be developed to prevent or minimize this shifting.

- So far, the functioning of the prototype was shown in a study where 8 persons performed 27 upper body postures. More application oriented studies can be conducted e.g. in sports or rehabilitation.
- Body posture detection with strain sensors is limited in the accuracy (e.g. shifting). Also tight-fitting garments is not everyone's cup of tea. Therefore, it might be better finding other methods (e.g. using accelerometers [5, 50]) and putting more effort in their textile integration. First approaches can be found e.g. in [48].

A

Strain Patterns Measured with Reference Method

In Chapter 2, a reference strain measurement method was presented using an optical tracking system. The measured strain patterns are shown in this Appendix.

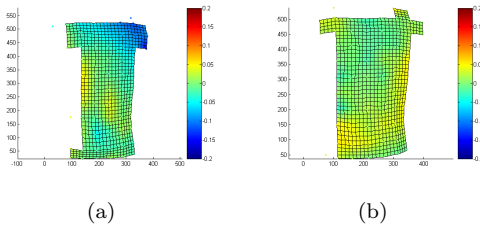


Figure A.1. Rotation of trunk to the right. Fig. A.1(a): strain in horizontal direction, Fig. A.1(b): strain in vertical direction.

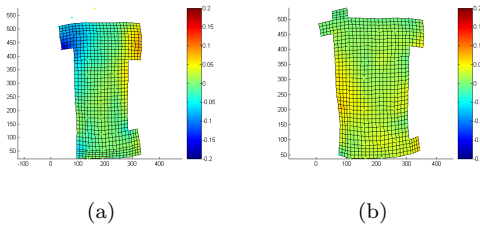


Figure A.2. Rotation of trunk to the left. Fig. A.2(a): strain in horizontal direction, Fig. A.2(b): strain in vertical direction.

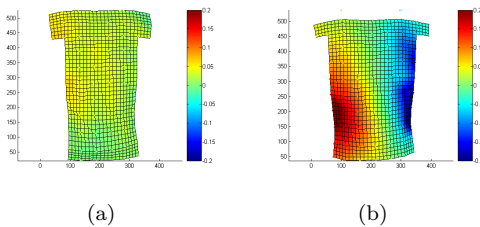


Figure A.3. Bending trunk sideways to the right. Fig. A.3(a): strain in horizontal direction, Fig. A.3(b): strain in vertical direction.

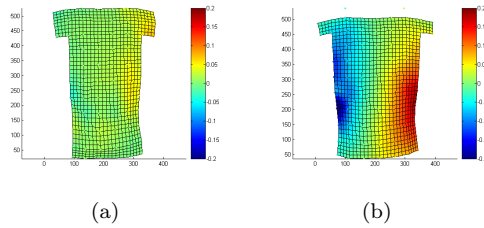


Figure A.4. Bending trunk sideways to the left. Fig. A.4(a): strain in horizontal direction, Fig. A.4(b): strain in vertical direction.

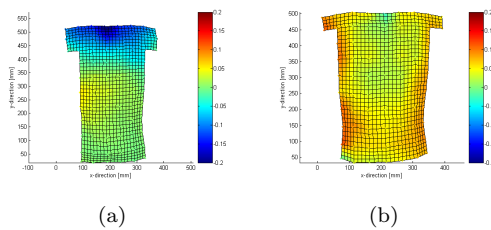


Figure A.5. Lifting both shoulders. Fig. A.5(a): strain in horizontal direction, Fig. A.5(b): strain in vertical direction.

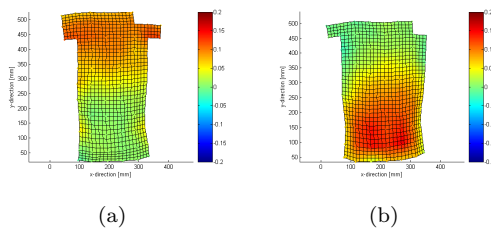


Figure A.6. Slumped. Fig. A.6(a): strain in horizontal direction, Fig. A.6(b): strain in vertical direction.

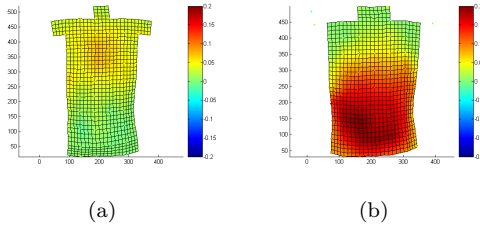


Figure A.7. Bending trunk forward (keeping arms along trunk). Fig. A.7(a): strain in horizontal direction, Fig. A.7(b): strain in vertical direction.

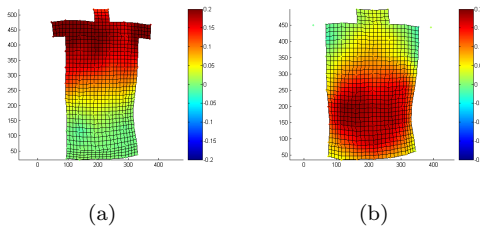


Figure A.8. Bending trunk forward (arms down). Fig. A.8(a): strain in horizontal direction, Fig. A.8(b): strain in vertical direction.

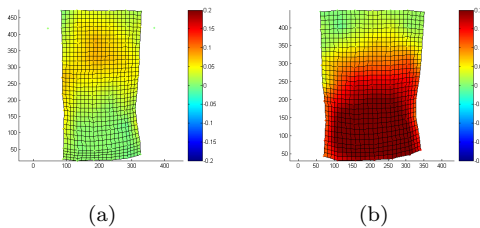


Figure A.9. Bending trunk strongly forward (keeping arms along trunk). Fig. A.9(a): strain in horizontal direction, Fig. A.9(b): strain in vertical direction.

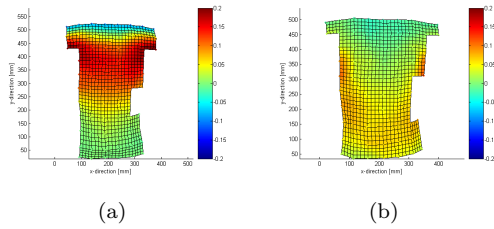


Figure A.10. Arms to the front. Fig. A.10(a): strain in horizontal direction, Fig. A.10(b): strain in vertical direction.

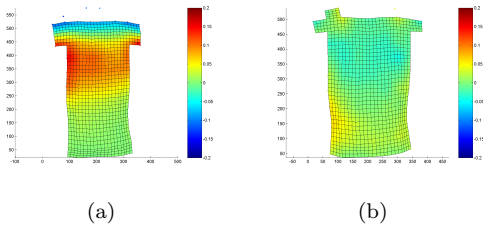


Figure A.11. Arms to the sides. Fig. A.11(a): strain in horizontal direction, Fig. A.11(b): strain in vertical direction.

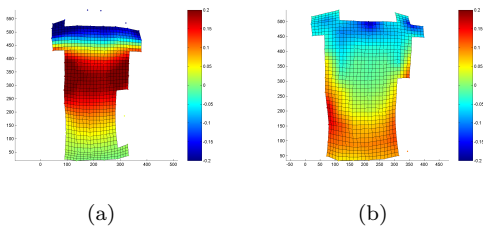


Figure A.12. Arms overhead. Fig. A.12(a): strain in horizontal direction, Fig. A.12(b): strain in vertical direction.

B

Simulated Strain Patterns

In this Chapter, the data used for the optimization of the sensor positions (Chapter 6) is visualized. Always the body posture used for the simulation and the calculated strain patterns (in horizontal and vertical direction) are shown.

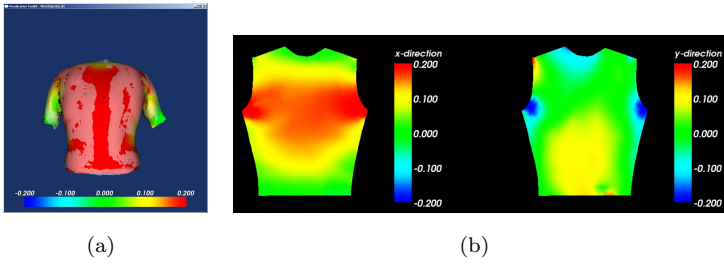


Figure B.1. Posture 1: Bending forward. Fig. B.1(a): Simulated posture. Fig. B.1(b): Calculated strain pattern in horizontal and vertical direction respectively.

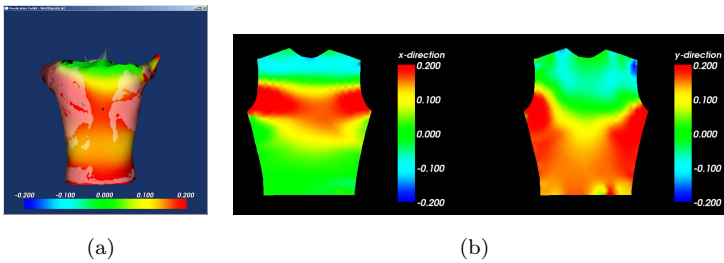


Figure B.2. Posture 2: Arms to the front. Fig. B.2(a): Simulated posture. Fig. B.2(b): Calculated strain pattern in horizontal and vertical direction respectively.

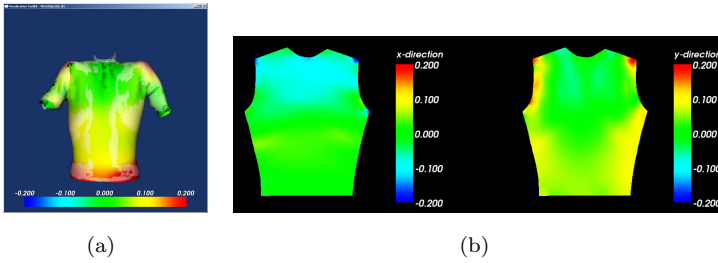


Figure B.3. Posture 3: Lifting shoulders. Fig. B.3(a): Simulated posture. Fig. B.3(b): Calculated strain pattern in horizontal and vertical direction respectively.

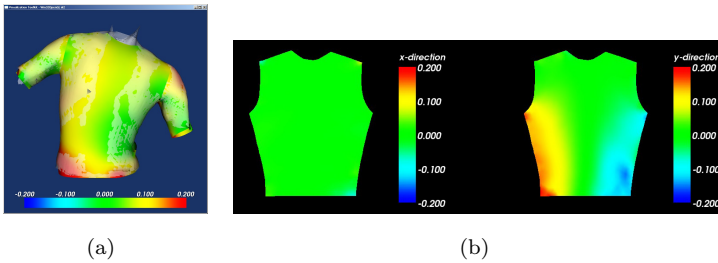


Figure B.4. Posture 4: Bending to the right. Fig. B.4(a): Simulated posture. Fig. B.4(b): Calculated strain pattern in horizontal and vertical direction respectively.

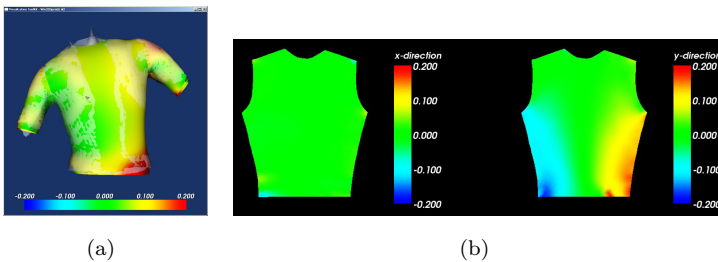


Figure B.5. Posture 5: Bending to the left. Fig. B.5(a): Simulated posture. Fig. B.5(b): Calculated strain pattern in horizontal and vertical direction respectively.

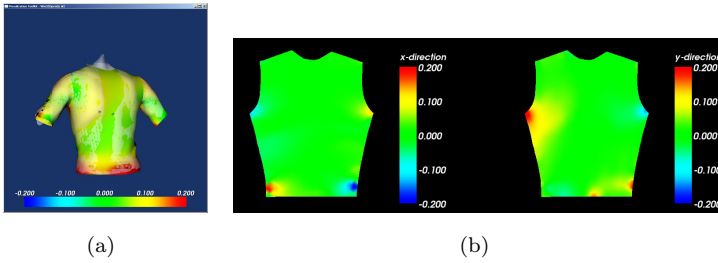


Figure B.6. Posture 6: Rotation to the left. Fig. B.6(a): Simulated posture. Fig. B.6(b): Calculated strain pattern in horizontal and vertical direction respectively.

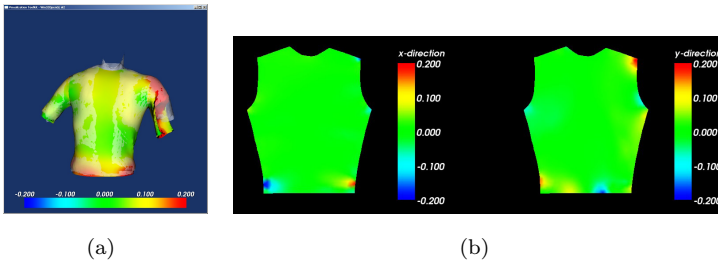


Figure B.7. Posture 7: Rotation to the right. Fig. B.7(a): Simulated posture. Fig. B.7(b): Calculated strain pattern in horizontal and vertical direction respectively.

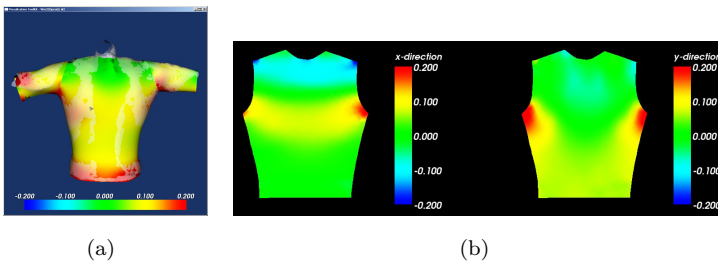


Figure B.8. Posture 8: Arms to the side. Fig. B.8(a): Simulated posture. Fig. B.8(b): Calculated strain pattern in horizontal and vertical direction respectively.

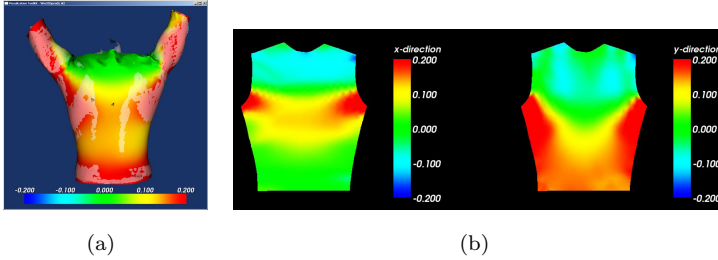


Figure B.9. Posture 9: Arms upwards. Fig. B.9(a): Simulated posture. Fig. B.9(b): Calculated strain pattern in horizontal and vertical direction respectively.

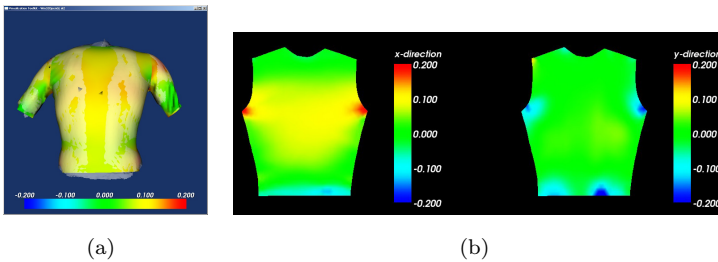


Figure B.10. Posture 10: Slumped posture. Fig. B.10(a): Simulated posture. Fig. B.10(b): Calculated strain pattern in horizontal and vertical direction respectively.

C

Simulated Strain Patterns after Shift of Shirt at Waistline

In this Chapter, the data used for the analysis in Section 7.4 (Upwards Shift of Shirt at Waistline) is visualized for a shift of 3cm. Always the calculated strain patterns (in horizontal and vertical direction) are shown.

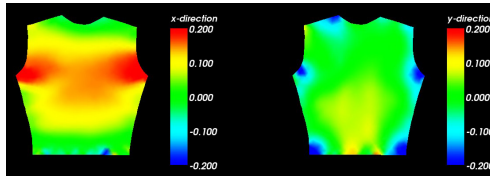


Figure C.1. Posture 1: Strain pattern while bending forward (see Fig. B.1(a)) after shirt moved upwards by 3cm. left: horizontal, right: vertical

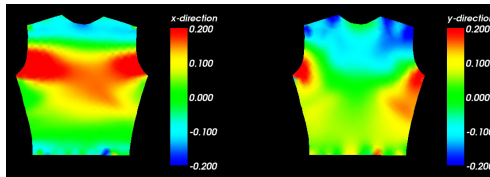


Figure C.2. Posture 2: Strain pattern while holding arms to the front (see Fig. B.2(a)) after shirt moved upwards by 3cm. left: horizontal, right: vertical

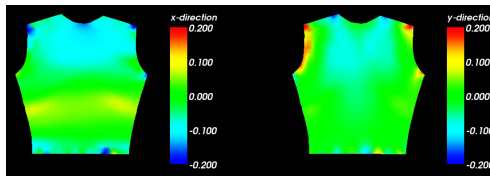


Figure C.3. Posture 3: Strain pattern while lifting the shoulders (see Fig. B.3(a)) after shirt moved upwards by 3cm. left: horizontal, right: vertical

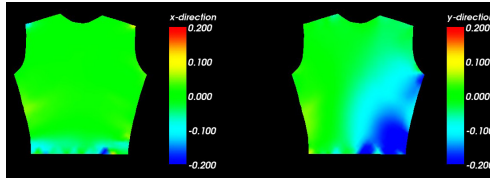


Figure C.4. Posture 4: Strain pattern while bending to the right (see Fig. B.4(a)) after shirt moved upwards by 3cm. left: horizontal, right: vertical

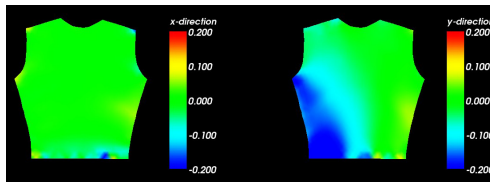


Figure C.5. Posture 5: Strain pattern while bending to the left (see Fig. B.5(a)) after shirt moved upwards by 3cm. left: horizontal, right: vertical

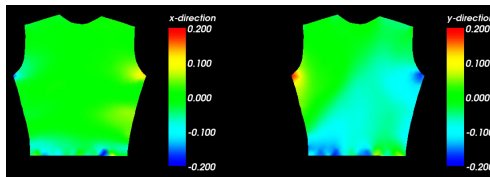


Figure C.6. Posture 6: Strain pattern while rotating to the left (see Fig. B.6(a)) after shirt moved upwards by 3cm. left: horizontal, right: vertical

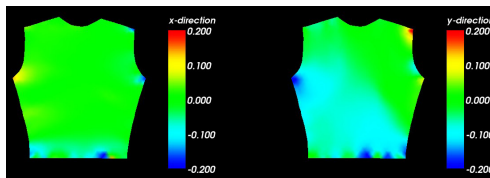


Figure C.7. Posture 7: Strain pattern while rotating to the right (see Fig. B.7(a)) after shirt moved upwards by 3cm. left: horizontal, right: vertical

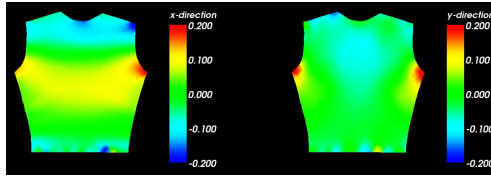


Figure C.8. Posture 8: Strain pattern while holding the arms to the side (see Fig. B.8(a)) after shirt moved upwards by 3cm. left: horizontal, right: vertical

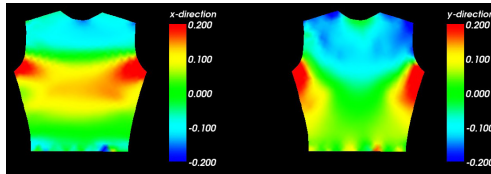


Figure C.9. Posture 9: Strain pattern while holding the arms upwards (see Fig. B.9(a)) after shirt moved upwards by 3cm. left: horizontal, right: vertical

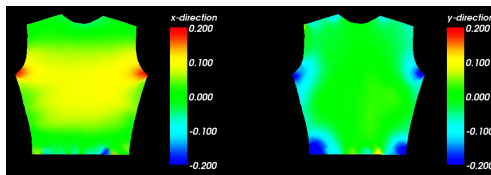


Figure C.10. Posture 10: Strain pattern while slumping (see Fig. B.10(a)) after shirt moved upwards by 3cm. left: horizontal, right: vertical

D

Simulated Strain Patterns for Different Body Proportions

In this Chapter, the data used for the analysis in Section 7.5 (Does Method Still Work for Different Body Proportions?) is visualized. Always the calculated strain patterns (in horizontal and vertical direction) are shown.

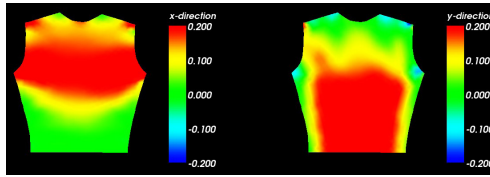


Figure D.1. Posture 1: Strain pattern while bending forward (see Fig. B.1(a)). left: horizontal, right: vertical

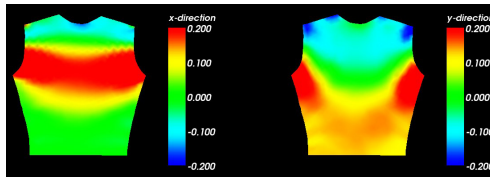


Figure D.2. Posture 2: Strain pattern while holding arms to the front (see Fig. B.2(a)). left: horizontal, right: vertical

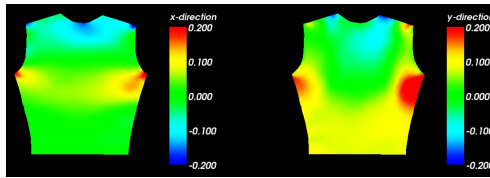


Figure D.3. Posture 3: Strain pattern while lifting the shoulders (see Fig. B.3(a)). left: horizontal, right: vertical

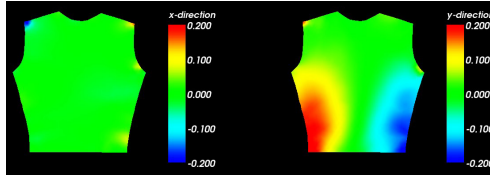


Figure D.4. Posture 4: Strain pattern while bending to the right (see Fig. B.4(a)). left: horizontal, right: vertical

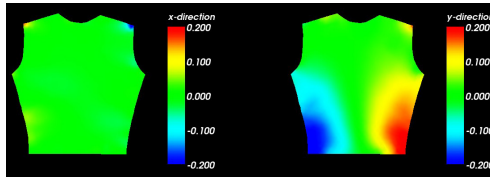


Figure D.5. Posture 5: Strain pattern while bending to the left (see Fig. B.5(a)). left: horizontal, right: vertical

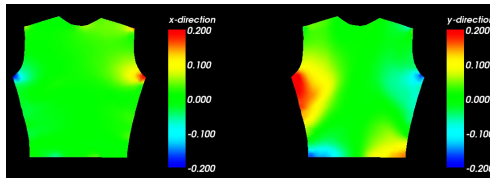


Figure D.6. Posture 6: Strain pattern while rotating to the left (see Fig. B.6(a)). left: horizontal, right: vertical

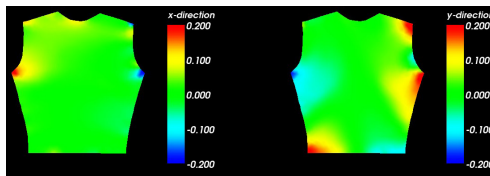


Figure D.7. Posture 7: Strain pattern while rotating to the right (see Fig. B.7(a)). left: horizontal, right: vertical

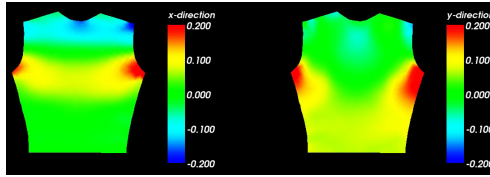


Figure D.8. Posture 8: Strain pattern while holding the arms to the side (see Fig. B.8(a)). left: horizontal, right: vertical

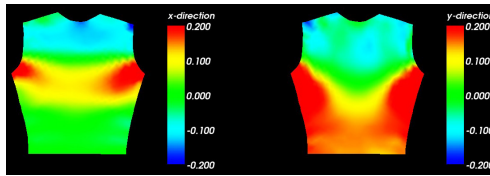


Figure D.9. Posture 9: Strain pattern while holding the arms upwards (see Fig. B.9(a)). left: horizontal, right: vertical

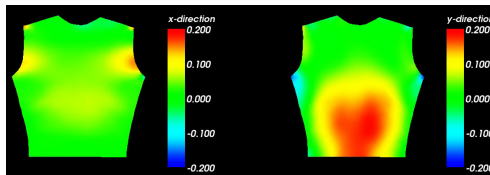


Figure D.10. Posture 10: Strain pattern while slumping (see Fig. B.10(a)). left: horizontal, right: vertical

Glossary

Symbols

Name	SI Unit	Meaning
A		transformation matrix
c		class
C		all classes c
D	kg/s	damping
d	m	distance between two cameras in an optical tracking system
$d_{reference}$	m	distance between two markers in the reference posture
$d_{posture}$	m	distance between two markers in the posture to be compared
dx	m	change in particle position in one iteration step
dt	sec	time step
E	N/m ²	Young's modulus
F	N	force
F		a set of features
F_a, F_b, F_c	N	force in a particle
F_i^D	N	damping force of particle i
F_i^G	N	gravitation force of particle i
F_s		a set of selected features
f		feature
f_s		selected feature
G	m/s ²	gravity
$I(c, f)$		mutual information between class c and feature f
l_0	mm	initial length of the sensor
Δl	mm	change in length of the sensor

m, m_a, m_b	kg	particle mass
N		number of time steps for closing a seam
N_C		total number of classes
P_a, P_b, P_c		particle position of the deformed triangle
$P(c, f)$		joint probability of feature f and class c
$P(c)$		probability of a certain class c
$P(f)$		probability of a feature f
R_0	Ω	initial resistivity of the sensor
ΔR	Ω	change in the electrical resistivity
U, V		directions of the deformed triangle (corresponding to the original directions of the thread in the textile)
$u_{a,b,c}, v_{a,b,c}$		particle position of the original triangle
x_a, x_b		particle positions
\dot{x}_a, \dot{x}_b		particle velocity
x_t		particle position at time t
β		weighting factor
ϵ	$\cdot 100\%$	strain
σ	N/m^2	stress
μ		poisson's ratio

l_0 and R_0 are the initial length and resistivity respectively, l and R the length and resistivity at maximal strain)

Acronyms and Abbreviations

AHRS	Attitude and Heading Reference Systems
BPMM	body posture and movement measurement
CE	conductive elastomer
ECG	electrocardiogram
EL	elastomer
EMPA	interdisciplinary research and services institution for material sciences and technology development within the ETH Domain
EPDM	ethylene-propylenediene rubber
EVA	ethylene-vinyl acetate
FEM	Finite Element Model
GA	Genetic Algorithm
IR	infrared
MI	Mutual Information
MIFS	Mutual Information Feature Selection
PA	polyamide
PCB	printed circuit board
PPy	polypyrrole
PU	polyurethane
SD	standard deviation
SSP	simulated strain patterns
TPE	thermoplastic elastomer

Bibliography

- [1] www.dowcorning.com/content/rubber/silicone-rubber.aspx, July 14th 2008. 27
- [2] www.c3d.org, July 16th 2008. 16
- [3] www.friendly-sensors.de/produkte_gesundheit_sonosens.php, July 16th 2008. 5
- [4] www.mocapsolutions.com, July 16th 2008. 14
- [5] www.moven.com, July 16th 2008. 4, 106
- [6] www.vicon.com, July 16th 2008. 12, 13
- [7] www.vtk.org, July 16th 2008. 53
- [8] Novonic, www.novonic.de/web/novonic.nsf/id/pa_novonic_data.html, July 25th 2008. 6, 8
- [9] www.bekaert.com/bft/products/innovative%20textiles/base%20materials/yarns.htm, July 25th 2008. 6
- [10] www.micro-coax.com/pages/technicalinfo/aracon/aracon_about.asp, July 25th 2008. 6
- [11] www.ohmatex.dk/index.php?id=16&main_id=1&sprog=engelsk, July 25th 2008. 6
- [12] www.statex.biz/eng/index.php?varx=garne, July 25th 2008. 6
- [13] www.softswitch.co.uk/technology/freeform.html, July 29th 2008. 8
- [14] D. Akin and J. Braden. Neutral buoyancy technologies for extended performance testing of advanced space suits. In *33rd International Conference on Environmental Systems*, 2003. 5
- [15] J. Ascough, H. Bez, and A. Bricis. A simple finite element model for cloth drape simulation. *International Journal of Clothing Science and Technology*, 8(3):59–74, 1996. 54

- [16] D. Baraff and A. Witkin. Dynamic simulation of non-penetrating flexible bodies. In *SIGGRAPH'92*, Chicago, 1992. 59
- [17] R. Battiti. Using mutual information for selecting features in supervised neural net learning. *IEEE Trans Neural Netw.*, 5(4): 537–550, 1994. 78
- [18] R. Boulic, P. Glardon, and D. Thalmann. From measurements to model: the walk engine. In *Proc. of 6th Conf on Optical 3D Measurement Techniques, Zurich International Archives of the Photogrammetry, Remote Sensing and Spatial Information Sciences*, 2003. 12
- [19] R. Boulic, M. C. Silaghi, and D. Thalmann. Visualization of local movements for optimal marker positioning. In *First International Workshop on Articulated Motion and Deformable Objects (AMDO 2000)*, 2000. 12
- [20] D. Breen. A survey of cloth modeling methods. In L. A K Peters, ed., *Cloth Modeling and Animation*. 2000. 54
- [21] D. Breen, D. House, and M. Wozny. Predicting the drape of woven cloth using interacting particles. In *Proc. Siggraph 94, Comp. Graph. Proc.*, pp. 365–372, 1994. 55
- [22] A. Burton, F. Balagué, G. Cardon, H. Eriksen, Y. Henrotin, A. Lahad, A. Leclerc, G. Müller, and A. van der Beek. Chapter 2: European guidelines for prevention in low back pain. *European Spine Journal*, 15(Suppl. 2):136–168, 2006. 4
- [23] F. Busetti. Genetic algorithms overview, <http://citeseer.ist.psu.edu/busetti01genetic.html>, july 16th 2008. Technical report, 2001. 80
- [24] B. Chen and M. Govindaraj. A physically-based model of fabric drape using flexible shell elements. *Textile Research Journal*, 65(6):324–330, 1995. 54
- [25] Y. S. Cho, T. Komatsu, M. Takatera, and H. Park. Posture and depth adjustable 3d body model for individual pattern making. *International Journal of Clothing Science and Technology*, 18(2): 96–107, 2006. 50, 51

- [26] C. Cochrane, B. Kim, V. Koncar, and C. Dufour. Multipurpose textile based sensors. In H. Mattila, ed., *Intelligent Textiles and Clothings*, p. 324. Woodhead Publishing Limited, Cambridge, 2006. 25
- [27] C. Cochrane, V. Koncar, M. Lewandowski, and C. Dufour. Design and development of a flexible strain sensor for textile structures based on a conductive polymer composite. *Sensors*, 7:473–492, 2007. 25, 31
- [28] F. Cordier and N. Magnenat-Thalmann. Real-time animation of dressed virtual humans. In *Eurographics*. Blackwell Publishers, 2002. 55
- [29] F. Cordier, P. Volino, and N. Magnenat. Integrating deformations between bodies and clothes. *The Journal of Visualization and Computer Animation*, 12(1):45–53, 2001. 58
- [30] N. Das, T. Chaki, and D. Khastgir. Effect of axial stretching on electrical resistivity of short carbon fibre and carbon black filled conductive rubber composites. *Polym Int.*, 51:156–163, 2002. 25
- [31] M. Di Rienzo, F. Rizzo, G. Parati, G. Brambilla, M. Ferratini, and P. Castiglioni. Magic system: a new textile-based wearable device for biological signal monitoring. applicability in daily life and clinical setting. In *27th Annual International Conference of the Engineering in Medicine and Biology Society (IEEE-EMBS)*, pp. 7167–7169, 2005. 8
- [32] L. Dunne. *Minimally Invasive Sensing of Body Position and Movement Using Body-Garment Interactions*. Phd, University College Dublin, 2007. 5
- [33] L. Dunne, S. Brady, B. Smyth, and D. Diamond. Initial development and testing of a novel foam-based pressure sensor for wearable sensing. *J NeuroEngineering Rehabil*, 2(4), 2005. 5, 7
- [34] L. Dunne, P. Walsh, B. Smyth, and B. Caulfield. Design and evaluation of a wearable optical sensor for monitoring seated spinal posture. In *Proc. of ISWC*, Montreux, 2006. 5
- [35] J. Edmison, M. Jones, Z. Nakad, and T. Martin. Using piezoelectric materials for wearable electronic textiles. In *Sixth Inter-*

- national Symposium on Wearable Computers (ISWC 2002)*, pp. 41–48, 2002. 5
- [36] Y. Ehara, H. Fujimoto, S. Miyazaki, M. Mochimaru, S. Tanaka, and S. Yamamoto. Comparison of the performance of 3d camera systems ii. *Gait & Posture*, 5(3):251–5, 1997. 13, 15
- [37] J. W. Eischen, S. Deng, and T. G. Clapp. Finite-element modeling and control of flexible fabric parts. *IEEE Computer Graphics and Applications*, 16(5):71–80, 1996. 54
- [38] O. Etmuss, M. Keckeisen, and W. Strasser. A fast finite element solution for cloth modelling. In *Proceedings of Pacific Graphics 2003*, 2003. 54
- [39] J. Farrington, A. J. Moore, N. Tilbury, J. Church, and P. D. Biemond. Wearable sensor badge and sensor jacket for context awareness. In *Proc. of ISWC*, pp. 107–113, 1999. 5, 24
- [40] L. Flandin, Y. Bréchet, and J.-Y. Cavaillé. Electrically conductive polymer nanocomposites as deformation sensors. *Composites Science and Technology*, 61:895–901, 2001. 26, 27
- [41] J. Fraden. *Handbook of Modern Sensors: Physics, Designs, and Applications*. AIP Press, 1997. 32
- [42] C. Frigo, M. Rabuffetti, D. C. Kerrigan, L. C. Deming, and A. Pedotti. Functionally oriented and clinically feasible quantitative gait analysis method. *Medical and Biological Engineering and Computing*, 36(2):179–185, 1998. 12
- [43] L. Gan, N. G. Ly, and G. P. Steven. A study of fabric deformation using nonlinear finite elements. *Textile Research Journal*, 65(11): 660–668, 1995. 54
- [44] P. Gibbs and H. Asada. Wearable conductive fiber sensors for measuring joint movements. In *IEEE International Conference on Robotics and Automation (ICRA '04)*, vol. 5, pp. 4753–4758, 2004. 5, 8, 24
- [45] T. Giorgino, S. Quaglini, F. Lorussi, and D. De Rossi. Experiments in the detection of upper limb posture through kinesthetic strain sensors. In *International Workshop on Wearable and Implantable Body Sensor Networks (BSN'06)*, 2006. 5

- [46] D. Goldberg. *Genetic Algorithms in Search, Optimization, and Machine Learning*. Addison-Wesley Publishing Company, Inc., 1989. 80
- [47] A. Griesser, T. P. Koninckx, and L. V. Gool. Adaptive real-time 3d acquisition and contour tracking within a multiple structured light system. In D. Azada, ed., *12th Pacific Conference on Computer Graphics and Applications (PG2004)*, pp. 361–370. IEEE Computer Society, October 2004. 51
- [48] M. Hamedi, R. Forchheimer, and O. Inganäs. Towards woven logic from organic electronic fibres. *Nature Materials*, 6, 2007. 7, 106
- [49] G. A. Hansson, P. Asterland, N. G. Holmer, and S. Skerfving. Validity and reliability of triaxial accelerometers for inclinometry in posture analysis. *Med Biol Eng Comput*, 39(4):405–13, 2001. 4
- [50] H. Harms, O. Amft, D. Roggen, and G. Tröster. Smash: A distributed sensing and processing garment for the classification of upper body postures. In *Third International Conference on Body Area Networks (BodyNets08)*, Tempe, AZ, 2008. 4, 7, 106
- [51] G. F. Harris and J. J. Wertsch. Procedures for gait analysis. *Arch Phys Med Rehabil*, 75(2):216–225, 1994. 12
- [52] J. H. Holland. *Adaption in Natural and Artificial Systems*. The University of Michigan Press, 1975. 79
- [53] D. House and D. Breen. *Cloth Modeling and Animation*. A.K. Peters Ltd., 2000. 59
- [54] J. Katz. Lumbar disc disorders and low-back pain: Socioeconomic factors and consequences. *Journal of Bone and Joint Surgery*, 88 (Suppl 2):21–24, 2006. 4
- [55] S. Kawabata, M. Niwa, and H. Kawai. The finite deformation theory of plane weave fabrics. *The Journal of the Textile Institute*, (64):21–83, 1973. 54
- [56] T. Kirstein. *Produktentwicklung für körpernahe Bekleidung unter Berücksichtigung der textilen Materialeigenschaften*. Phd, Universität Dresden, 2001. 24

- [57] T. Kirstein, M. Lawrence, and G. Tröster. Functional electrical stimulation (fes) with smart textile electrodes. In *International Workshop on a new generation of wearable systems for e-health*, 2003. 8
- [58] R. Kohavi and G. John. Wrappers for feature subset selection. *Artificial Intelligence*, 97(1-2):273–324, 1997. 74
- [59] J. Lander. Devil in the blue faceted dress: Real-time cloth animation. *Game Developer*, 1999. 55
- [60] D. Lehn, C. Neely, K. Schoonover, T. Martin, and M. Jones. e-tags: e-textile attached gadgets. In *Communication Networks and Distributed Systems Modeling and Simulation Conference*, 2004. 7
- [61] T. Löher, A. Neumann, L. Böttcher, B. Pahl, A. Ostmann, R. Aschenbrenner, and H. Reichl. Smart pcbs manufacturing technologies. In *6th International Conference on Electronics Packaging Technology*, 2005. 7
- [62] G. Li and P. Buckle. Current techniques for assessing physical exposure to workrelated musculoskeletal risks, with emphasis on posture-based methods. *Ergonomics*, 42(5):674–695, 1999. 3
- [63] Y. Li, X. Cheng, M. Leung, J. Tsang, X. Tao, and M. Yuen. A flexible strain sensor from polypyrrole-coated fabrics. *Synthetic Metals*, 155:89–94, 2005. 24
- [64] I. Locher. *Technologies for Systems-on-Textile Integration*. Phd, ETH Zurich, 2006. 7, 8
- [65] F. Lorussi, E. P. Scilingo, M. Tesconi, A. Togenetti, and D. De Rossi. Strain sensing fabric for hand posture and gesture monitoring. *IEEE Transaction of Information Technology in Biomedicine*, 3:372 – 381, 2005. 25
- [66] M. Maccioni, E. Orgiu, P. Cosseddu, S. Locci, and A. Bonfiglio. Towards the textile transistor: Assembly and characterization of an organic field effect transistor with a cylindrical geometry. *APPLIED PHYSICS LETTERS*, 89(14):143515, 2006. 7
- [67] N. Magnenat Thalmann and D. Thalmann. Computer animation. *ACM Computing Surveys*, 28(1):161–163, 1996. 12

- [68] T. Martin, M. Jones, J. Edmison, and R. Shenoy. Towards a design framework for wearable electronic textiles, 2003. URL citeseer.ist.psu.edu/martin03towards.html. 4
- [69] C. Mattmann, O. Amft, H. Harms, F. Clemens, and G. Tröster. Recognizing upper body postures using textile strain sensors. In *Proc. of 11th International Symposium on Wearable Computers (ISWC07)*, Boston, 2007. 39
- [70] C. Mattmann, F. Clemens, and G. Tröster. Patent: Recognizing upper body postures using textile strain sensors, t-07-066, us60/976,806, 2007. 25
- [71] C. Mattmann, F. Clemens, and G. Tröster. Sensor for measuring strain in textile. *Sensors*, 8(6):3719–3732, 2008. 8, 23
- [72] C. Mattmann, T. Kirstein, and G. Tröster. A method to measure elongations of clothing. In *Proc. 1st International Scientific Conference Ambience 05*, September 2005. 11
- [73] C. Mattmann and G. Tröster. Design concept of clothing recognizing back postures. In *Proc. 3rd IEEE-EMBS International Summer School and Symposium on Medical Devices and Biosensors (ISSS-MDBS 2006)*, September 2006. 40
- [74] J. Meyer, P. Lukowicz, and G. Tröster. Textile pressure sensor for muscle activity and motion detection. In *10th IEEE International Symposium on Wearable Computers*, pp. 69–72, 2006. 7
- [75] A. Meyer-Heim, M. Rothmaier, M. Weder, J. Kool, P. Schenk, and J. Kesselring. Advanced lightweight cooling-garment technology: functional improvements in thermosensitive patients with multiple sclerosis. *Multiple Sclerosis*, 13(2):232–237, 2007. 8
- [76] U. Möhring, S. Gimpel, A. Neudeck, W. Scheibner, and D. Zschenderlein. Conductive, sensorial and luminescent features in textile structures. In *3rd International Forum on Applied Wearable Computing (IFAWC2006)*, Bremen, 2006. 8
- [77] H. Ng and R. Grimsdale. Computer graphics techniques for modeling cloth. *IEEE Computer Graphics and Applications*, 16(5): 28–41, 1996. 54

- [78] V. Ng-Thow-Hing. Revisiting the standart joint hierarchy. In *Game Developers Conference*, 2004. 52
- [79] C. Nørstebø. Intelligent textiles, soft products, www.ivt.ntnu.no/ipd/docs/pd9-2003/norstebo.pdf, july 16th 2008. Technical report, 2003. 8
- [80] M. Pacelli, G. Loriga, N. Taccini, and R. Paradiso. Sensing fabrics for monitoring physiological and biomechanical variables: E-textile solutions. In *Proceedings of the 3rd International Summer School and Symposium on Medical Devices and Biosensors (IEEE-EMBS)*, 2006. 8
- [81] B. Pahl, C. Kallmayer, R. Aschenbrenner, and H. Reichl. Ultrathin assemblies on flexible substrates. In *7th Electronic Packaging Technology Conference*, 2005. 7
- [82] S. Park and J. Hodgins. Capturing and animating skin deformation in human motion. *ACM Transaction on Graphics (SIGGRAPH 2006)*, 25(3):881–889, 2006. 12
- [83] H. Peng, F. Long, and C. Ding. Feature selection based on mutual information: Criteria of max-dependency, max-relevance, and min-redundancy. *IEEE Transactions on Pattern Analysis and Machine Intelligence*, 27(8):1226–38, 2005. 74
- [84] X. Provot. Deformation constraints in a mass-spring model to describe rigid cloth behavior. In *Graphics Interface '95*, 1996. 55
- [85] L. Rattfält, M. Lindén, P. Hult, L. Berglin, and P. Ask. Electrical characteristics of conductive yarns and textile electrodes for medical applications. *Medical and Biological Engineering and Computing*, 45(12):1251–1257, 2007. 8
- [86] D. Roggen, N. Bharatula, M. Stäger, P. Lukowicz, and G. Tröster. From sensors to miniature networked sensorbuttons. In *3rd Int. Conf. on Networked Sensing Systems (INSS06)*, pp. 119–122, 2006. 7
- [87] R. Sanchez, J. Liu, S. Rao, P. Shah, R. Smith, T. Rahman, S. Cramer, J. Bobrow, and D. Reinkensmeyer. Automating arm movement training following severe stroke: Functional exercises with quantitative feedback in a gravity-reduced environment.

- IEEE Transactions on Neural Systems and Rehabilitation Engineering*, 14(3):378–389, 2006. 4
- [88] J. Schumm. *Genetic Algorithm for Feature Selection*. Master thesis, RWTH Aachen, 2006. 79
- [89] H. Seo and N. Magnenat-Thalmann. An automatic modeling of human bodies from sizing parameters, 2003. 641487 19-26. 50, 51
- [90] H. Seo and N. Magnenat-Thalmann. An example-based approach to human body manipulation. *Graphical Models*, 66(1):1–23, 2004. Journal Paper. 51
- [91] A. Seyam. Mechanics of woven fabrics. *Textile Research Journal*, 60(7):389–404, 1990. 54
- [92] I. Silveira, F. Clemens, C. Bergmann, and T. Gaule. Flexible strain-sensitive sensors for application in human physiology. In *Materiais 2007*, Porto, Portugal, 2007. 26
- [93] I. Silveira, F. Clemens, C. P. Bergmann, and T. Gaule. Novel electrical conductive fibres using thermoplastic elastomer - carbon black composites. In *Brazilian MRS Meeting 2006*, 2006. 25
- [94] D. Terzopoulos, J. Platt, A. Barr, and K. Fleischer. Elastically deformable models. In *International Conference on Computer Graphics and Interactive Techniques (SIGGRAPH '87)*, vol. 21, pp. 205–214, Anaheim, 1987. ACM. 55
- [95] A. Tognetti, F. Lorussi, R. Bartalesi, S. Quaglini, M. Tesconi, G. Zupone, and D. De Rossi. Wearable kinesthetic system for capturing and classifying upper limb gesture in post-stroke rehabilitation. *J NeuroEngineering Rehabil*, 2(1):8, 2005. 5, 8, 25
- [96] A. Tognetti, F. Lorussi, M. Tesconi, and D. De Rossi. Strain sensing fabric characterization. In *Proc. of IEEE Sensors*, vol. 1, pp. 527–530, 2004. 25
- [97] A. Toney. A novel method for joint motion sensing on a wearable computer. In *Proc. of ISWC*, pp. 158–159, 1998. 5

- [98] J. van der Lee, I. Snels, H. Beckerman, G. Lankhorst, and R. Wagenaar. Exercise therapy for arm function in stroke patients: a systematic review of randomized controlled trials. *Clinical Rehabilitation*, 15(1):20–31, 2001. 3
- [99] A. Van Gelder. Approximate simulation of elastic membranes by triangulated spring meshes. *Journal of Graphics tools*, 3(2): 21–42, 1998. 55
- [100] K. Van Laerhoven and O. Cakmakci. What shall we teach our pants? In *Proc. of ISWC*, pp. 77–83, 2000. URL citeseer.ist.psu.edu/vanlaerhoven00what.html. 4
- [101] P. Volino, M. Courchesne, and N. Magnenat. Versatile and efficient techniques for simulating cloth and other deformable objects. In *International Conference on Computer Graphics and Interactive Techniques*, pp. 137–144, 1995. 55
- [102] P. Volino and N. Magnenat. Implicit midpoint integration and adaptive damping for efficient cloth simulation. In *CASA 2005*, vol. 16, 3-4, pp. 163–175. John Wiley and Sons Ltd., 2005. 55
- [103] P. Volino and N. Magnenat-Thalmann. *Virtual Clothing: Theory and Practice*. Springer, 2000. 61, 62
- [104] P. Volino and N. Magnenat-Thalmann. Accurate garment prototyping and simulation. *Computer-Aided Design & Applications*, 2(Nos. 1-4), 2005. 55, 56, 57, 72, 104
- [105] J. Weil. The synthesis of cloth objects. *ACM SIGGRAPH Computer Graphics*, 20(4):49 – 54, 1986. 54
- [106] P.-B. Wieber, F. Billet, L. Boissieux, and R. Pissard-Gibollet. The humans toolbox, a homogeneous framework for motion capture, analysis and simulation. In *submitted to the ninth ISB Symposium on 3D analysis of human movement*, Valenciennes, France, 2006. 52
- [107] X. Zhang, K. W. Yeung, and Y. Li. Numerical simulation of 3d dynamic garment pressure. *Textile Research Journal*, 72(3): 245–252, 2002. 54
- [108] H. Zhou and H. Hu. A survey - human movement tracking and stroke rehabilitation. Technical Report CSM-420, 2004. 12

Curriculum Vitae

Personal Information

Corinne Mattmann
Born July 18th 1978, Lucerne, Switzerland
Citizen of Wallisellen ZH, Switzerland

Education

- 2004–2008 PhD studies in information technology and electrical engineering (Dr. sc. techn.) at ETH Zurich, Switzerland
- 1999–2004 MSc studies in information technology and electrical engineering (Dipl. El.-Ing. ETH) at ETH Zurich, Switzerland
- 1999 Language studies in Cannes, France and Bournemouth, England
- 1991–1998 Gymnasium (Matura, Typus C) at Kantonsschule Hochdorf and Reussbühl, Switzerland
- 1985–1991 Primary school in Eschenbach, Switzerland

Professional Experience

- 2004–2008 Research and teaching assistant at Electronics Laboratory, ETH Zurich, Switzerland
- 2003 Internship with Sensirion, Zürich, Switzerland:
Building a testing environment for flow sensor.
- 2002 Internship with Bruker AG, Fällanden, Switzerland:
Accuracy measurements of different temperature sensors.
- 2001 Internship with Siemens Metering, Zug, Switzerland:
Writing software to test current measurement systems.
- 1998–1999 Internship with RUAG, Emmen, Switzerland.